Experimental Study of the Durability of Textile Reinforced Cementitious Composites

For Outdoor Applications of Sandwich Panels

Jens De Koster

Master thesis submitted under the supervision of
prof. dr. ir. Tysmans Tine and dr. ir. arch. Remy Olivier

The co-supervision of
ir. De Munck Matthias

In order to be awarded the Master's Degree in
Civil Engineering

Academic year
2016-2017

Study of the Durability of Textile Reinforced Composites
For Outdoor Applications of Sandwich Panels

Jens De Koster

Vrije Universiteit Brussel
Pleinlaan 2, 1050 Brussels

Master of Science in
Civil Engineering

jens.de.koster@vub.ac.be

June 2017

Keywords: *Textile Reinforced Cementitious Composite, Tensile behaviour, Environmental loading, Freeze-thaw, Heat-Rain*

Abstract

Sandwich panels show excellent possibilities towards low-energy building solutions. Although, regarding the application of sandwich panels for outdoor applications, a durable performance is required. This work investigates the mechanical performance of textile reinforced cementitious composites (TRC) with an alkali resistant glass textile when exposed to durability cycles, namely 100 freeze-thaw cycles, 50 heat-rain cycles and combination of both. The characterization of the tensile behaviour was done by means of non-destructive and uniaxial tensile test. The loss in mechanical performance of the aged specimens seems to be governed by the physical damage attributed to durability loading. Further investigation on the micro-scale processes will be of interesting use to entirely understand the degradation processes. Knowledge and quantification of this loss is essential for the design of sandwich panels for renovation purposes.

Acknowledgement

The completion of this thesis could not have been possible without the participation and assistance of so many people of the MeMC Department whose names may not all be enumerated. Their contributions are sincerely appreciated and gratefully acknowledged. However, I would like to express my deep appreciation particularly to the following:

- promotor **prof. dr. ir. TYSMANS Tine** and co-promotor **dr. ir. REMY Olivier** for the general supervision and availability for questions,
- supervisor **ir. DE MUNCK Matthias** for the day to day supervision and assistance where needed,
- **ir. TSANGOURI Eleni** for the assistance with non-destructive testing,
- **ir. BOULPAEP Frans**, **VAN DEN NEST Gabriël** and **DEBONDT Daniel** for the assistance and help in the laboratory,
- my parents for the endless support and the opportunity to start this Civil Engineering studies,
- my fellow students for the mutual support and the pleasant working atmosphere.

List of tables

List of figures

Table of Contents

1. Introduction

1.1 Problem statement

The increasing energy- and insulation requirements in Flanders, Belgium, cause the need for low-energy building solutions for new buildings and renovation purposes. The maximal U-value for renovation and new buildings in Belgium is set to 0.24 W/m²K since 1 January 2017. [Vlaamse Overheid 2016] This corresponds to an EPS-core with a thickness of at least 130mm. In the construction industry, a common structural insulating wall element consists of a structural load-bearing layer, a heat insulation layer and an outer facing. The total thickness of such an element varies between 20 and 27 centimeters. [De Munck 2014]

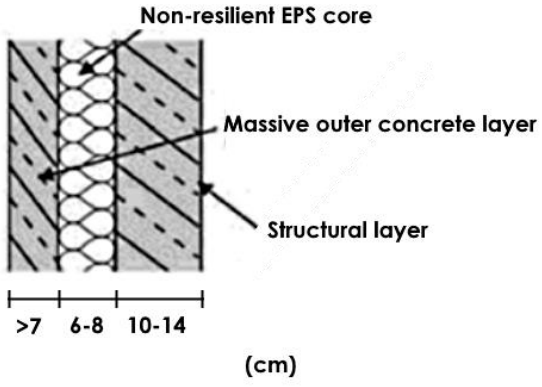

Structural component	Thickness
Structural load-bearing	10-14 cm
Insulation layer	6 cm
Outer facing	> 7 cm

Figure 1 Common structural wall element [De Munck 2014]

This master thesis focusses on the renovation industry, where the insulation requirements in combination with the structural properties and dimensions are of essential need. Sandwich panels offer the ultimate solution due to their substantial decrease in thickness and weight while maintaining mechanical performance.

Sandwich panels are assembled wall elements consisting of a rigid core sandwiched between two layers of structural board. These constructions use the fact that the core of a panel that is loaded in bending does not carry much in-plane stresses and does not represent the surface of the panel. The core can thus be made from a different, more lightweight and/or less expensive material. Solutions are found in lightweight insulating materials, such as a rigid polyurethane foam (PUR/PIR), expanded polystyrene foam (EPS), phenolic foam, cellular glass and even mineral wool to meet the fire prevention requirements. [Craig 2004] Sandwich panels are therefore an ideal solution for high energy efficiency regarding insulation and have already been produced for commercial purposes under the terminology of structural insulated panels (SIP). Figure 2 shows typical dimensions of such a sandwich panel.

The **mechanical requirements** will be governed by the Serviceability and Ultimate Limit state requirements. The Serviceability Limit State requires a high stiffness to limit deflections caused by external loading, such as bending of the panel, while for the Ultimate Limit State, interest is found in the ultimate strength of the material. These requirements will be attributed to the structural boards, which may exist out of metal sheets, plywood, cement, polymers or oriented strand board (OSB). [Zenckert 1995]

Metal, polymer and wood faced insulating sandwich panels have a wide field of application, because of their excellent mechanical performance. For metal faced insulating sandwich panels, the ability of strain hardening, and therefore improved fire safety, are additional benefits. One of the main drawbacks of these panels in the renovation industry is found in the sustainability and esthetics.

Textile Reinforced Cementitious Composites (TRC) will be used for this purpose because of their relative high stiffness and the resistance of the fibres to corrosion. In addition, TRC has an excellent fire resistance. [De Munck 2014] These properties will govern a good global performance compared to other materials used for renovation purposes as wood and polymers. A typical TRC sandwich panel is displayed in Figure 3.

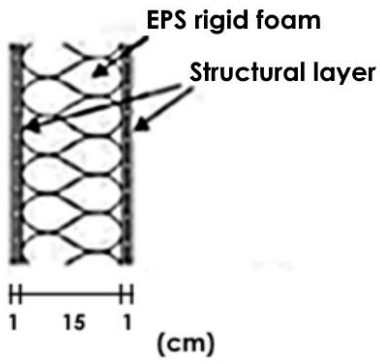

Figure 2 Dimensions of the investigated sandwich panels

Figure 3 Textile Reinforced Cement Faces on Sandwich panels for renovation [De Munck 2014]

In addition, these lightweight sandwich panels have a decreased **impact on the environment**, because of the reduced $C0_2$ production compared to a concrete structural wall element (Figure 1). Also, every kilo saved in the construction results in less energy needed to move the material, saving the environment from enormous amounts of pollutants. [Craig 2004]

Since the lightweight sandwich panels will be directly exposed to outer weathering conditions, the choice of the material of the structural layer should also be based on **durable performance**. Within the research of this master thesis, the mechanical behaviour of TRC faces exposed to outer weathering conditions will be investigated.

1.2 Objectives and Outline

The main objective of this master thesis is to enlarge the knowledge on, and quantify the influence of environmental loading on the mechanical performance of Textile Reinforced Cementitious Composites for Outdoor Application of Sandwich Panels. This knowledge is of importance considering a durable design of such sandwich panels regarding the Serviceability and Ultimate Limit States. This work is part of a bigger project-joint between the CRH Structural Concrete Belgium NV and the Vrije Universiteit Brussel, in the context of the PhD research of ir. De Munck Matthias (Vrije Universiteit Brussel).

Originally, one of the objectives of this master thesis was to investigate the influence of environmental loading on sandwich beams existing of an inner EPS core of 150 mm sandwiched between two TRC faces with a thickness of 10 mm. Due to technical problems with the provided climate chambers, testing of this sandwich beams have never taken place but could be of interest for further investigation. Nevertheless, the opportunity has presented itself to get into deeper detail on the study of durability on Textile Reinforced Cementitious composites in particular.

This master thesis covers a brief state of the art study on the durability of Textile Reinforced Cementitious Composites by exposing TRC specimens to environmental loading cycles. These environmental cycles approximate the environmental loading experienced by sandwich panels for outdoor applications.

Next, the methods used within this master thesis can be found; 72 prismatic specimens with nominal dimensions of 500 mm in length, 50 mm in width and 10 mm thick have been produced using a hand lay-up technique. An extensive experimental program is carried out, where 27 specimens will be used as virgin specimens, 18 specimens will be subjected to 100 freeze-thaw cycles, 9 specimens will be exposed to 50 heat-rain cycles and 18 specimens to a combination of both.

Afterwards, mechanical loading is executed using uniaxial tensile tests on the different specimens. The mechanical tests were continuously monitored by Digital Image Correlation. Interpretation of these results give information on the crack pattern and strain evolution during the mechanical tests. An investigation on the global mechanical performance is done by focusing on the influence of environmental loading on several mechanical properties with eye on the Serviceability and Ultimate Limit State requirements of sandwich panels. The discussion of these results can be found in chapter 4. The investigated properties are briefly described in what follows.

The first cracking strength is a critical value regarding SLS requirements, since crack initiation takes place at this stress level. Although, this interpretation must be done with care, since some may interpret the formation of cracks as an exceedance of the SLS requirements, while others may interpret the crack formation and propagation until a certain width as an acceptable SLS condition.

To limit deflections in the sandwich panels that is loaded in bending, the composite's stiffness is of important use. Within this work, the evolution of the stiffness during environmental loading is monitored using a non-destructive resonalyser test. Additionally, non-destructive Ultrasonic Pulse Velocity tests have been conducted on a limited amount of specimen to compare both techniques. Finally, the effective material stiffness is deduced from the stress-strain curves obtained after mechanical uniaxial tensile tests before and after environmental loading.

The maximum tensile strength is defined by the maximum tensile stress and forms the most important parameter concerning the ULS requirements. This work discusses the influence of environmental loading on the ultimate strength, as well as the failure mode of the specimens.

Regarding the failure mode which can be attributed to fibre pull-out or fabric failure. A study on the material's stiffness and the efficiency factor of the fabrics is carried out. This property is characterized by the third and last stage regarding the ACK model developed by Aveston, Cooper and Kelly (1971).

With respect to the durable performance of TRC, an investigation on the number of cracks is carried out and related to the environmental loading. This crack investigation, in particular the opening of the cracks, is of essential use to determine the sensitivity to aggressive substances. Therefore, deeper detailing on the average crack width and crack interdistance is carried out at the level of ultimate failure.

Finally, evolution of the above enumerated properties on virgin specimens and environmental-loaded specimens is discussed and summarized in a conclusion. A brief enumeration of possible fields of interest are designated for further investigation on this topic.

2. State of the Art

2.1 Introduction

Textile Reinforced Cementitious Composite (TRC) is a construction material consisting of high-performance filament yarns of glass, polymeric or carbon fibre and a fine-grained cementitious matrix. In the majority of the existing and prospective applications of TRC, fabrics made of glass fibres with a high resistance to alkalis (AR glass) are used [Butler 2010]. These cement-based composites reinforced with fabrics allow to obtain thin and lightweight structures characterized by a relatively high tensile strength. Despite the brittle nature of cementitious materials, TRC composites behave completely different behaviour in tension. [Remy 2012] Figure 4 displays an example of a TRC composite.

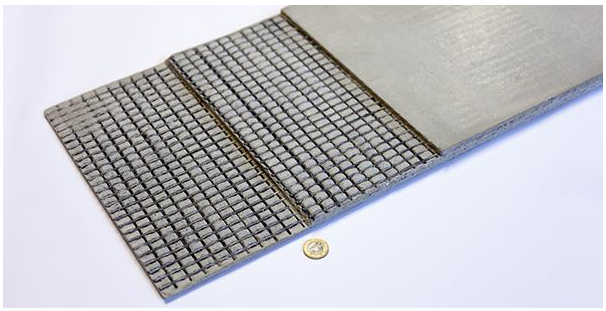

Figure 4 An example of a TRC composite [Sigmund 2014]

The development of TRC is based on the experiences with Glass fibre Reinforced Cementitious Composites (GFRC). A drawback of the reinforcement with chopped strands is the partial un-oriented distribution of the fibres over the total cross section, reducing their effectiveness. In contrast, in TRC, the fibres are aligned as two-dimensional fabrics in the direction of the tensile stresses. This leads to a higher utilization of the reinforcement material and better load-bearing properties of the component. [Butler 2010, Colombo 2015] In comparison to conventional glass fibre reinforced concrete (GFRC), this results in a reduction of up to 80% in the fibre reinforcement necessary and to an essential increase in efficiency of the fibre utilization. [Butler 2010]

The characteristics of TRC have proven their advantages to build slender, lightweight, modular and freeform structures, taking away the risk of corrosion. [Portal 2014] Nowadays, Textile Reinforced Cementitious composites are already used in existing structures as a pedestrian bridge in Germany (Figure 5) [Hegger 2010] and the development of thin, self-supporting sandwich panels (Figure 5). [Tomoscheit]

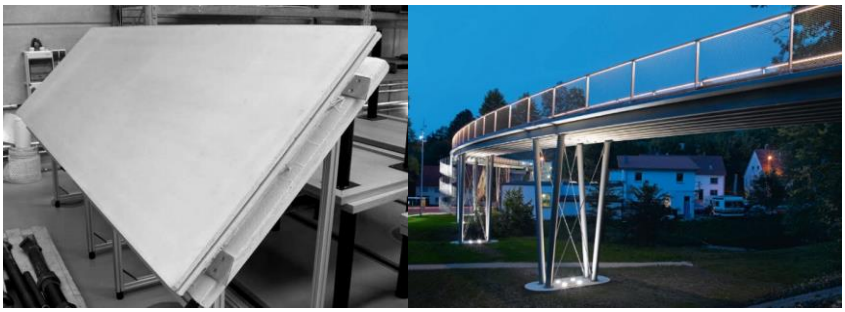

Figure 5 Thin, self-supporting sandwich panel (Insu-Shell) [Tomoscheit] and a pedestrian Bridge of TRC, Germany [Hegger 2010]

This chapter contains a brief overview of the different components of TRC, followed by a discussion of the mechanical behaviour of such a composite, consisting typically out of a pre-cracking stage, a multiple cracking stage and a post-cracking stage. This mechanical behaviour is theoretically approached by the ACK theory, developed by Aveston, Cooper and Kelly (1971). Finally, within the topic of durability on TRC, an overview of the degradation processes observed after accelerated ageing of TRC is assessed on microscale on one hand, while on the other hand the effect of durability cycles on the mechanical behaviour of TRC is established.

2.2 Components of TRC

2.2.1 Fibres and textiles as reinforcement

The fibre materials used in Textile Reinforced Cementitious Composites can vary a lot. [Cuypers 2008] Table 1 displays the properties of some frequently used fibre materials. In order to guarantee the composite's mechanical behaviour, four essential aspects [Remy 2012] need to be taken into account:

1. The fibre's material properties
2. The amount of fibres inserted in the matrix (fibre volume fraction)
3. The structure of the fibrous textiles
4. The fibre to matrix bond

Fibrous textiles are made from rovings which themselves consist of some hundreds to thousands of single fibres (filaments). This will cause that the textiles can be aligned in the direction of the tensile forces, resulting in better tensile behaviour of the composite. [Colombo 2015]

To guarantee a good mechanical performance, interest is found in a high Young modulus, tensile strength and ultimate elongation. According to Bentur et al., glass, aramid, carbon, steel and asbestos fibres satisfy those requirements.

Table 1 Properties of suitable fibre reinforcement materials for cement composites

Fibre	Diameter (μm)	Specific density (-)	Elastic Modulus (GPa)	Tensile strength (MPa)	Ultimate elongation (%)
Steel	5-500	7.84	200	0.5-2.0	0.5-3.5
Glass	9-15	2.6	70-80	2-4	2-3.5
Asbestos Crocidolite	0.02-0.4	3.4	196	3.5	2.0-3.0
Asbestos Chrysolite	0.02-0.4	22.6	164	3.1	2.0-3.0
Aramid	10-12	1.44	63-120	2.3-3.5	2-4.5
Carbon	8-9	1.6-1.7	230-380	2.5-4.0	0.5-1.5
Acrylic	18	1.18	14-19.5	0.4-1.0	3
Polyethylene	25-1000	0.92-0.96	5	0.08-0.60	3-100
Polypropylene	20-400	0.9-0.95	3.5-10	0.45-0.76	15-25

Due to the thin layered sandwich panels, steel reinforcements are unlikely to use due to their sensitivity to corrosion. The use of asbestos causes health problems and can therefore no longer be used in construction. Adding the cost as a third parameter, glass fibres show the most economical advantage and will therefore be used in this thesis. [Tysmans 2010]

2.2.2 Cementitious matrix

The cementitious matrix used for TRC applications must fulfill particular requirements. The most important requirement for the cementitious matrix used in the Textile Reinforced Cementitious composite is the alkalinity of the matrix. On the long term, the latter will have an (negative) influence on the mechanical behaviour of the fibres. Therefore, either Alkali Resistant glass fibres, either avoiding the use of alkaline OPC-based mortars, can be used to prohibit this limitation. [Remy 2012]

To guarantee a good bonding and, therefore, a good load bearing behaviour, full penetration of the fabrics in the matrix is another important requirement. The geometry of the fabrics limits the maximum grain size of the matrix to values varying between 2 and 4 mm [Brameshuber 2006]. Of course, the coarser the geometry of the fabrics, the smaller the allowable grains. Also, the consistency of the matrix plays an important role dependent on the fabric geometry. The smaller the mesh size of the fabrics, the more fluid the matrix consistency must be.

2.3 Mechanical behaviour

In compression, TRC follows a linear elastic behaviour, while in tension, a non-linear behaviour is observed (Figure 6). The main advantages of this material are the ability to orient the reinforcement in the direction of the tensile forces, the bi-axial load capacity and the unrequired concrete cover. [Colombo 2015] This bi-axial load capacity is of important use in the application of outdoor sandwich panels, since the sandwich constructions use in-plane stress distributions.

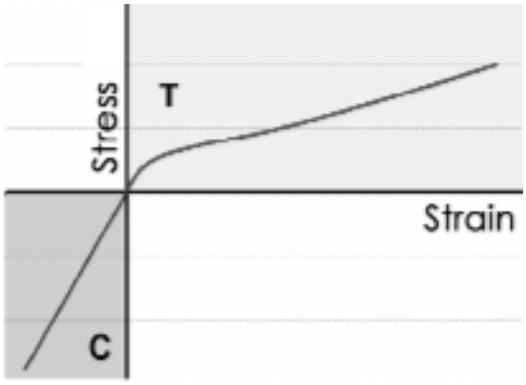

Figure 6 Mechanical behaviour TRC: Linear elastic behaviour in compression, non-linear in tension [Remy 2012]

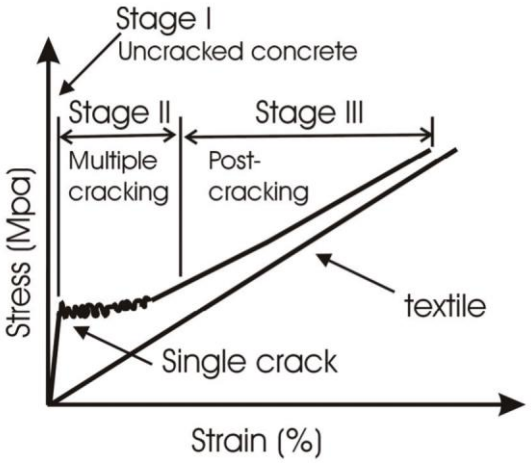

Figure 7 Mechanical behaviour TRC under uniaxial loading [Tysmans 2010]

The typical non-linear tensile behaviour of TRC, represented in Figure 7, can be divided in three stages. [Brameshuber 2006]

Stage I – Pre-cracking represents a linear elastic behaviour in the assumption of a perfect bond. The E-modulus during this stage accords to an uncracked composite and follows the "law of mixtures".

Stage II – Multiple cracking occurs when the tensile strength of the cementitious matrix is reached. In order to have a post cracking behaviour as in Figure 7, the fibre volume fraction should be above a critical value, otherwise the composite will fail. The first crack is formed when the matrix's tensile strength is reached, meaning that the fibres are debonded from the matrix, causing a frictional bond instead of an adhesive ('perfect') bond. Frictional stress transfers the forces further in the matrix. The stress strain curve shows numerous "jumps", which indicate abrupt, brief partial unloading of the specimen due to formation of new cracks and therefore redistribution of deformations over the specimen's length.

Stage III – Post-cracking occurs when no further cracks occur. All the load is now taken by the fibres until fibre failure or fibre pull-out occurs. Therefore, the Young modulus should equal the one of the fibres in this stage. The offset in the stress – strain curve between the composite and the reinforcement is called the tension stiffening effect. [Butler 2010]

Aveston, Cooper and Kelly (1971) developed a theoretical model for these phenomena, hereby referred to as the ACK theory. This model is described briefly below and displayed in Figure 8.

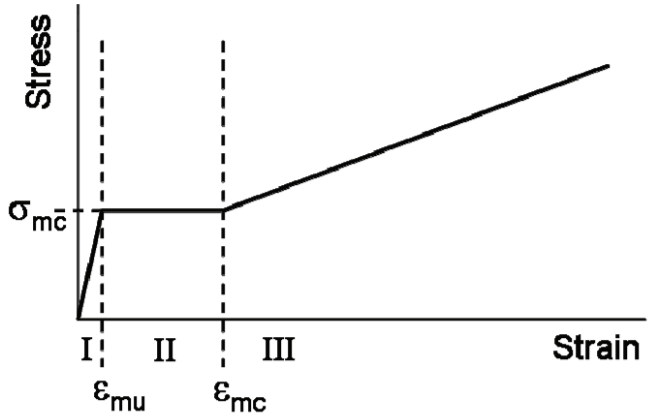

Figure 8 Theoretical modelling: ACK theory [Tysmans 2010]

During **stage I – Pre-cracking**, the composite is uncracked and both the matrix and the fibres contribute to the global stiffness following the "law of mixtures", assuming a perfect bond. The latter results in an equal strain in the fibres and the matrix, developing the following formula

$$E_{c1} = E_f V_f + E_m V_m \tag{1}$$

Where E_f and E_m Young modulus of the fibres and matrix respectively
V_f and V_m volume fraction of the fibres and matrix respectively

At the start of **stage II – Multiple cracking**, the matrix's tensile failure stress σ_{mu} is reached and cracks start to initiate and propagate along the composite. According to the ACK-theory, strain in the composite equals strain in the matrix

$$\sigma_{mc} = \frac{E_{c1}\sigma_{mu}}{E_m} \tag{2}$$

As mentioned in 2.2.1 Fibres and textiles as reinforcement, the composite behaviour will only occur if the fibre volume fraction is bigger than a critical value. (σ_{mu} and σ_{fu} are the matrix tensile failure and fibre tensile failure respectively)

$$V_f > \frac{\sigma_{mu}}{-\frac{E_f}{E_m}\sigma_{mu} + \sigma_{mu} + \sigma_{fu}} \tag{3}$$

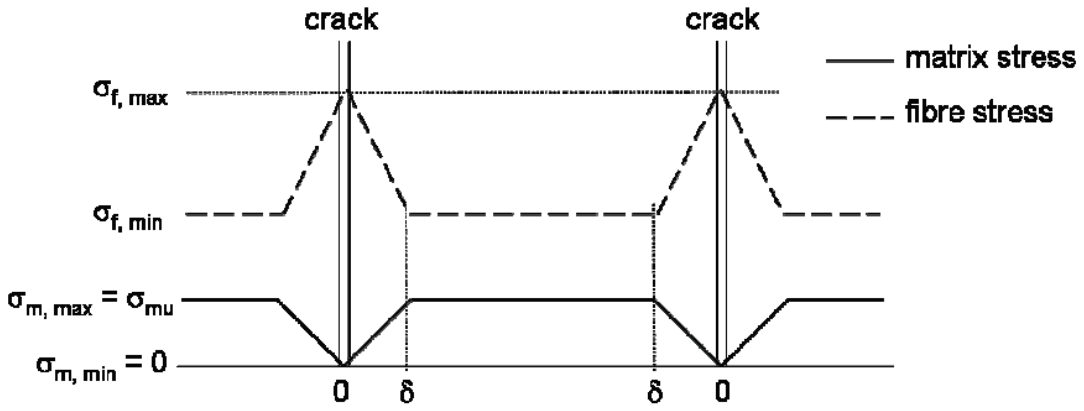

Figure 9 Stress distribution around a crack [Tysmans 2010]

Figure 9 displays the normal stress distribution in the matrix and fibre along a crack in the material. While the stress in the fibre increases towards a crack, the stress in the matrix decreases towards zero in the crack and will be equal to the matrix tensile strength (σ_{mu}) at the debonding length δ . The latter is defined as the transition stage over which the stress in the matrix is lower than σ_{mu}, meaning that no new cracks will occur within this stage. This implies that if the distance between two cracks is bigger than 2δ, the matrix will reach his maximum tensile stress and new cracks will occur. Cuypers et al. (2008) uses a stochastic model which is equivalent to the geometrical car parking problem, introducing a formula for the end of the multiple cracking stage

$$\langle \varepsilon_{mc} \rangle = (1 + 0.666\alpha)\frac{\sigma_{mu}}{E_m} \tag{4}$$

$$\alpha = \frac{E_m V_m}{E_f V_f} \tag{5}$$

Stage III – Post-cracking is then represented by the relative stiffness of the fibres

$$E_{c3} = E_f V_f \tag{6}$$

2.4 Durability

To guarantee the main features of TRC such as its high tensile strength and ductile behaviour as well as its high ultimate strain (strain capacity) which have many possible applications in both new structures and renovation applications, no significant degradation of mechanical and esthetical performance should occur with increasing age. These eventual negative effects affecting the latter must be known in advance in order to be considered in the design of structural members made of TRC, such as sandwich panels for renovation purposes. Within this section, an overview of the degradation processes observed after accelerated ageing of TRC is assessed on microscale on one hand, while on the other hand the effect of durability cycles on the mechanical behaviour of TRC is established.

2.4.1 Degradation processes

Accelerated aging of TRC made of AR glass fibres and a cement-based matrix is mainly governed by the same damage mechanisms as glass-fibre-reinforced concrete. [Butler 2010] These changes in mechanical performance result from deterioration of the armoring fibres, alterations in the matrix itself and/or changes in the bond between matrix and fibres. Butler et al. (2010) differentiates four damage mechanisms, as described as follows.

(1) Corrosion of the AR-glass fibres due to alkaline attacks of OH^- ions in the pore solution

Majumdar et al. (1977) observed that the mechanical performance of glass fibres is influenced by the alkalinity and temperature of the environment. Increasing of the latter decreases the glass fibres strength and stiffness significantly. The alkalinity of a concrete mixture results from Portland cement reacting with water during the hydration phase. Healthy concrete has a high pH varying between 12 and 13,5, which classifies concrete as highly alkaline. [AC Tech 1996] For these reasons, fabrics made of glass fibres with a high resistance to alkalis are used for TRC applications. To improve the resistance of glass in highly alkaline environments, addition of 16-20% by mass zirconium dioxide is provided, generating a protective layer immediately after the start of an alkaline attack on the glass network and slowing down the diffusion of OH- ions into the bulk glass. This reduces further glass network breakdown in high alkaline pore solutions significantly and is defined as AR-glass.

Complete preclusion of the glass degradations is impossible because of increasing glass deterioration with increasing pH value of the pore solution and with temperature, as proved by Majumdar et al. (1977)

A solution for delaying this corrosion process is found in the application of organic polymer sizes to the filament surfaces immediately after spinning the glass filament. Gao et al. (2004) noticed that the thickness of the polymer size reduces rapidly when in contact with pore solution or even water, but stops after short time and one third of the initial size of the layer is remained, providing extra protection to the glass fibres.

(2) Static fatigue of the AR-glass filaments in highly alkaline surroundings under critical growth of surface flaws

Spinning process of the glass filament or chemical attacks can induce tiny surface defects, reducing the strength of the fibres significantly. These latter experience local stress concentrations when the filament is strained. In case of high constant stresses (e.g. uniaxial tension) and presence of water, the growth of such defects is fostered, especially in an alkaline environment and at higher temperatures. According to Zinck et al. (2001), reduction and delaying of these stress concentrations can be governed by application of polymer size at the filament surface.

(3) Enhanced bond between fibres and matrix by continuous hydration and precipitation of hydration products in the interface matrix-fibre

Increasing bond stress is governed by improving the contact surface between fibres and matrix. During the hydration process of the binder, the interface stage becomes denser, increasing the ability to take up shear stress at matrix cracks. Another ability is the local bending of the filaments which are oriented non-orthogonal to the matrix cracks. During the hydration process, the flexibility of the fibres is reduced due to precipitation of hydration products and an enhanced bond between matrix and fibres. Portlandite $[\mathrm{Ca(OH)_2}]$ is the predominant precipitation product and growth of the latter can cause notching at the fibre surface, causing brittle mechanical behaviour instead of ductile behaviour of the composite. Also, these crystals will cover the filaments and will tend towards spalling when straining, inducing discontinuities which will result in stress concentrations.

According to several investigations of Purnell et al. (2001) and Orlowsky et al. (2008), the delayed failure of AR glass filaments is supposed to dominate the other mechanisms. On the opposite, the Institute of Construction Materials at TU Dresden [Hempel 2005] indicates that the phase conversion in the fibre matrix interface is much more significant regarding the changes in mechanical properties of the composites in time and thus in respect of TRC durability.

Within this research, Butler et al. (2010) investigated above statements on TRC with a reinforcement ratio of 1,35% parallel to the direction of uniaxial loading. Three fine-grained matrix concrete mixtures are used, each differentiated from the others with respect to alkalinity, hydration kinetics and granulometry of the binder. The binder of matrix M3 consist entirely of Portland cement, resulting in a high alkalinity since no buffering of pozzolanic additives is governed. On the opposite, the binder of matrix M1 consists of a blast furnace cement in rich in ground, granulated blast furnace slag, governing a strong buffer to alkalinity by addition of fly ash and micro silica. Composition of M2 is between both M1 and M3. Accelerated aging was governed by placing the specimen in a fog room (40°C, 99% RH) for 28, 56, 90, 180 and 360 days. Matrix M1 showed a pH reduction from 12.4 to 1.8, while matrix M3, which contained no pozzolana, exhibited a nearly constant pH level of approximately 12.7.

Table 2 Compositions of the fine-grained concretes, masses in kg/m³ concrete [Butler 2010]

Matrix composition	M1 (kg/m³)	M2 (kg/m³)	M3 (kg/m³)
CEM I 32.5 R	-	557	861
CEM III/B 32.5 NW-HS-NA	550	-	-
Fly ash	248	251	-
Microsilica suspension 50 mass% powder, 50 mass% water	55	56	-
Sand 0-1 mm	1101	1114	1148
Water	248	251	287

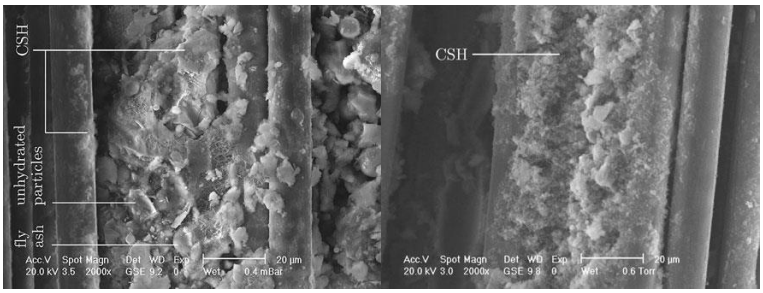

Figure 10 ESEM image of AR glass filaments in matrix M1 (left) and M3 (right) after 28 days of standard storage [Butler 2010]

The significantly higher Portland cement clinker content of matrix M3 leads to a faster hydration process and with it to a homogeneous structure of CSH (calcium silicate hydrate) phases, even after 28 days of standard storage (Figure 10), governing a well-developed bond between fibres and filaments. CSH is the main product of hydration of Portland cement and is primarily responsible for the strength in cement based materials. Therefore, higher stresses are observed in the stress strain curves for M3 instead of M1, where slower hydration and therefore less CSH formation is experienced. (Figure 11)

Accelerated aging on TRC specimens made of M1 and M2 show an increase in the overall stress levels. This is contributed to an intensive participation of latent hydraulic and pozzolanic binder constituents in the hydration process under favorable conditions of the fog room.

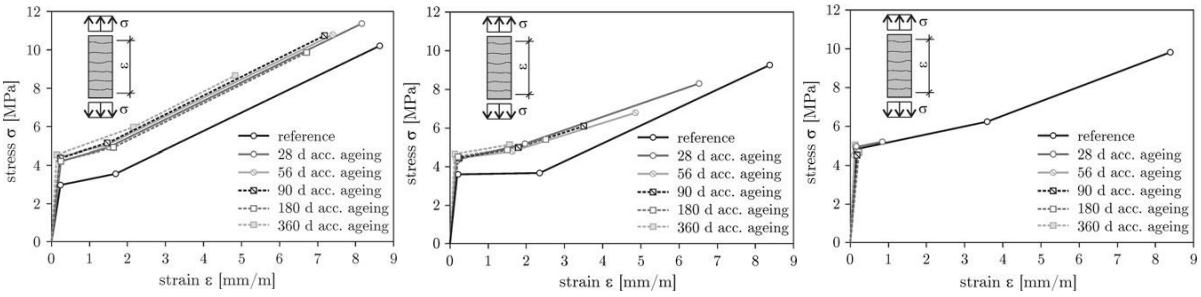

Figure 11 Stress-strain curves for TRC made with matrix M1, M2, M3 (left to right); accelerated aging at 40°C/99% RH, reference storage at 20°C/65% RH [Butler 2010]

However, accelerated aging decreases drastically the mechanical performance of TRC composed of M3 matrix. Essential cause of this observation is found in the high pH level of the pore solution, which is perpetuated by the continuous new formation of Portlandite due to continuous Portland cement hydration in the moist environment of the fog chamber (Figure 12). These Portlandite crystals between matrix and filaments are easy to split and provide a bad load bearing bond. Additional effects of these crystals can be found in notched fibre surfaces as well as growth of surface defects. All these effects can cause failure at relative low loads, resulting in a quasi-brittle mechanical behaviour of the composite.

In the case of composites made of relatively alkali-poor matrices (M1 and M2), the hydration of CEM III cement causes a lower production of $Ca(OH)_2$. Additionally, the portlandite is continuously consumed by the pozzolans in the formation of CSH phases. Delicate hydration products (CSH phases) are formed on the filament surfaces, resulting in a favorable bond, governing the ductile behaviour of the composite. The latter is caused by the ability of partial debonding and slip of a filament near a crack. This homogeneous CSH structure (Figure 12) provides load bearing still after 360 days of aging.

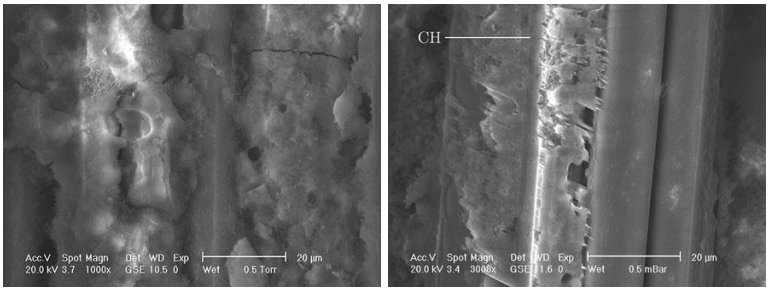

Figure 12 ESEM image of AR glass filaments in matrix M1 after 360 days of accelerated aging (left) and in matrix M3 after 28 days of accelerated aging (right) [Butler 2010]

(4) Physical effects such as freeze-thaw damage and abrasion

According to Neville [Neville 1996], freezing – thawing damage finds its origin in the dilating pressure due to the freezing of the water in the capillary pores. When this pressure exceeds the tensile force of the matrix, damage will occur. The dilating pressure is related to the following factors:

- the pore system of the hardened cement
- the degree of saturation
- permeability
- Water to cement ratio

Few investigations on freezing-thawing behavior can be found for Textile Reinforced Cementitious Composites. Although, freezing-thawing can affect the cement paste and therefore the bond between fabric and mortar, which is the main mechanism governing the tensile behaviour of TRC.

2.4.2 Effect of durability loading cycles on the mechanical behaviour TRC

Colombo et al. (2015) investigated the residual tensile behaviour of textile reinforced concrete samples in uncracked and cracked configuration when subjected to freezing-thawing cycles. The matrix consisted of a high strength mortar and a perfect bond is assumed with the AR glass fabric. The specimens tested in the experiment are characterized by a reinforcement ratio of 3.2%. Manufacturing of the specimens was done using a hand lay-up.

Uncracked and pre-cracked specimen were subjected to 25, 50, 75, 100, 150 and 500 freezing-thawing cycles according to Procedure A of the ASTM C 666 /C666 M -03 (1997) standards.

Figure 13 [Colombo 2015] shows the average results of the stress-strain curves after different (imposed) number of freezing – thawing cycles. It can be seen that freeze-thaw cycles have a negative effect on the ultimate strength of the Textile Reinforced Cementitious composite (Figure 14a), resulting in a decreasing Efficiency Factor (Figure 14d) of the material. This may be due to a degradation of the bond strength of the matrix.

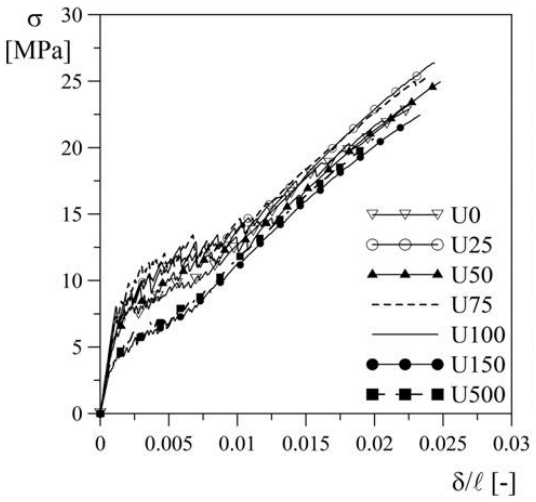

Figure 13 Average stress-strain curves after different number of freezing - thawing cycles [Colombo 2015]

Looking at the first cracking strength, a clear decrease is observed for a higher amount of cycles. The latter is clearly visible after 100 cycles (Figure 14c), which states a matrix degradation. A reduction up to 40% of the initial first cracking strength is experienced with increasing cycles.

Figure 14b shows that an increasing number of cycles goes together with a decrease in total ultimate strain of the specimen.

The global mechanical behaviour (Figure 13) seems to be similar to the average reference (U_0) specimen, which may be related to an autogenous healing phenomenon and late hydration.

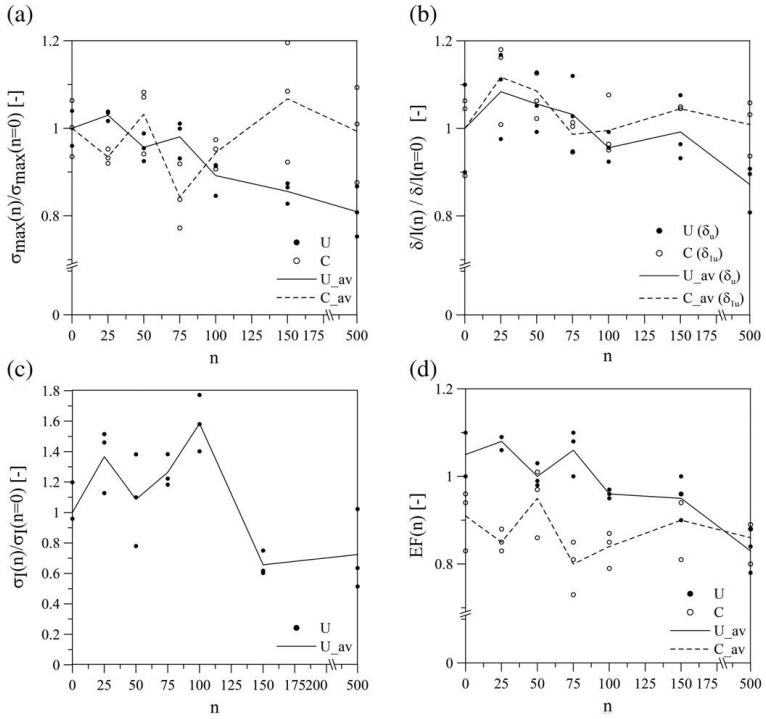

Figure 14 Test results: (a) peak strength vs. number of cycles, (b) peak normalized displacement vs. number of cycles, (c) first cracking strength vs. number of cycles and ((d) EF vs. number of cycles [Colombo 2015]

An interesting observation is shown in Figure 15a, where H crack propagation can be observed between two neighbouring cracks. This may result in a longitudinal crack propagation, as illustrated in Figure 15b. The latter may cause spalling of the mortar cover, exposing the fabric. The phenomena of longitudinal crack propagation occurs close to the maximum tensile strength of the composite, therefore, no delamination will occur in Serviceability Limit State.

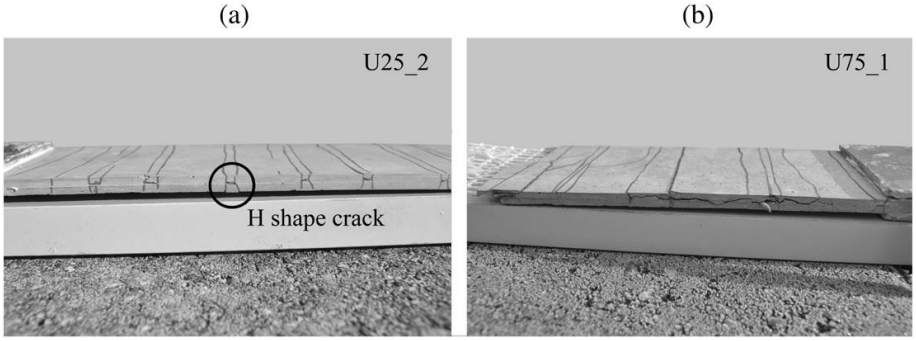

Figure 15 Specimens after tensile test: H crack propagation (a) and longitudinal crack propagation (b) [Colombo 2015]

Remy O. (2012) [Remy 2012] subjected GFR.IPC specimens to a series of climatic tests according to the EN 12467 (2004) standard. During these climatic tests, evaluation of the stiffness was determined by non-destructive testing, based on flexural resonance frequencies using the resonalyser test method. Within his research, both unidirectional and 2D randomly reinforced specimens were subjected to 100 freeze-thaw cycles, with a fibre-volume fraction of 23% and 26% respectively. This is an important difference with the specimens investigated by Colombo et al. (2015). No deterioration of the stiffness was observed. At the end of 100 cycles, the residual strength was measured and compared to the reference specimens and no significant decrease was observed.

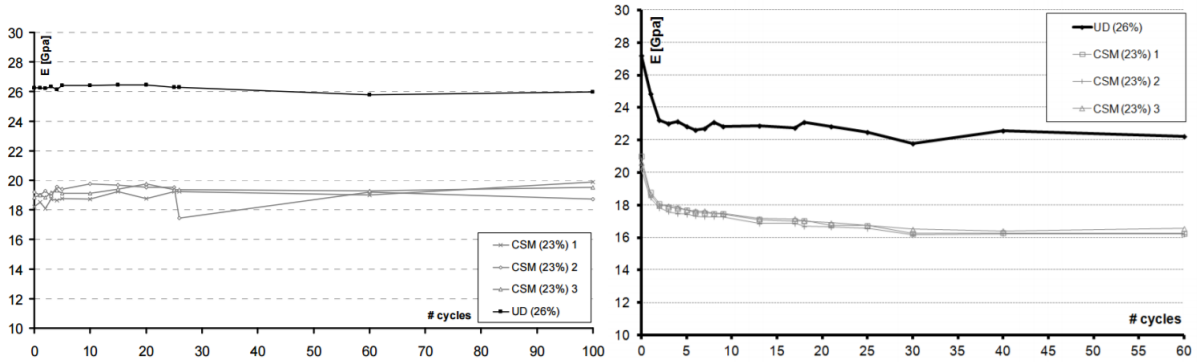

Figure 16 Evolution of the stiffness during freeze-thaw cycling (left) and wetting-drying (right) using a non-destructive technique [Remy 2012]

The same procedure was followed to evaluate the stiffness during 60 wetting-drying cycles, following the EN 12467 (2004) standards. A continuous decrease of the stiffness is noticeable and displayed in Figure 16. The drop in stiffness was majorly observed in the 2 initial cycles. After 30 cycles, the loss in stiffness was about 20% and further cycling had no further significant effect on the stiffness.

A possible declaration of this phenomena can be contributed to shrinkage during the first few heating cycles. This shrinkage is restrained due to the presence of fibrous materials, causing microcracks.

The typical geometry of these microcracks can be seen with the eye and is studied by Hwang et al. (1984). An optical micrograph of this pattern is displayed in Figure 17.

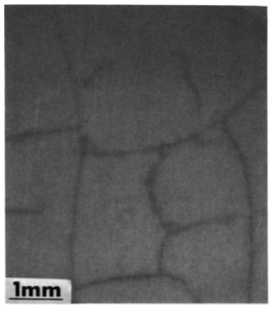

Figure 17 Cracks induced due to Shrinkage of Portland Cement Paste [Hwang 1984]

However, few investigations on the influence of environmental loading on mechanical behavior can be found for Textile Reinforced Cementitious Composites. This master thesis presents the results of experimental research aimed at understanding the deterioration of the tensile behavior of TRC subjected to freeze-thaw cycles, heat-rain cycles and a combination of both.

3. Materials and Methods

To investigate the residual tensile behavior of Textile Reinforced Cementitious composites subjected to environmental loading, an extensive experimental program was carried out. The test specimens are made using a hand lay-up technique by reinforcing a mortar matrix with two layers of AR glass fabric. Note that the selection of these materials is imposed by the CRH group for commercial purposes. This section covers the involved materials in the casting procedure are briefly described, as well as the test set-up and the adapted test procedure.

3.1 Composite preparation

The **matrix** of the investigated TRC is «VWS POLYSTYREEN KLEEFSTOF TM 282» characterized by a water to binder ratio equal to 0.125. The product information [Tillman 2016] states that processing 50 kg of the cement results in 25 dm³ of matrix. The design for 1 m³ of the mix is shown in Table 3.

Table 3 Matrix design per m³, water to cement ratio 0.125 [Tillman 2016]

Component	Content
Tillman VWS Polystyrene Kleefstof TM 282	2000 kg/m³
Water	125 L/m³

The mechanical properties of the matrix were quantified via bending and compressive tests on prismatic specimens of the matrix following the European Standards (EN 196-1:2016 Methods of testing cement – Part 1: Determination of strength). Table 4 displays the average results of the density (ρ), the flexural strength ($f_{ct,f}$), tensile strength (f_{ctm}) and the compressive strength (f_{cc}) of the matrix.

Table 4 Mechanical properties cementitious matrix

	ρ (kg/m^3)	$f_{ct,f}$ (MPa)	f_{ctm} (MPa)	f_{cc} (MPa)
Average	1753,82	4,96	2,18	29,60
STD	25,05	0,56	0,25	4,49

The tensile strength was deduced from the bending tensile strength via the formula proposed in the fib Model code 2010 [Walraven 2010]:

$$f_{ctm} = A_{fl} . f_{ct,f} \quad (7)$$

Where $A_{fl} = 0{,}44$ is chosen according to Walraven et al. (2010) and an experimental investigation in the PhD thesis of Colombo (2015).

The **fabrics** used in the composites consist of AR-glass rovings, which are finished to a squared mesh structure. The product name is Isoltex KNAUFF. For more details on the AR-glass fabric, a reference is done to section 2.2.1 and the product information sheet [Knauff 2016]. The geometry and mechanical properties of the fabric are displayed in Figure 18.

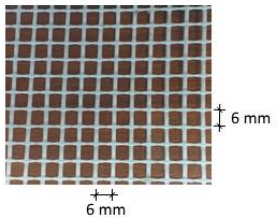

Roving distance	6**mm** x 6**mm**
Weight	220 g/m^2
Tensile force	2500 N/50mm

Figure 18 Geometry of the AR glass fabric [Knauff 2016]

The composite specimens used in the experimental investigation are rectangular and have a nominal length (l) of 475 mm, a nominal width (w) of 50 mm and have a thickness (t) of 10 mm. These specimens were cut out of bigger plates (500 mm by 500 mm by 10 mm) produced using a hand lay-up technique and are characterized by a nominal reinforcement ratio of 1,69 %, which corresponds to two 2D-fibre nets in a plate of 10mm thickness. (Figure 19)

$$V_f = \frac{nA_w}{\rho_f \, d_{sample}} = \frac{2 \text{ x } 220 \frac{g}{m^2}}{2600 \frac{kg}{m^3} \text{ x } 10 \text{ mm}} = 1{,}69 \text{ \%} \tag{8}$$

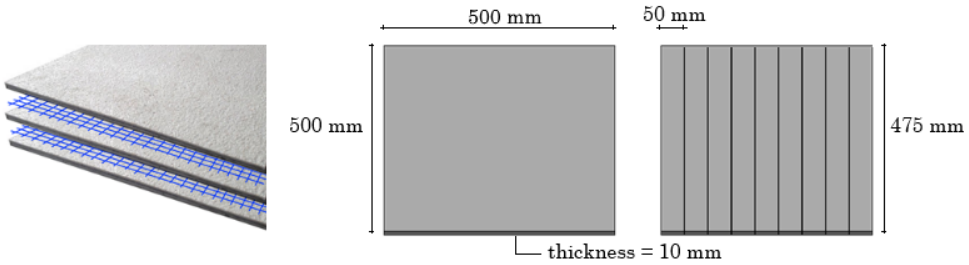

Figure 19 TRC composition using a hand lay-up technique and cutting of the specimen out of plates

A first layer of the matrix was spread onto the formwork's bottom plate and smoothened. A reinforcement fibre net was positioned and lightly pressed into the first matrix layer. After spreading out a second layer of matrix onto the latter mixture, a second reinforcement fibre net was positioned and lightly pressed into the matrix. A third and last cover of matrix was added and smoothened to fill the formwork. The date of production, demolding and cutting of every plate can be found in Annex A. The environment of the laboratory had temperatures ranging between 17 °C and 25 °C during production. The relative humidity ranged between 45 % and 60 %. The used mortar was very adhesive and therefore difficult to process, causing unavoidable voids in the specimen. Additionally, human errors on the smoothening of the plates caused a loss of planarity in the specimen's surface. During the production process, no use was made of rails keeping the reinforcing fibre nets in place. This will cause an unknown eccentricity of the fabric inside the specimen, precluding the perfect symmetry of the specimen itself. After curing the plates in air (environmental conditions of the laboratory) for more than 28 days, cutting of each plate into 9 specimens was employed. (Figure 19)

3.2 Environmental Loading

3.2.1 Freeze-Thaw cycles

ASTM Standard C 666/C 666M -03 (1997) describes the (American) standard test method for resistance of concrete to rapid freezing and thawing. The nominal freeze-thaw cycle described by this test method shall consist of alternately lowering the temperature of the specimens from $(4 \pm 2)°C$ to $(-18 \pm 2)°C$ in not less than 2 nor more than 5 hours. (Figure 20)

NBN EN 12467 (2012) describes the (European) standard test method for resistance of Flat fibre-cement sheets to freeze-thaw cycles. Within this standard, the nominal freeze-thaw cycle is described by alternately lowering the temperature of the specimens from $(-20 \pm 4)°C$ to $(20 \pm 4)°C$ in not less than 2 nor more than 4 hours. (Figure 20)

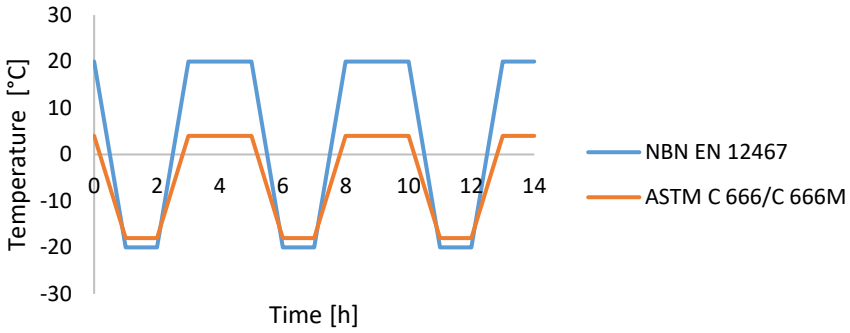

Figure 20 Freeze-thaw cycles according to ASTM and EN standards

Since no such standards exist (so far) for the resistance of TRC to freeze-thaw cycles, the author has decided to apply the NBN EN 12467 (2012) European Standards because of its more severe approach and the equivalence with TRC.

Following this standard, sheets intended for applications where they may be subjected to heat, moisture and severe frost are classified as Category A. Within this category, several types of tests are relevant such as the Freeze-Thaw test, which is performed as follows and visualized in Figure 21.

- Cool (freeze) in the chamber which shall reach a temperature of (-20 $\pm$ 4) °C within 1h and hold this temperature for a further 1h.
- Heat (thaw) in the water bath which shall reach a temperature of (20 $\pm$ 4) °C within 1h and hold this temperature for a further 1h.

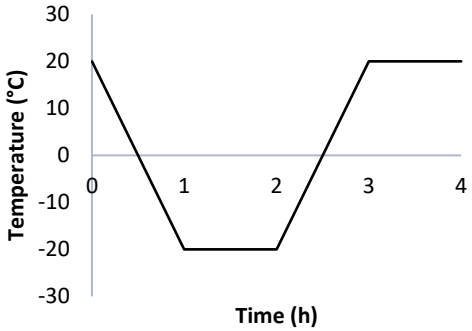

Figure 21 Evolution of temperature over one freeze-thaw cycle

According to the standards, 100 freeze – thaw cycles should be carried out for Category A. The freezer unit used in this procedure is a VÖTSCH® VC 4018. Since the freezing-thawing cycles could not be performed automatically with the available equipment and a manual approach was not practical, an approximated approach was carried out and is explained below.

The specimens are placed in a water bath for 48h before starting the freezing-thawing cycles, to fully saturate the specimen. Afterwards, every specimen is placed in a plastic bag and taped in such a manner that no external air can enter the bag.

By doing so, the amount of water in the specimen is captured inside the plastic bag during the freezing and thawing processes and will be used to damage the specimen. After 12 and 37 cycles, the specimens are again placed in a water bath for 48 hours to ensure the full saturation. Within the climate chamber, free air circulation was foreseen during the whole process.

A total overview of the planning for the freeze-thaw cycles can be found in Annex A.

3.2.2 Heat-Rain cycles

Following the standard *EN 12467 (2012) Fibre-cement flat sheets – Product specification and test methods,* specimens assigned to Category A should carry out up to 50 heat – rain cycles. The performance of this test is done by putting the samples into a frame, as described in the standards. Afterwards, the assembled frame is subjected to

- A water spray with over a period of 2h 50min $\pm$ 5min
- A pause of 10min $\pm$ 1min
- A radiant heat of (60$\pm$5) °C that shall be reached after 15min and will last over a period of 2h 50min $\pm$ 5min
- A pause of 10min $\pm$ 1min

Because of the very specific conditions on the equipment and procedure, an approximating test procedure is followed. Interpretation of the Heat-Rain procedure described in the European Standards tells us that the water spray is applied to cool down the sample in a continuous way. The provided time assures that the whole body is cooled to a uniform temperature.

Since the standards cover thermal treatment of plates instead of beams, a shorter procedure is applied in the thesis.

- Cool (rain) in the water bath which shall reach a temperature of (20 $\pm$ 4) °C within 30 minutes.
- Pause for 10min $\pm$ 1min
- Heat in the heating device with a radiant heat that reaches (60 $\pm$ 5) °C after 15 minutes and hold on for another 45 minutes.
- Pause for 10min $\pm$ 1min

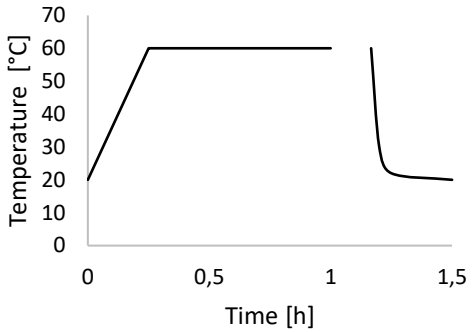

Figure 22 Evolution of temperature over one heat-rain cycle

The heating device used during these cycles is again a VÖTSCH® VC 4018. A total overview of the planning for the freeze-thaw cycles can be found in Annex A.

3.2.3 Experimental program

This work covers the production of 9 TRC plates with nominal dimensions of 500 mm in length, 500 mm in width and 10 mm in thickness, characterized by a nominal fibre-volume fraction of 1,69%. These plates are enumerated with the letters A to I. In theory, all the plates should have an identical composition. Although, this is not the case due to the hand lay-up technique, inducing plate-dependent human errors. Therefore, investigation on the influence of environmental loading is done on the level of the plates.

Every plate is cut in 9 samples. To obtain a statistically representative amount of results, these 9 samples were divided in 3x3 samples.

For plates A to F, 3 samples were taken as a reference, 3 samples were subjected to 100 freezing-thawing cycles and the remaining 3 samples were subjected to 100 freezing-thawing and 50 heat-rain cycles respectively. After durability loading, the samples are exposed to a uniaxial tensile test to characterize the mechanical performance. A schematic overview of this procedure is displayed in Figure 23.

With eye on the maximum reduction of human errors, a similar trend of mechanical behaviour is expected over these 6 plates. These 6 trends will be generalized by means of an overall conclusion.

For plates G, H and I, 3 samples were taken as a reference, while 3 other samples were subjected to 50 heat-rain cycles before subjection to mechanical loading. A schematic overview of this procedure is displayed in Figure 24.

Again, with eye on the maximum reduction of human errors, a similar trend of mechanical behaviour is expected over these 3 plates. These 3 trends will be generalized by means of an overall conclusion of the influence of 50 heat-rain cycles only.

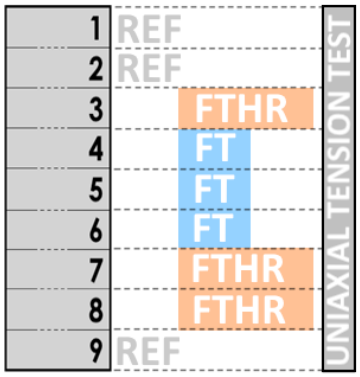

Figure 23 Methodology for plate A, B, C, D, E and F

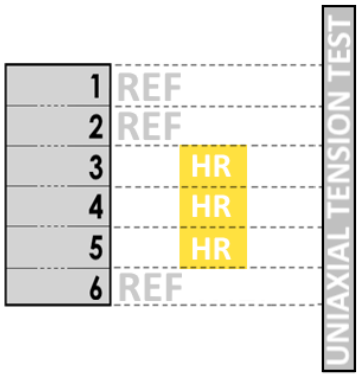

Figure 24 Methodology for plate G, H, I

For the ease of notation, virgin samples will be referred to as **REF loading case**, the 100 freezing-thawing cycles will be referred to as the **FT loading case** and the combination of 100 freezing-thawing and 50 heat-rain cycles will be referred to as the **FTHR loading case**. For plates G to I, the influence of 50 heat-rain cycles is investigated separately and will be referred to as the **HR loading case**.

This will lead to the following convention regarding reference to a specific sample:

(x)(i)_(type)

Where:	(x)	refers to the plate number (A, B, C, D, E, F, G, H or I)
	(i)	refers to the number of the specimen (1, 2 or 3)
	(type)	refers to the type of thermal treatment as explained above (REF, FT, FTHR or HR)

For example:

A1_FTHR

refers to a specimen from series A which is subjected to the FTHR loading case, being 100 freezing-thawing cycles and 50 heat-rain cycles respectively.

Table 5 *d*isplays the total number of specimens subjected to the different loading cases.

Table 5 Total number of specimens investigated during the thesis

	REF	FT	FTHR	HR
Number of specimens	27	18	18	9

3.3 Non-destructive testing methods

3.3.1 Resonalyser test setup

When subjecting the tested specimens to durability cycles, resonalyser tests have been performed on a frequent basis to evaluate the stiffness of the samples during the environmental loading. The resonalyser method [De Baere 2007] is a method used to identify the engineering constants of orthotropic materials in a non-destructive way by means of the resonance frequencies of freely suspended rectangular plates. For the investigation of this master thesis, interest lays in the first resonance frequency of a test beam with free boundary conditions (Figure 25) associated to a bending mode deformation due to excitation.

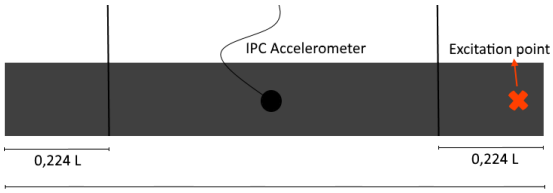

Figure 25 Resonalyser test setup

From this first resonance, determination of the Young's modulus of the material in longitudinal direction is possible according to the following equation [De Baere 2007]

$$E = 0{,}946\frac{\rho\, f^2 l^4}{t^2} \tag{9}$$

With E the Young's modulus of the beam $[MPa]$, ρ the specific mass of the investigated material $[kg/m^3]$, f the resonance frequency of the beam (measured) $[Hz]$, l the length of the beam $[m]$ and t the thickness of the beam $[m]$.

The exponential relation between Young's modulus and first resonance frequently and specimen dimensions will make it very sensitive for variations.

3.3.2 Ultrasonic Pulse Velocity

In addition to the resonalyser test method, Ultrasonic Pulse Velocity (UPV) is used to predict the material stiffness in a non-destructive way. This technique is used to determine a degree for the quality of a specimen, since it is a function of the bulk modulus, shear modulus and density of the material. Thus, concrete porosity and cracking influence the UPV because they directly affect the latter properties. Saint-Pierre 2016] The velocity of an ultrasonic pulse traveling in a solid material can be calculated using the following relation, as described in the NCHRP report 465 (2002) [Witczak 2002]

$$v = \sqrt{\frac{E\,(1-\mu)}{\rho\,(1+\mu)(1-2\mu)}} \tag{10}$$

A simplified setup is displayed in Figure 26. For a more detail overview for the needed equipment, the author refers to Saint-Pierre et al. (2016) and Witczak et al. (2002).

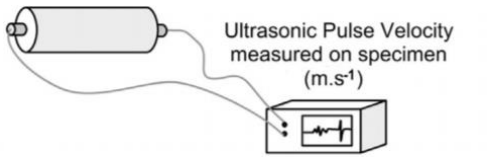

Figure 26 Ultrasonic Pulse Velocity Equipment [Saint-Pierre 2016]

This technique will be used to evaluate the stiffness after environmental loading. Results of this technique will be compared to the results of the resonalyser test.

3.4 Mechanical Loading

3.4.1 Uniaxial tension test procedure

After environmental loading of the samples, a uniaxial tensile test procedure is carried out following the RILEM TC 232-TDT recommendations. [Brameshuber 2016] To characterize the mechanical behaviour using an INSTRON® 5900 electromechanical press. Clamping of the samples was applied at top and bottom of the specimen using steel plates. Between the steel plates and the specimen, rubber is placed for a better distribution of the clamping pressure and thus minimize the damage associated to local crushing of the specimen (Figure 27). Load transfer is based on the coulomb friction. The tests were displacement-controlled by a rate of 1mm/min. Note that a small deviation of the RILEM TC 232-TDT recommendations (2016) is applied by using a steel pin to keep the specimen in position, requiring a hole at top and bottom of the specimen, which may cause additional stress concentrations.

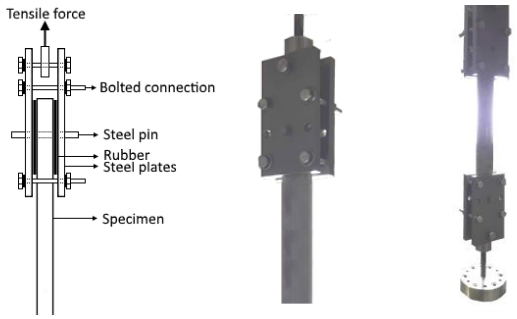

Figure 27 Uniaxial test equipment

3.4.2 Digital Image Correlation

During the uniaxial tension tests, Digital Image Correlation (DIC) is used to have a more accurate measurement of the strain and crack pattern. DIC is a non-contact optical technique for strain and displacement measurements. It is an accurate and cost-effective technique that has led to a wide use of applications [McCormick 2010]. Figure 28 shows the equipment needed for the DIC. [Harris 2017]

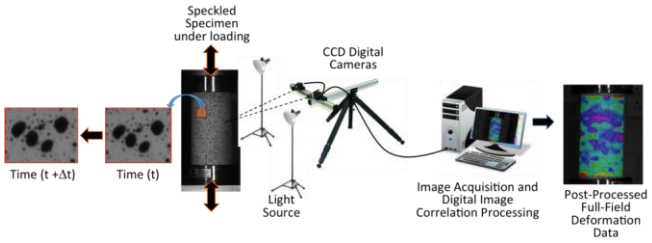

Figure 28 Digital Image Correlation: equipment [Harris 2017]

By use of the CCD Digital Cameras, the system tracks down blocks of pixels and compares digital photographs at different stages of deformations. This will result in a 2D and/or 3D deformation or strain field. [Harris 2017] [Satoru] To increase the effectiveness of the DIC, pixel blocks need to unique , randomly orientated and have a range of contrast and intensity levels. No special treatment of the tested surface needs to be done. Practical application of the pixels to the specimen's surface was done using special sieves. Figure 29 shows a typical speckle pattern used in this thesis.

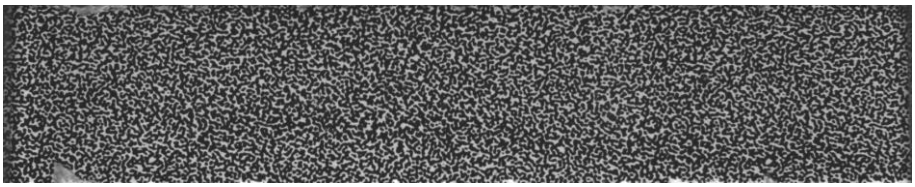

Figure 29 Typical speckle pattern

3.4.3 Theoretical Mechanical Behaviour

Theoretical modelling of the stress-strain curve of the Textile Reinforced Cementitious composite used in this master thesis is done following the ACK theory [Aveston 1971]. The TRC properties defining this stress-strain curve are based upon the material properties of the matrix and the fabrics and are calculated using equations (1) to (6) in section *2.3 Mechanical Behaviour.*

The obtained stress-strain curve displays the expected behaviour of a rectangular TRC specimen with nominal dimensions and a fibre-volume fraction of 1,69%. Due to the geometry of the fabrics (squared grid), only 50% of the fibres will take up the uniaxial tensile loads in the tensile test. This ''effective fibre-volume fraction'' is defined as V_f^* and equals 0,845% for the investigated specimens.

The composite behaviour as described by Aveston, Cooper and Kelly (1971) will only occur when a critical fibre-volume fraction is exceeded. This value can be calculated using equation (3) in section *2.3 Mechanical Behaviour.* The critical fibre-volume fraction to assure composite behaviour should exceed at least 0,22%.

The expected behaviour of the TRC specimens used in this research is depicted in Figure 30 and will be used to compare the effective TRC behaviour of the reference (virgin) specimens, defining the deviations on the theoretical model.

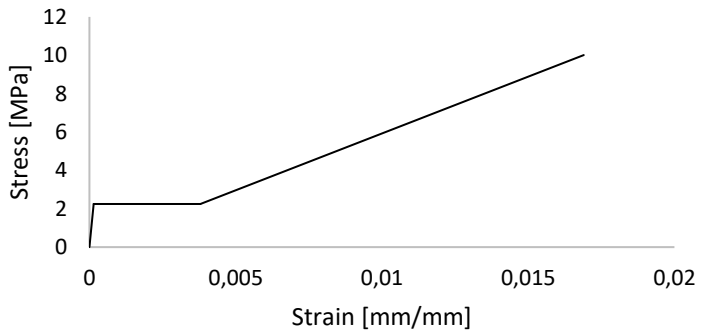

Figure 30 Expected stress-strain curve for all the specimens in this master thesis (V_f of 1,69%)

Table 6 Main properties of the AR glass fabric, Cementitious matrix and the TRC composite

AR glass fibre		
E_f	70	GPa
σ_{fu}	1	GPa
V_f	1,690	%
V_f^*	0,845	%
Cementitious matrix		
E_m	15	GPa
V_m	99,155	%
σ_{mu}	2,18	MPa

Textile Reinforced Cementitious Composite		
E_{c1}	15,47	GPa
σ_{mc}	2,25	MPa
ε_{mu}	1,45 E-04	-
ε_{mc}	3,79 E-03	-
E_{c3}	0,592	GPa
σ_{cu}	10,0	MPa
ε_{cu}	0,0169	-

4. Results and Discussion

4.1 General properties

Because of a hand lay-up production process of the samples, the average density per plate differs. An overview of the variation in density is given in Figure 31. The average density over all the plates equals $1732 \pm 103\ \mathrm{kg/m^3}$. After the cutting process of the plates into 9 specimens, every specimen is weight again to define the scatter on the plate's density.

Table 7 Density per plate

	A	B	C	D	E	F	G	H	I
AVG (kg/m³)	1707	1873	1807	1604	1807	1845	1656	1682	1606
STD	47	107	67	14	31	34	12	16	20

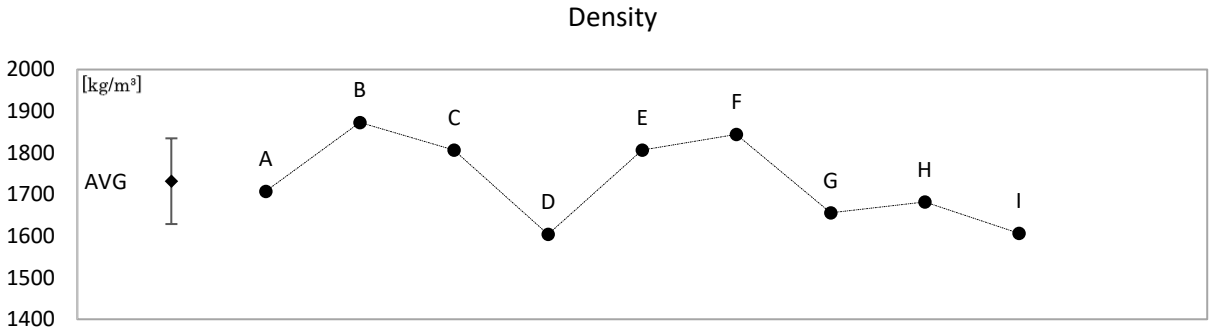

Figure 31 Density per plate

To have an idea on the amount of water taken up by the specimens subjected to freezing-thawing cycles (FT and FTHR), the latter are weighted before and after entering the water bath for 48 hours. Figure 32 displays the percentage of water ($\mathrm{M_{wet}} - \mathrm{M_{dry}}$) taken up after the water bath.

After 12 and 37 cycles, the specimens are again placed in a water bath for 48 hours to ensure the full saturation. To have an idea of the water loss, the specimens are weighted after 12, 37 and 65 freezing-thawing cycles. The specimens have also been weighted right after the water bath. These measurements showed that during the process, a water loss of maximum 17,3% was observed. The latter can find cause in the approximated method of freeze-thaw cycling by taking in and out the wet specimen out of the plastic bags, causing unavoidable water loss. Although, this relatively low loss of water proves that this method is a good approximation of the standards imposed by EN 12467 (2012).

It is a logical sequence that the density of the plates is inversely proportional to the degree of saturation of the specimen. This may indicate that the water is captured in the pores and is not used for hydration processes.

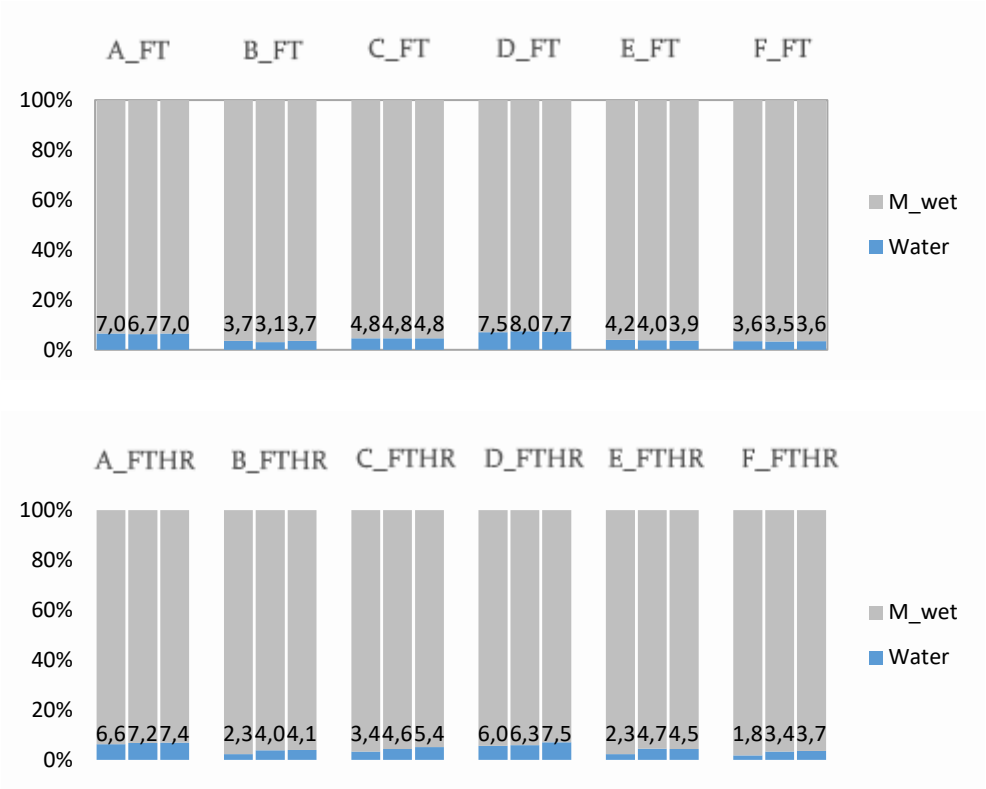

Figure 32 Saturation of the specimen

Saturation of specimens subjected to the HR loading case is not investigated in detail because, after every heat cycle, the samples have been placed in a water bath for 30 minutes, governing a continuous, full saturation of these specimens.

4.2 Environmental Loading

When subjecting the tested TRC specimen to durability cycles, non-destructive test methods have been performed at frequent number of cycles to determine the evolution of the specimens' stiffness. This section covers the observations with the Resonalyser test method and the Ultrasonic Pulse velocity method.

4.2.1 Resonalyser test results

For the specimens subjected to the FT loading case (100 freeze-thaw cycles), resonalyser tests have been performed after 1, 2, 3, 6, 12, 17, 22, 27, 37, 50, 65, 76 and 100 cycles. Out of these results, the stiffness of every specimen could be determined. Note that the results received from resonalyser tests are an overestimation compared to the results received after mechanical loading. This may be addressed to the fact that the resonalyser test displays the material's stiffness under no external load (corresponding to the initial stiffness at 0MPa), while the stiffness obtained after mechanical loading is deduced from the first linear part in the stress-strain curve (corresponding to a stress range instead of an unloaded situation). Although they can be used as a qualitative approximation of the evolution of the stiffness. On Figure 33 it can be noticed that the stiffness of series B_FT, C_FT and E_FT is unaffected after the FT loading case, which was also observed by Remy (2012) [Remy 2012]. For series A_FT and D_FT, having the lowest density, a degradation in the stiffness is observed after a certain amount of cycles. These observations may demonstrate the presence of cracks induced by durability loading.

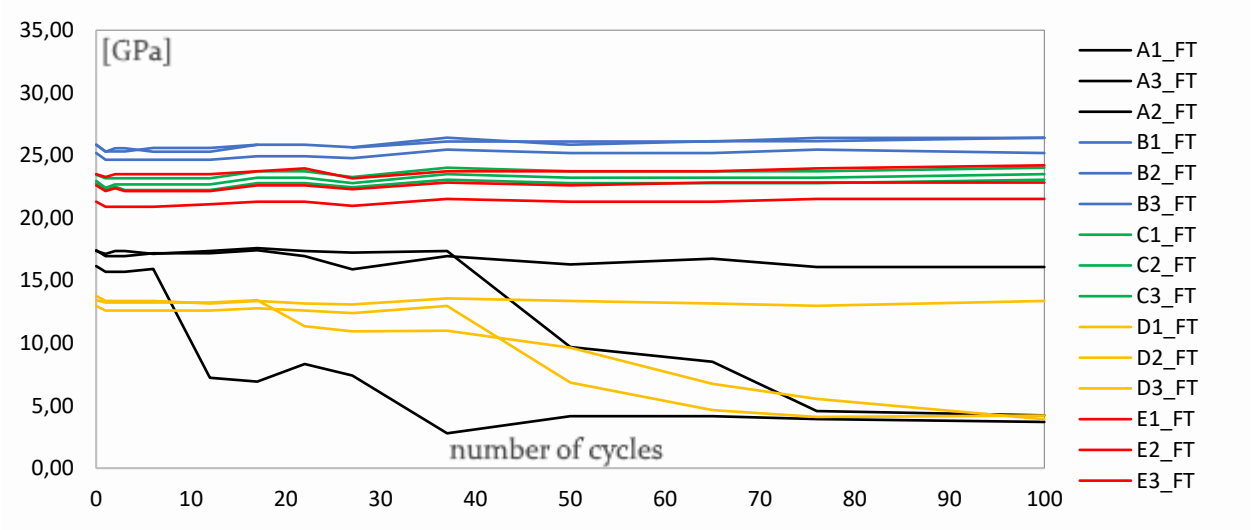

Figure 33 Evolution of the stiffness during FT cycling

Further confirmation on these durability induced cracks is found in the DIC images right before the first load drop was experienced in the stress-strain curve during the mechanical uniaxial tensile loading. As for example, the DIC images of series B_FT (no degradation, Figure 33) and series A_FT (degradation in 2 out of 3 specimens, Figure 33) are shown in Figure 34 and are in accordance with the resonalyser results show in Figure 33. Although, on the DIC images of series A_FT it can clearly be noticed that all the samples are showing durability cracks. For DIC images of all the specimens, the author refers to Annex C.

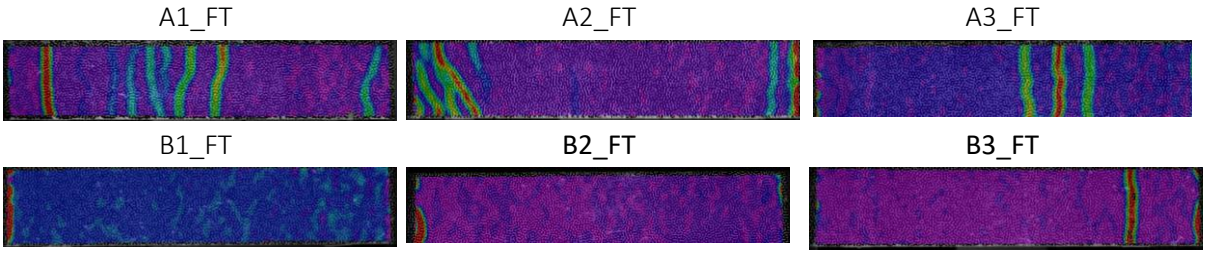

Figure 34 DIC images of durability induced cracks for series B_FT and A_FT

The specimens subjected to the FTHR loading case (100 freeze-thaw cycles and 50 heat-rain cycles) have been monitored with the resonalyser after 1, 2, 4, 6, 12, 20 and 50 heat-rain cycles. During the subjection to the freeze-thaw cycles within this loading case, the above trend is assumed and no resonalyser tests have been performed during the freeze-thaw cycles. The evolution of the stiffness during the 50 heat rain cycles of the FTHR loading case are displayed in Figure 35.

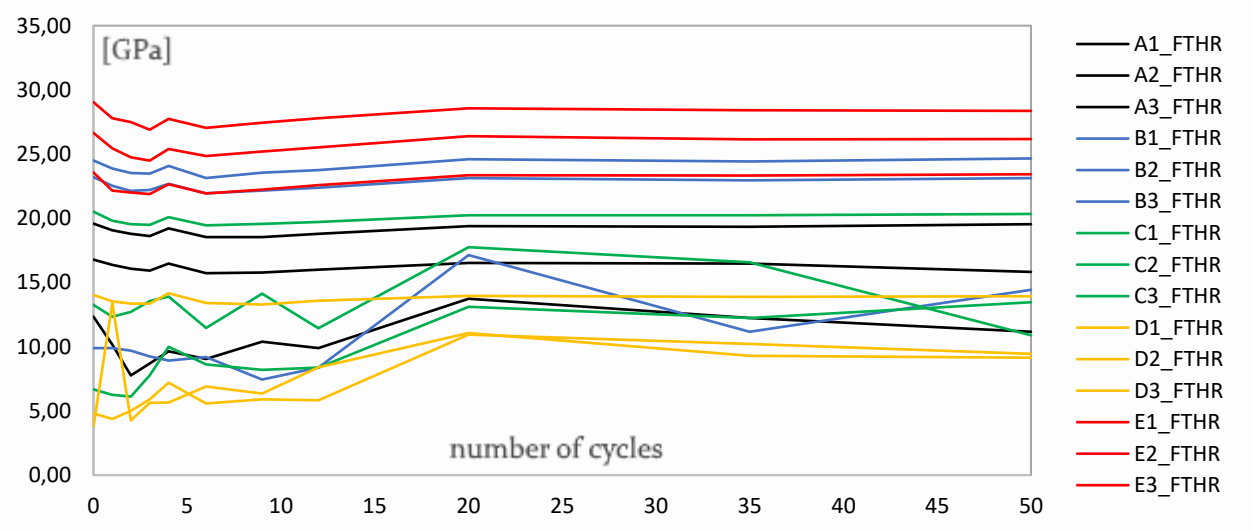

Figure 35 Evolution of the stiffness during FTHR cycling

Again, it can be noticed that series A_FTHR and D_FTHR (having the lowest density relatively to other series) are the most sensitive to durability loading, as depicted in Figure 36. Although, a small in crease of the stiffness may be linked to a late hydration process and/or a self-healing process. For the DIC images related to the specimens, the author refers to Annex C. The

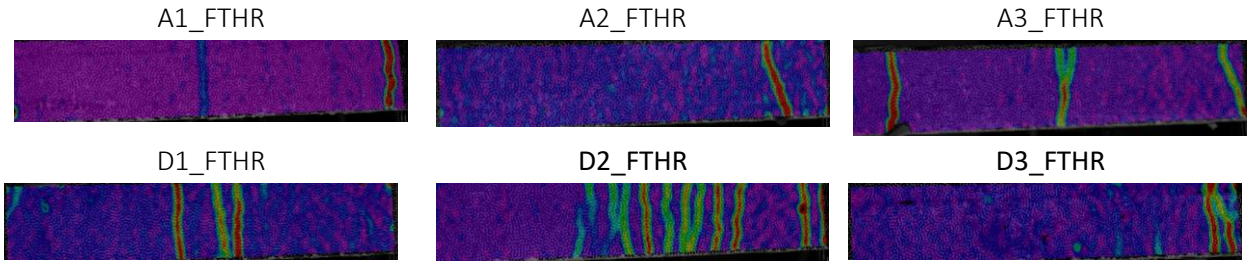

Figure 36 DIC images of durability induced cracks for series A_FTHR and D_FTHR

stiffness at cycle 0 in Figure 35 corresponds to the situation after 100 freeze-thaw cycles. Quantitative comparison to Figure 33 shows that 2 out of 3 specimen of series C_FTHR and specimen B1_FTHR experienced an enormous decrease in stiffness, which indicates the presence of durability cracks.

The same procedure is repeated for specimens subjected to the HR loading case (50 heat-rain cycles). Resonalyser tests have been performed after 1, 2, 4, 6, 12, 20 and 50 heat-rain cycles. On Figure 37 it can be noticed that, except for G1_HR, no degradation is observed.

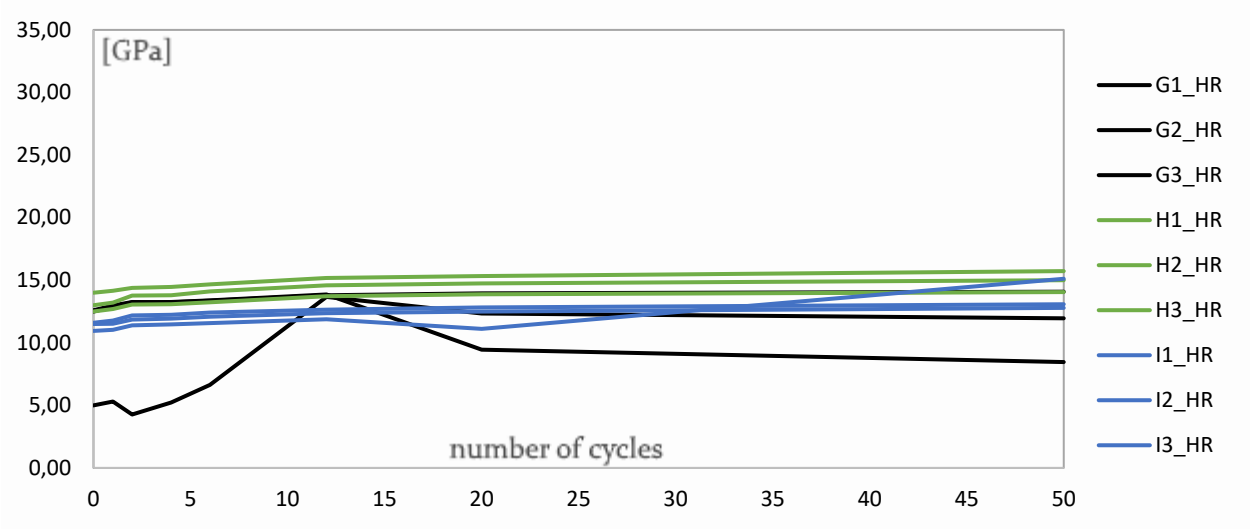

Figure 37 Evolution of the stiffness during HR cycling

Nevertheless, a lot of initial (durability) cracks were observed for series G_HR, as displayed in Figure 38.

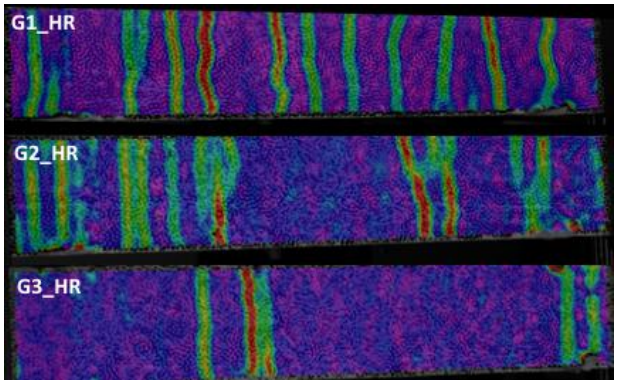

Figure 38 Damaged series G_HR

In short, resonalyser results are a good qualitative approximation for the evolution of the stiffness during environmental loading cycles. For a quantitative approach of the stiffness, an overestimation is observed in comparison with the effective stiffness, which can be addressed to the fact that the resonalyser test displays the material's stiffness under no external load (corresponding to the initial stiffness at 0MPa), while the stiffness obtained after mechanical loading is deduced from the first linear part in the stress-strain curve (corresponding to a stress range instead of an unload situation). Although, this qualitative approach is a very beneficial feature regarding the non-destructive origin of the test method.

4.2.2 Ultrasonic Pulse Velocity

Before testing the samples under uniaxial load, wave pulse velocity tests have been applied on all the specimens subjected to the FTHR and HR loading case to check their "health". Specimens A_FTHR, B_FTHR, C_FTHR, D_FTHR, E_FTHR, F_FTHR, G_HR, H_HR and I_HR have been tested and the wave pulse velocity has been recorded. (Figure 39) For the ease of interpretation, the specimens later on submitted to the FTHR loading case are displayed in blue, while the specimens destined for the HR loading case are displayed in orange.

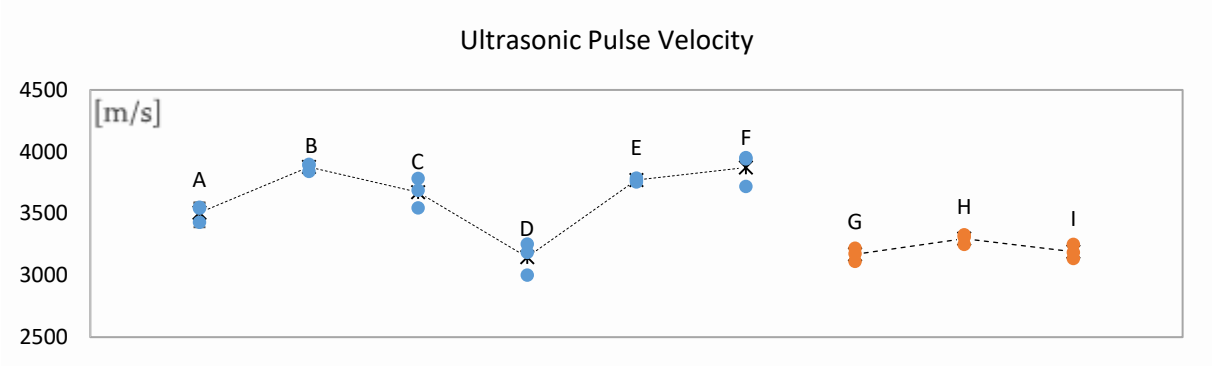

Figure 39 Wave pulse velocity for samples A to F (after subjection to FTHR) and samples G, H (after subjection to HR)

As a first, small conclusion, we can see that the density is directly proportional to the wave pulse velocity, which corresponds to the observations of Saint-Pierre et al. (2016) Out of these Ultrasonic Pulse Velocity results, the Young's modulus can be determined as described in 3.3.2.

Figure 40 displays the average value and STD of the Young's modulus for samples A to F after FTHR cycles and for samples G to I after HR cycles. A remarkable observation is found in the differences in STD, which are much higher for the resonalyser test results. This phenomenon may find cause in the exponential relation between Young's modulus and first resonance frequently and specimen dimensions, as can be noticed in equation (10) in section *3.3 Non-destructive testing methods*. All the values and their STD are tabulated in annex D for the reader's information.

Despite the differences, both techniques how the same tendency between the plates, namely a lower initial Young's modulus for series A, D and G, H, I.

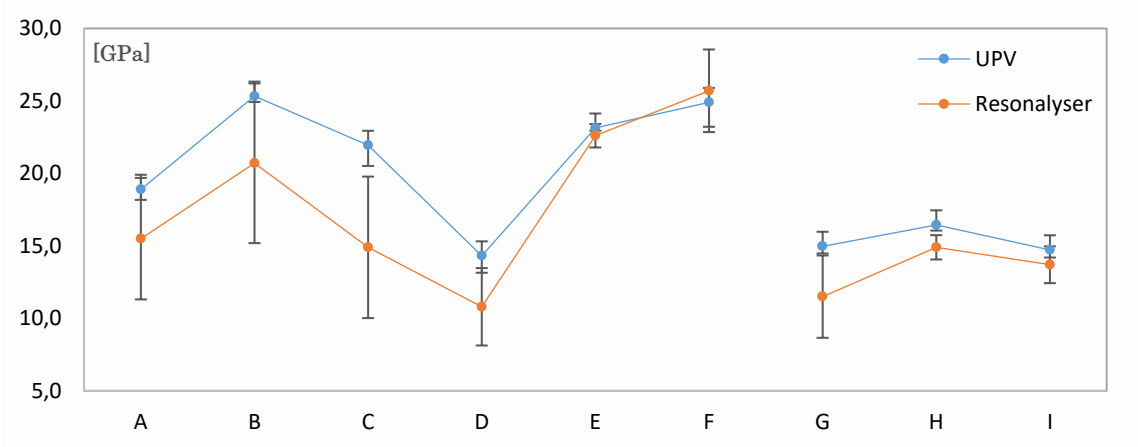

Figure 40 Young's modulus for samples A to F after FTHR cycles; and samples G, H and I after HR cycles

4.2.3 Durability cracks

Before going into detail on the global mechanical behaviour characterized by the uniaxial test, an investigation is done on the crack pattern induced by durability loading of the tested specimen. This is done to get a better understanding of the mechanical performance after uniaxial tensile testing. During the mechanical loading, Digital Image Correlation (DIC) is used to measure strains (and thus cracks) in the specimen.

Following the theoretical approximation of Aveston, Cooper and Kelly (1971), the first crack appears when the matrix's tensile strength is reached, resulting in a load drop in the stress-strain curve. Analysis of the results of the DIC shows that, for most of the specimens, certain cracks have already been formed before the first load drop. This observation is most remarkable on the specimens subjected to durability loading, concluding that durability cycles induce irreversible damage to the specimen by means of crack initiation, hereafter referred to as durability cracks. Figure 41 displays this tendency by showing 2 random specimens from every loading case. Important to mention is that all the results concerning cracks are derived from the DIC images, which only show part of the entire specimen due to the mechanical clamping equipment, as shown in Figure 27. All other DIC images can be retrieved in Annex C.

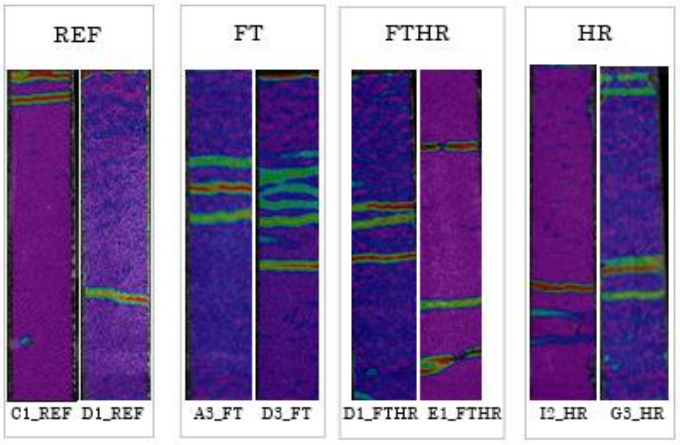

Figure 41 Durability cracks on 2 virgin specimens, 2 specimens subjected to FT, 2 specimens subjected to FTHR and 2 specimens subjected to HR

To be entirely sure whether these cracks are purely linked to the durability cycles, a closer look is taken to DIC images of specimen D2_FT before occurrence of the first load drop (at 1,99 kN).

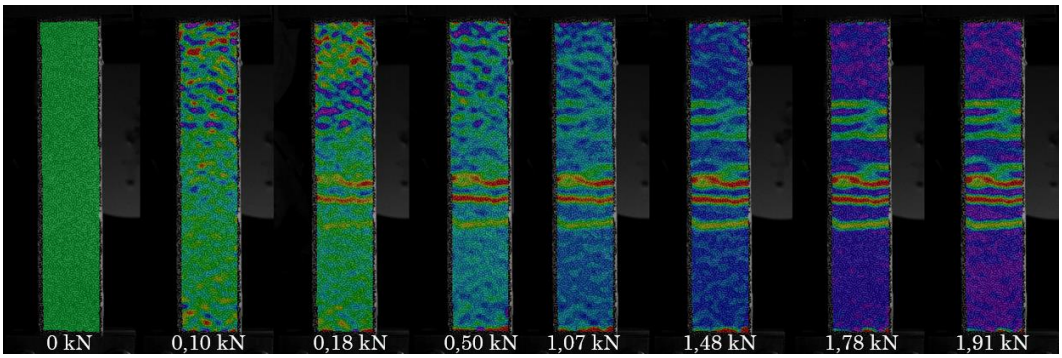

Figure 42 Evolution of durability cracks of specimen D2_FT before first load drop (due to mechanical loading)

Visual observation of Figure 42 proves that the durability cracks initiate at lower load levels and grow with increasing loads instead of having an abrupt appearance (which would go together with a load drop in the stress-strain curve). This indicates that above statements are correct.

Quantification of these durability cracks is done for all the specimens and summarized in Table 8. Note that the values displayed in this table are an averaged value of 3 specimens, explaining, for example, the appearance of 2,3 cracks which is physically incorrect. Although, this value is not rounded for further interpretation. Notations (*) and (**) are introduced to define the rejection of one respectively two specimens out of three. This may be due to early mechanical failure in the clamps or missing DIC images.

The block diagram displayed in Figure 44 shows the total number of durability cracks per specimen. The colors refer to the type of loading; grey represents the reference case, while blue represents the FT loading case, orange the FTHR loading case and yellow the HR loading case.

Table 8 Durability cracks

	A	B	C	D	E	G	H	I
REF $[-]$	1,0	$0{,}0^{**}$	2,0	1,3	$0{,}0^{*}$	1,3	0,3	3,5
FT $[-]$	4,3	0,7	1,7	5,7	0	–	–	–
FTHR $[-]$	2,3	0,7	$1{,}0^{*}$	4,7	2,0	–	–	–
HR $[-]$	–	–	–	–	–	10,0	2,3	$3{,}7^{*}$

Observation of these results shows that plates A, D, G, H and I are the most sensitive to crack initiation after durability loading. Remarkable to note is that those plates have a relatively lower density (Figure 31) than the other plates, as was already (partially) observed with the resonalyser tests. The black line represents the inversed value of the Young's modulus of every specimen. It can be noticed that a correlation is found between this value and the number of durability cracks. Note that the Young's modulus in this correlation is calculated out of the stress-strain curves obtained after mechanical loading.

4.2.4 Microcracks due to restricted shrinkage

During the application of the Heat-rain cycles within the FTHR and HR loading cases, specimens were heated up to 60°C within one hour and are abrupt cooled down by placing them in a water bath of ± 20°C. When taking the specimens out of the water, microcracks were clearly visible due to water infiltration. The appearance of these microcracks finds cause in the restricted shrinkage of the matrix due to the reinforcing fabrics. This observation matches with the experiences of Remy (2012) [Remy 2012] and the geometry of the microcracks answers the investigation of Majumdar et al. (1977).

Figure 43 Appearance of shrinkage cracks after heat-rain cycles

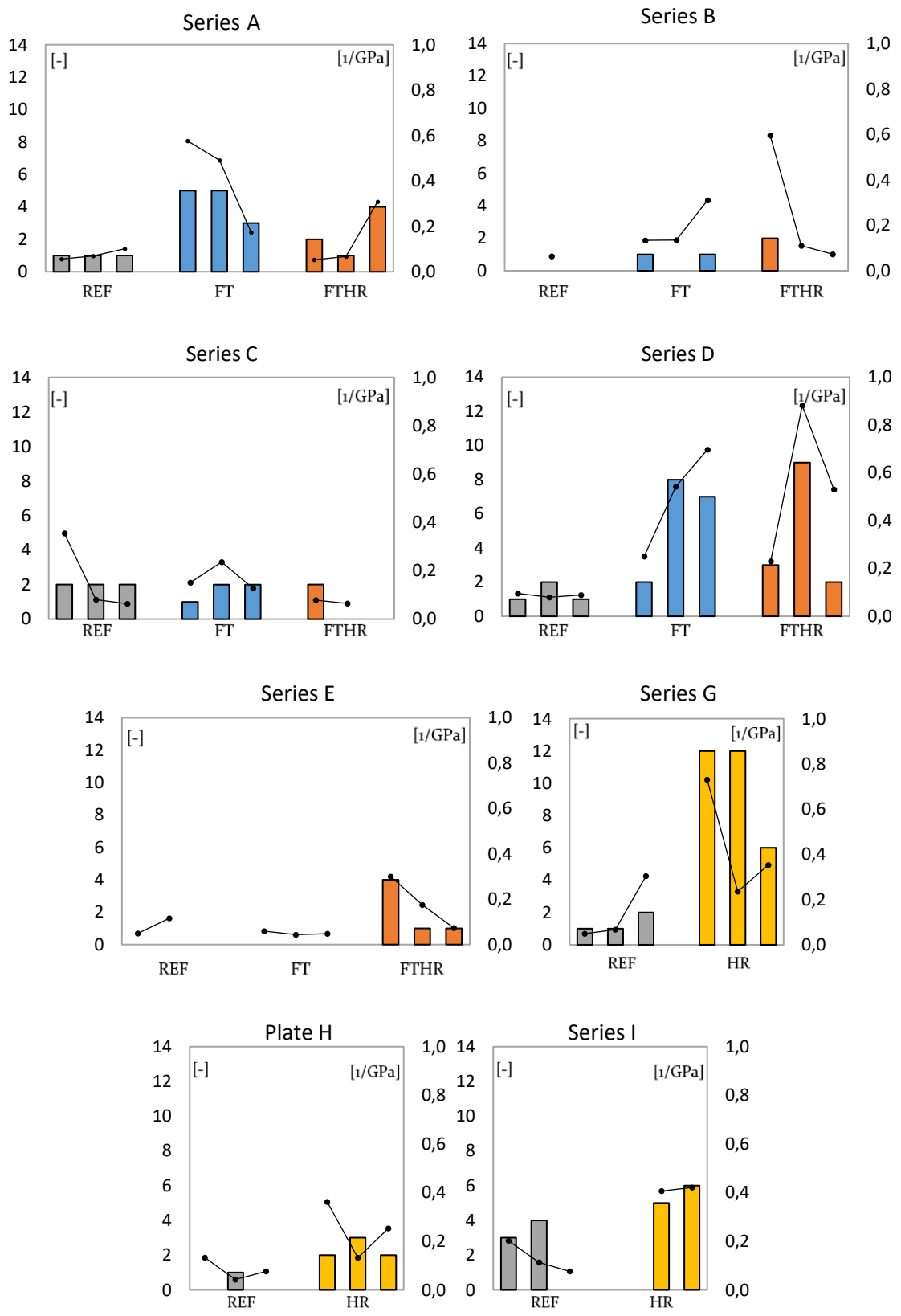

Figure 44 Durability cracks are inversely proportional to the material's stiffness

4.3 Mechanical loading

4.3.1 Overview of the uniaxial tension test results

An interpretation of the mechanical behaviour of the reference samples in comparison to those submitted to durability cycles is displayed in this chapter.

This chapter captures all the results of series A to I. For plates A to F, a distinction is made between

- 3 Reference samples [REF]
- 3 Samples subjected to 100 freezing-thawing cycles [FT]
- 3 Samples subjected to 100 freezing-thawing and consecutively 50 heat-rain cycles [FTHR]

For plates G to I, a distinction is made between

- 3 Reference samples [REF]
- 3 Samples subjected to 50 heat-rain cycles [HR]

Figure 48 shows the average mechanical behaviour of the reference compared to the theoretical ACK model. In these results, the three stages that typically characterize the TRC behaviour under tensile loading can be observed very well. The grey shaded area on each graph represents the scatter on the results, since an average of 3 specimens is taken per plate.

First cracking occurs when the tensile strength of the matrix is reached and then, multiple cracking of the matrix occurs in the strain-hardening stage (stage II). The final branch is characterized by the volume fraction and geometry of the fibres. Finally, composite failure is caused by fabric failure or fibre pull-out. In practice, some of the specimens showed early failure due to unexpected stresses induced by a misaligned set-up in the clamps. The latter have been rejected in the analysis of the results and are referred to with (*) or (**) for rejection of 1 respectively 2 specimens. Within this context, specimens cut out of plate F showed early failure or exceptional mechanical behaviour for 6 out of 9 samples. Therefore, the author decided to reject plate F in the further discussion of the results.

A typical evolution of the crack pattern of a reference specimen is illustrated in Figure 45, where specimen D3_REF is used as an example. In this example the final failure occurs at the level of the first crack, which is not always the case.

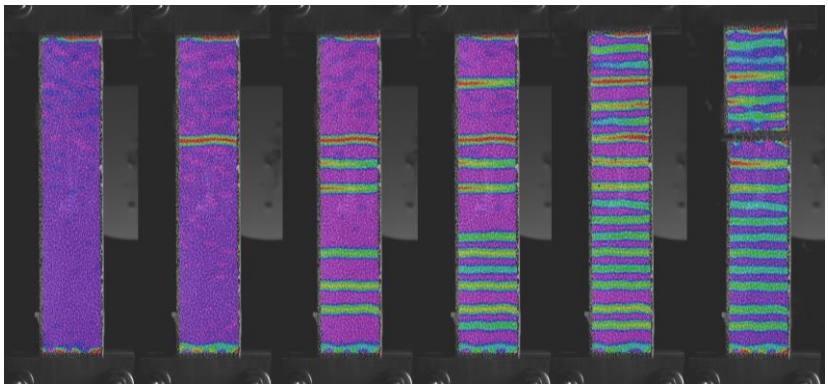

Figure 45 Evolution of the crack pattern (D3_REF)

Figure 46 displays a percental comparison of the experimental values of the first cracking stress (σ_{mc}), stiffness in the first stage (E_{c1}) and stiffness in the third stage (E_{c3}) to the theoretical values obtained by the ACK theory for the different series (Figure 48). It can be noticed that the average values of the first cracking strength and stiffness in the first stage don't deviate significantly from the expected value. This is a degree for the quality of the produced specimens. On the other hand, the stiffness in the third stage deviates significantly from the expected value. This may find cause in hand-layup preparation of specimen, resulting in a non-planarity of the fabrics.

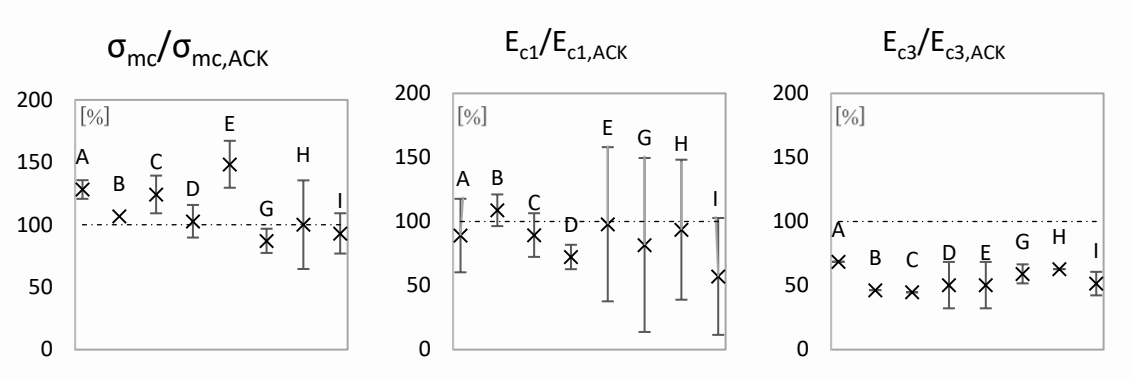

Figure 46 Percental deviation of mechanical reference behaviour to the ACK model

Figure 47 displays an overview of the mechanical properties that will be investigated in this section:

- First cracking strength (1)
- Strain and stress at end of the Multiple Cracking stage (2)
- E_1 modulus (3)
- E_3 modulus (4)
- Ultimate strength (5)
- Total number of cracks at failure (6)
- Average crack width (7)
- Average crack interdistance (8)

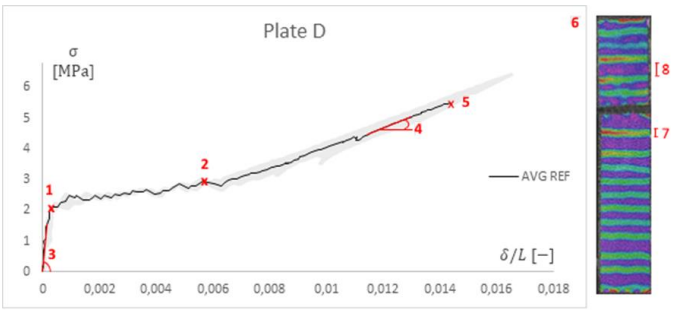

Figure 47 Investigated mechanical properties

As already explained, parameters (1), (2) and (3) are related to the Serviceability Limit State, while parameters (4) and (5) are related to the Ultimate Limit State. Crack investigation is done by inspecting parameters (6), (7) and (8) and cannot be classified under a specific Limit State. Although, cracks improve the sensitivity to aggressive substances to deteriorate the composite. For a full overview of all these results per specimen, the author refers to Annex B.

Afterwards, a discussion of the results will lead to a global conclusion. Figure 49 displays the results of the uniaxial tension tests for reference specimens and specimens subjected to environmental loading. The shaded area represents the scatter on the results. In what follows, every property stated above will be investigated separately. In order to keep a well-structured overview, the scatter on every property is not depicted in the according figures, but is displayed in table-form and can be found in Annex D.

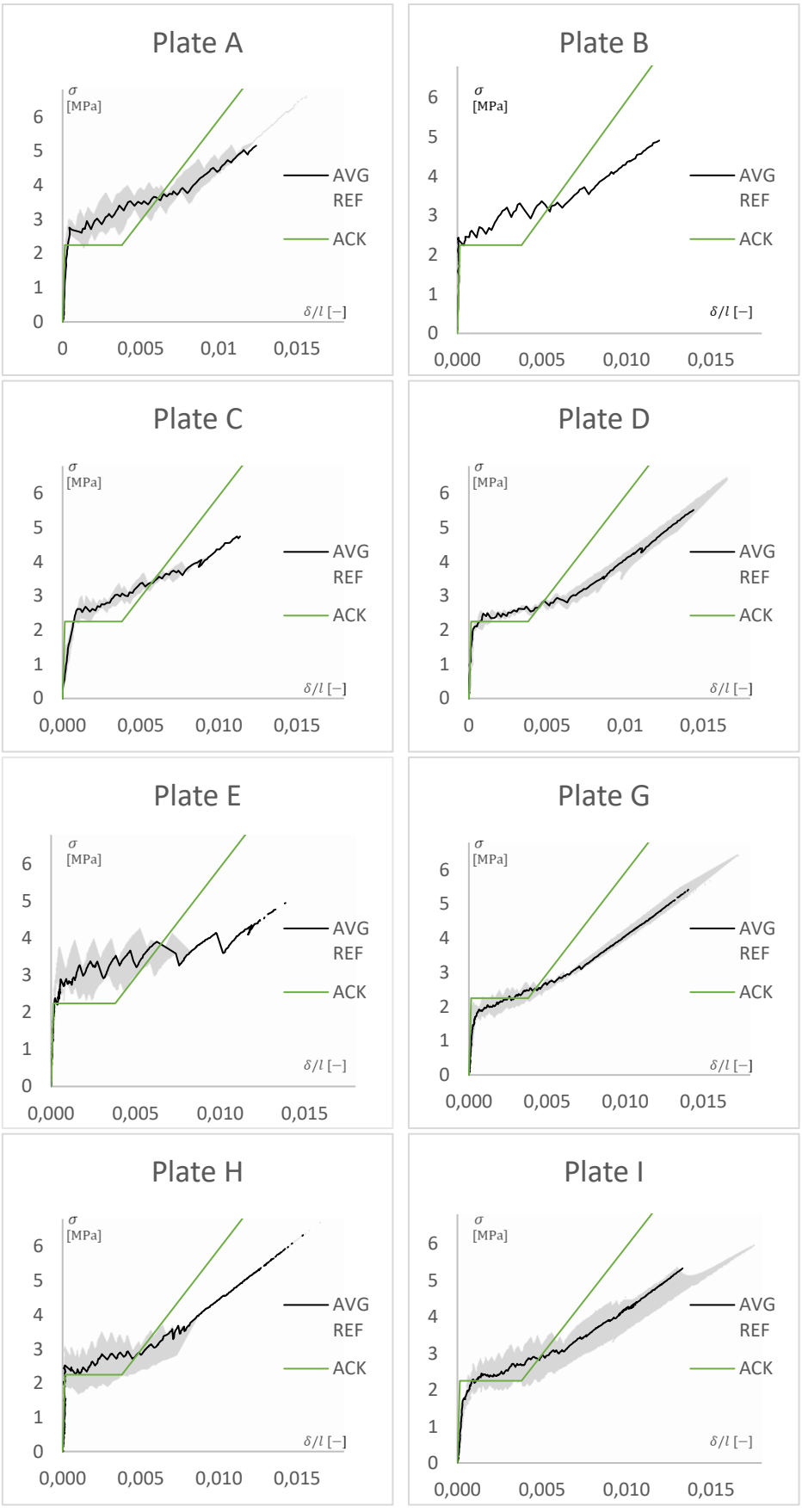

Figure 48 Average behaviour of the reference specimens compared to the theoretical ACK model

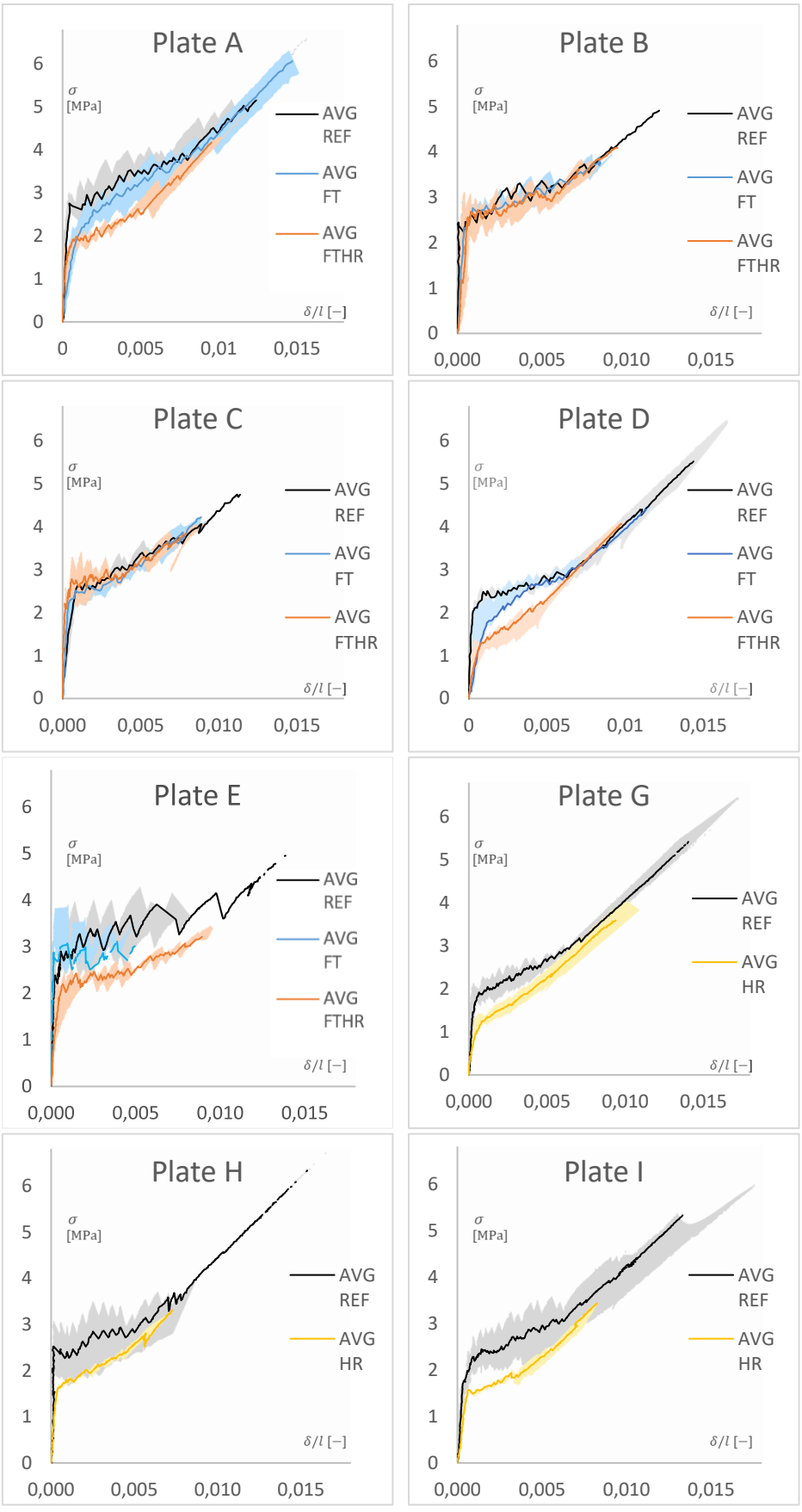

Figure 49 Average influence of durability cycles to the reference situation

4.3.2 Mechanical properties

Within this investigation, the author wants to stress on some designations. For the ease of explanation, example is taken for series D.

Series D consists of 9 specimens, whom 3 are used as reference samples, 3 are subjected to the FT loading case and 3 are subjected to the FTHR loading case. For each set of 3 specimens, the above enumerated mechanical properties are investigated and are averaged over every set. This means that, per investigated property, 3 average values will represent the behaviour of the Reference case, the FT loading case and the FTHR loading case respectively. Standard deviations on these results are not depicted in the according figures to keep a well-structured overview. For a quantification of these Standard deviations, the author refers to Annex D.

4.3.2.1 First cracking strength

In the design of sandwich panels for outdoor applications, the first cracking strength is related to the Serviceability Limit State conditions and should be interpret with care, since one may interpret the formation of cracks as an exceedance of the SLS requirements, while others may interpret the crack formation and propagation until a certain width as an acceptable SLS condition.

In theory, the first crack appears when the tensile strength of the matrix is reached and is therefore only dependent on the matrix's density and quality. Important to note is that the durability loading cases already induced durability cracks before subjection to the uniaxial tension test. Sometimes even reference samples showed some initial cracks.

These durability cracks are classified as irreversible damage to the material and, according the ACK model, the multiple cracking stage is already reached. Therefore, during this thesis, the "first cracking strength" is referred to as the first load drop observed in the stress-strain curve obtained by Digital Image Correlation after the uniaxial tension test.

A general decrease in first cracking strength for increasing durability cycles is observed on Figure 49. To quantify this observation, an investigation on all the specimen of plate A to I is done.

Figure 50 displays the evolution of the first cracking strength for increasing durability loading. Compared to the density per plate (Figure 31), these results show that the first cracking strength is proportional to the density. More in particular, series D has the lowest density and shows the lowest cracking strength in the reference situation, as well as in the FT case as in the FTHR case. Although, deviations of this theory can be observed but are not significant, considering the scatter on the results.

Taking a closer look to the evaluation of the first cracking strength within every series subjected to different durability loading cases, a general decrease is observed after the FT loading case (except for series B and E) FTHR loading and HR loading.

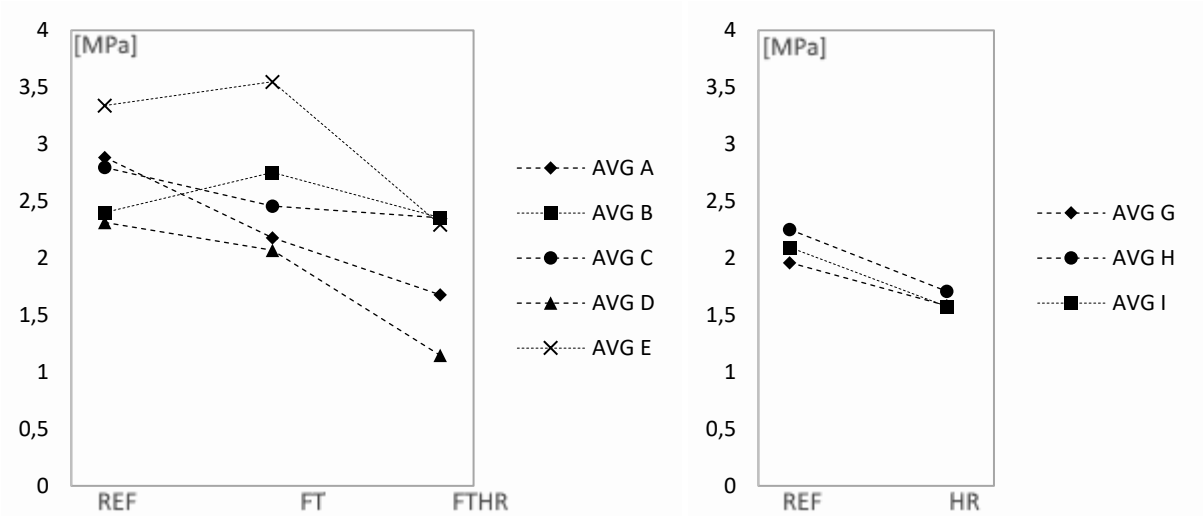

Figure 50 Evolution of the first cracking strength

Table 9 Percental evolution of the first cracking strength after mechanical loading compared to the reference case

	A	B	C	D	E	G	H	I
REF [MPa]	2.885	2.400**	2.796	2.313	3.340*	1.960	2.251	2.094
FT [%]	▼24,5	▲14,7	▼12,2	▼10,6	▲6,3	–	–	–
FTHR [%]	▼41,8	▼1,8	▼15,8*	▼50,4	▼31,3	–	–	–
HR [%]	–	–	–	–	–	▼19,3	▼24,8	▼24,8*

After subjecting the specimen to **the FT loading case**, a decrease in first cracking strength is observed between 24,5%, and 10,6%. This decrease is a logical result regarding the initiated damage attributed to durability cracks (Table 8) induced by this loading case. Series B and E show the highest density among the series and deviations on the general trend (an increasing first cracking strength is observed for series B and E) may be linked to late hydration processes governing the formation of CSH phases, resulting in an increase in first cracking strength, as investigated by Butler et al. (2010) Other series show a relatively lower density, which may indicate that all the hydration processes have already occurred before (or during) the FT loading case, resulting in a decrease of first cracking strength after FT loading.

Further subjection to **the FTHR loading case** reduces the first cracking strength even more by values varying from 1,8% to 50,4%. Within these results, a clear correlation is observed with the density. By now, series B and E are also showing a decrease in first cracking strength which may indicate that the late hydration processes have been stopped. Series B shows the highest density, resulting in the lowest decrease in first cracking strength after FTHR cycles, while series D has the lowest density, resulting in the highest decrease in first cracking strength. This phenomenon may be attributed to the formation of portlandite crystals (chemical origin) and/or a degradation of the bond between fibres and matrix (physical origin) due to environmental loading.

The same trend can also be noticed for the series G, H and I subjected to **the HR loading case**, with a decrease in first cracking strength varying between 19,3% and 24,8%. A percental evolution of the first cracking strength with respect to the reference value is shown below for every loading case.

In short, it can be concluded that the influence of the durability cycles on the first cracking strength is strongly related to the density of the matrix, which corresponds with the theoretical model presented by Aveston, Cooper and Kelly (1971). Late hydration processes in specimen with relative higher densities will govern the formation of CSH phases, even after the FT loading case. These CSH phases govern a well-developed bond between fibres and matrix, resulting in an increased first cracking strength. On the opposite, degradation of the first cracking strength may find cause in a deterioration of the bond between fibres and matrix, which can be attributed to the formation of portlandite crystals in the fibre matrix stage or to physical freeze-thaw damage in the pores of the matrix.

4.3.2.2 End of the Multiple Cracking stage

The end of the multiple cracking stage is characterized by the final crack and introduces stage III, where the tensile load is fully taken by the fabrics. Variation on the strain at the end of the Multiple Cracking stage are attributed to the durability cycles and can be related to microscale processes. A possible explanation of the observed results in this master thesis is attributed to the observations of the microscale processes studied by many authors. These observations have been briefly summarized in section *2.4 Durability*.

It can be noticed that, after **the FT loading case**, a decrease varying from 25,9% up to 63,6% is observed for series B, C and E compared to the reference situation. Series A and D have a relative lower density than the latter and show an increase between 6,2 and 10,6% in strain at the end of the Multiple Cracking stage. These increases are not significant and, considering the scatter on the results, it can be concluded that the FT loading case doesn't influence these series. For series B, C and E, the decrease in strain can be attributed to the higher density which fosters the formation of portlandite between matrix and filaments, causing a bad load bearing bond. [Butler 2010] Another possible explanation is the deterioration of the fabrics due to the high alkali environment of the matrix. One of these (or both) assumptions may be the cause of the decrease in strain at the end of the Multiple Cracking stage for the series with a relative higher density.

After subjecting to **the FTHR loading case**, a decrease varying from 14,4% up to 45,2% is observed with respect to the reference case, while a small increase is observed for series B, C and E with respect to the FT loading case. In order to understand this increase, a study on the microscale behaviour should be executed in order to evaluate these mechanisms. The general decrease can be linked to the fact that, during FTHR cycling, exposure to temperatures up to 60°C is experienced. This high temperature in combination with the possible high alkali content of the matrix may cause deterioration of the fabrics. [Zinck 2001]

This conclusion can be extended for **the HR loading case**, where a decrease varying from 16,7% up to 53,0% is observed.

It should be noticed that the investigation on the end of the multiple cracking stage should be handled with care. A decrease in strain could be attributed to the formation of durability cracks, meaning that the multiple cracking stage is already reached before mechanical testing. This decrease in strain is therefore not related to the formation of less cracks. On the other hand, a decrease in strain could effectively be linked to a bad load bearing bond attributed to the formation of portlandite. To draw

clear conclusions on the strain at the end of the multiple cracking stage, a deeper study is recommended.

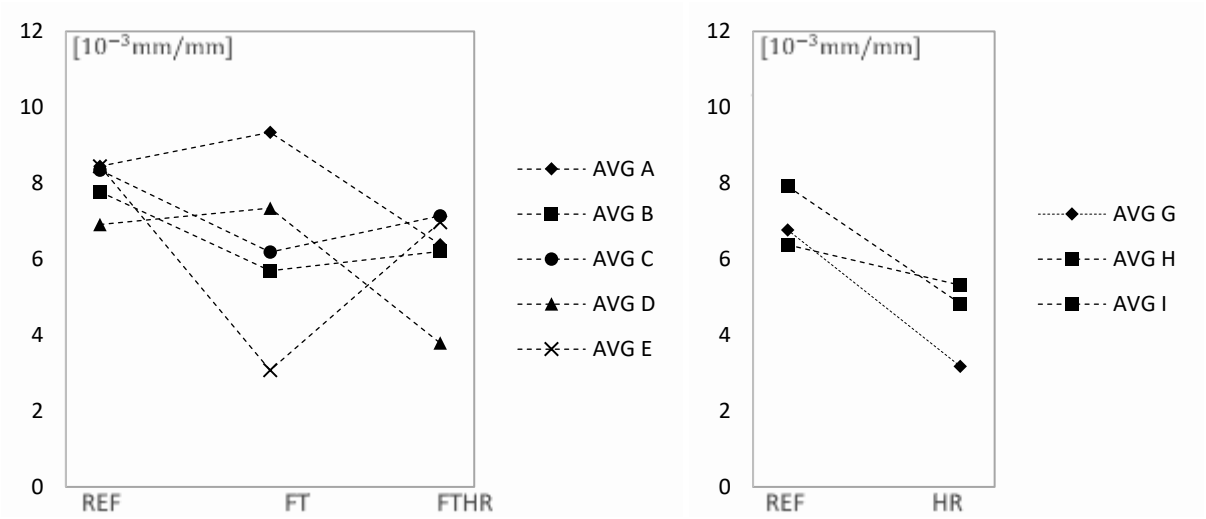

Figure 51 Evolution of the strain at the end of the Multiple Cracking stage

Table 10 Percental evolution of the strain at the end of the Multiple Cracking stage

	A	B	C	D	E	G	H	I
REF $[10^{-3}]$	8,446**	7,774**	8,345*	6,914*	8,451*	6,772	7,923**	6,378
FT [%]	▲10,6	▼26,8	▼25,9	▲6,2	▼63,6	–	–	–
FTHR [%]	▼34.4	▼20,2	▼14,4*	▼45,2*	▼17,5	–	–	–
HR [%]	–	–	–	–	–	▼53,0	▼39,0*	▼16,7*

The observations of the strain at the end of the Multiple cracking stage can be extended to the according stress. These results are shown in Figure 52. Globally, the last cracking stress decreases after exposure to durability cycles. A small increase of 9,1% is observed for series A after exposure to FT cycling, but this small increase may be attributed to the scatter on the results, since 2 out of 3 specimens have been rejected in the reference case of series A. Again, to draw clear conclusions on this investigated parameter, a deeper study should be carried out.

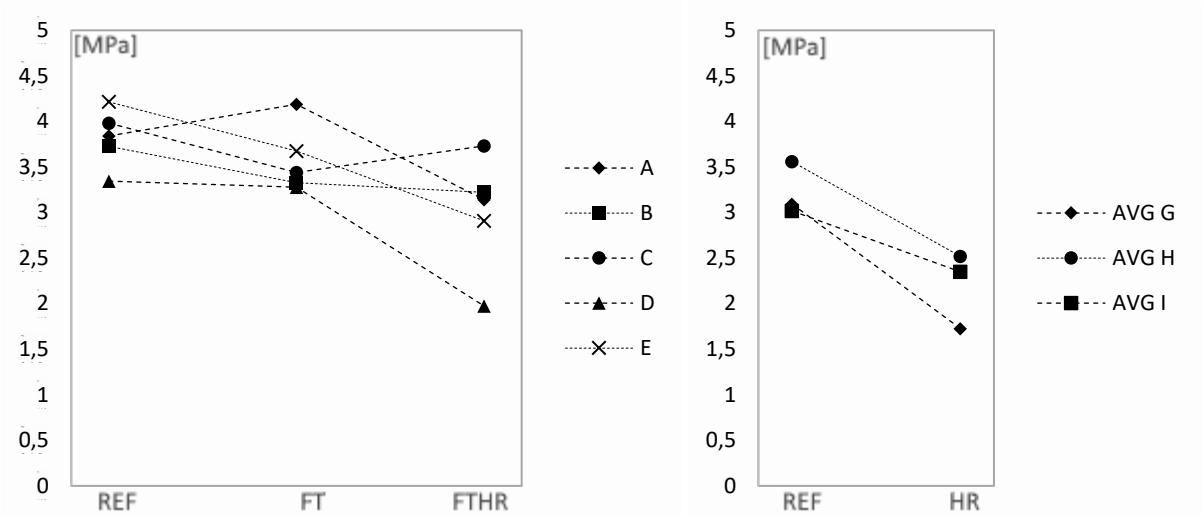

Figure 52 Evolution of the last cracking strength

Table 11 Percental evolution of the last cracking strength after mechanical loading compared to the reference case

	A	B	C	D	E	G	H	I
REF [MPa]	3,84**	2.727**	3.982*	3.345*	4,215*	3.093	3.560**	3.018
FT [%]	▲9,1	▼10,7	▼13,6	▼2,0	▼17,6	–	–	–
FTHR [%]	▼19,2	▼13,5	▼6,3*	▼59,0*	▼31,0	–	–	–
HR [%]	–	–	–	–	–	▼44,2	▼29,2*	▼22,1*

4.3.2.3 Stiffness Stage I

Regarding the Serviceability Limit State conditions on the outdoor applications of sandwich panels, the material's stiffness is an important parameter to consider since sandwich panels are mainly loaded in bending. The stiffer the material, the more resistance it can offer to these loads. Evolution of this parameter under environmental loading is thus essential regarding the durability of such a sandwich panel.

The Young's modulus decreases after exposing the specimen to a Durability loading case of type FT, while a slight increase is again noticed for further Durability loading to FTHR compared to FT. The only exceptional result is found for series E subjected to FT cycling, where an increase of Young's modulus is observed.

As a logical sequence, the higher the density, the higher the initial Young's modulus in reference state. This trend is followed. The only extremity in this trend is found in specimen B, which may find cause in the fact that 2 out of 3 specimens were rejected and no statistical representative number of specimens was considered in the reference state.

After subjection to **the FT loading case**, a decrease of E modulus is found between 39,6% and 78,7%, with an exceptional increase for series E (Table 12). Again, the more cracks induced by the durability cycles (see Table 8**)**, the lower the Young's modulus, which completely strikes with the ACK theory.

The exceptional behaviour of the series E can be declared that no cracks were induced by the freeze-thaw cycles for these specimens, which may find cause in the increased thickness of the specimen's set, inducing a decrease in the fibre-volume fraction that approximates the critical value. This may

point to a loss of composite behaviour and result in a higher initial stiffness (and first cracking strength) explained in section *4.3.2.5 Ultimate Strength.*

After subjecting the specimens to **the FTHR loading case**, a slight increase is observed compared to FT loading case, while a global decrease compared to the reference situation is observed. This increase can be explained because less cracks were present on specimens subjected to FTHR cycling, which may be due to late hydration processes, healing the cracks initiated in the FT loading case. Again, to be entirely sure on these assumptions, a deeper study on microscale is recommended.

The same trend of results is found for **the HR loading case**, where a decrease between 67,8% and 78,1% is perceived.

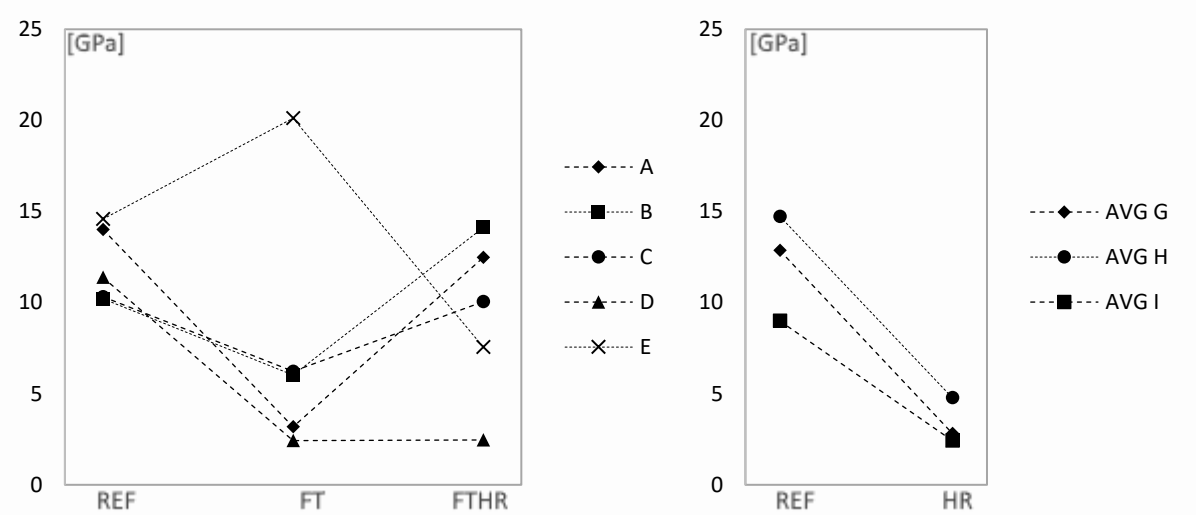

Figure 53 Young's modulus stage I

Table 12 Percental evolution of the Young modulus (stage I) after mechanical loading compared to the reference case

	A	B	C	D	E	G	H	I
REF [GPa]	14,01	15.62**	10,32	11,38	14,58*	12,86	14,73	8,99
FT [%]	▼77,3	▼41,0	▼39,6	▼78,7	▲38,0	–	–	–
FTHR [%]	▼11,0	▲38,3	▼2,7*	▼78,4	▼48,2	–	–	–
HR [%]	–	–	–	–	–	▼78,1	▼67,8	▼73,1*

It is remarkable that above trends were not seen with the resonalyser test method, where, after FT cycles, a degradation of the stiffness was only observed for series A and D (Figure 33).

Figure 54 displays the variation on the E modulus for non-destructive testing techniques (UPV, resonalyser) and destructive uniaxial tensile testing (UTT). These results cover the specimen that were subjected to FTHR loading (series A to E) and to the HR loading case (series G to I). Remind that series F have been rejected after UTT.

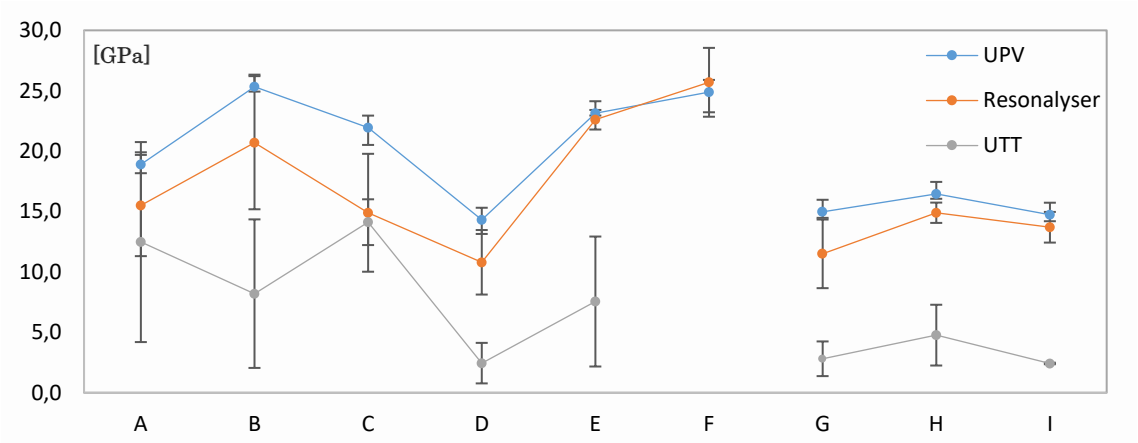

Figure 54 Young's modulus according to Resonalyser test method, Ultrasonic Pulse Velocity (UPV) and uniaxial tension tests (UTT) for series A to E subjected to FTHR cycling and series G to I subjected to HR loading

It can be concluded and confirmed that the results of the resonalyser tests are a good qualitative indication for non-reversible damage, but are not fully reliable to make final conclusions. Although, they can be used as a backing for the interpretation of the mechanical test results.

In short, it can be noticed that the more durability cracks (environmental damage) are present, the more decrease is observed in stiffness. The presence of the durability cracks indicates that the multiple cracking stage has already been reached. This means that the initial damage was already experienced by the composite, resulting in a decrease of the stiffness as investigated by Butler et al. (2010) and displayed in Figure 55. Analysis of the experimental results proves that the investigated non-destructive test results are a good qualitative indication for the indication durability damage and therefore the stiffness of the composite. Although, these results should be interpreted with the required expertise and can be used as a backing for the interpretation of the mechanical test results.

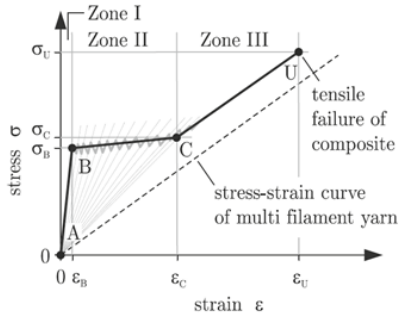

Figure 55 Degradation of the stiffness according the ACK theory [Butler 2010]

4.3.2.4 Stiffness Stage III

The ultimate strength of the composites will be governed during stage III of the ACK theory developed by Aveston, Cooper and Kelly (1971). Within this stage, external loading is fully taken by the fabrics. Therefore, a deeper investigation on the stiffness of the composite during this stage is investigated below.

Since the fibre volume fraction and the nominal dimensions of the cross section are equal for all the specimens, the global trend of evolution of the Young's modulus in the last stage of the ACK theory [Aveston 1971] should be approximately the same. Regarding the reference specimens, the average stiffness equals $0{,}321\ \mathrm{GPa}$ with a standard deviation of $0{,}030\ \mathrm{GPA}$, which is a deviation of 45,8% regarding to the theoretical expected value according to the ACK theory.

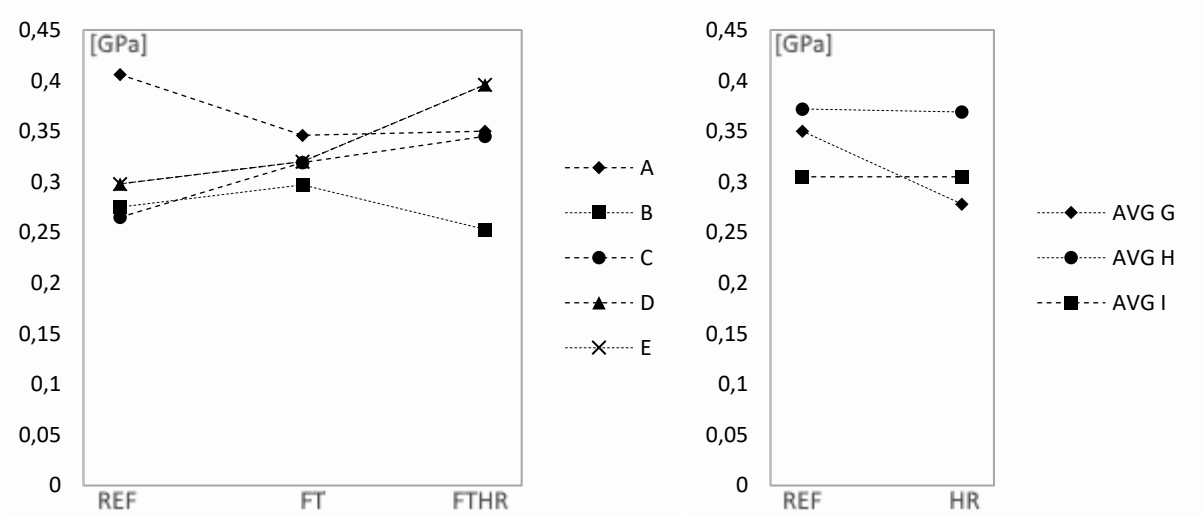

Figure 56 E modulus stage III

The theoretical E_{c3}-value of $0.592\ \mathrm{GPa}$ may find cause in the non-planarity of the fabrics and the hand layup preparation of the specimen. Another possible cause can be found in a deterioration of the fabrics during the rolling process of the latter, causing surface flaws, lowering the fabric's performance. In any case, deterioration of the fibre performance due to high temperatures and high alkalinity for this amount of cycles cannot be confirmed, since no information is given on the pH of the used matrix and no significant deterioration is observed in comparison with the reference samples.

4.3.2.5 Ultimate Strength

Regarding the Ultimate Limit State, focus is found on the ultimate strength, which is defined by the ultimate stress and strain. To determine the influence of durability cycles on the ultimate strength of the specimens, a closer look is taken to the specimen that didn't fail in the clamps. Figure 57 displays the specimens of series D at failure. It can be noticed that specimens D1_REF and D3_REF have failed in the clamps, and will therefore not be considered for the analysis of the ultimate strength. The failure mode for all specimens can be found in Annex B.

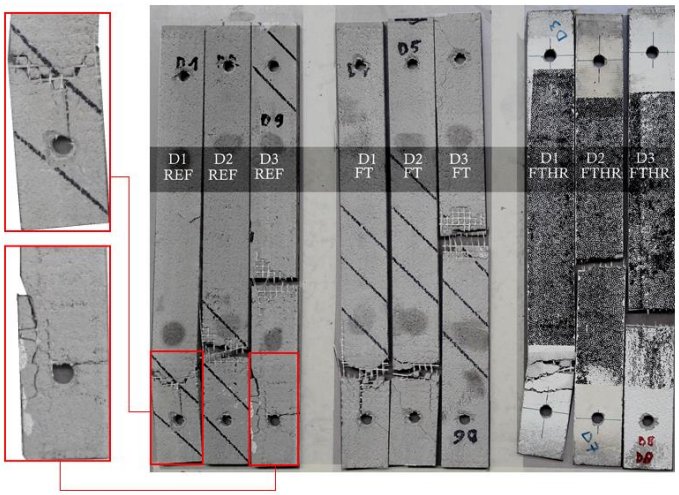

Figure 57 Failure of series D with a close-up for D1_REF and D3_REF, where failure in the clamps caused early failure

A general trend of decreasing in ultimate strength after subjection to durability loading is found in Figure 58.

After subjection to **the FT loading case**, a decrease in ultimate stress between 10,1% and 25,4% is observed. Further subjection of the specimens to **the FTHR loading case**, a decrease in ultimate stress between 9,6% and 33,5% is observed compared to the reference situation. Comparison of these results to the FT loading case shows that no significant decrease is observed, except for series A. Therefore, the FT loading case caused already most of the damage in the material. Declaration on these results may be attributed to physical and chemical damage during the environmental loading. Physical damage is related to the cycles causing damage in the pores of the matrix, while chemical damage may be related to the formation of precipitation phases such as portlandite, causing a bad load bearing between fibres and matrix and/or notching of the fabrics, which may result in a more brittle composite behaviour.

Although, subjecting the series to **the HR loading case** results in a decrease from 40,7% up to 54,7%. These deteriorations may again be attributed to the formation of portlandite, affecting the performance of the fabrics and enhancing the brittleness of the composite. In addition, a possible explanation of this relatively higher degradation compared to FT and FTHR can be found in the negative effect of the pH level of the matrix in combination with high temperatures, as investigated by Majumdar et al. (1977) .

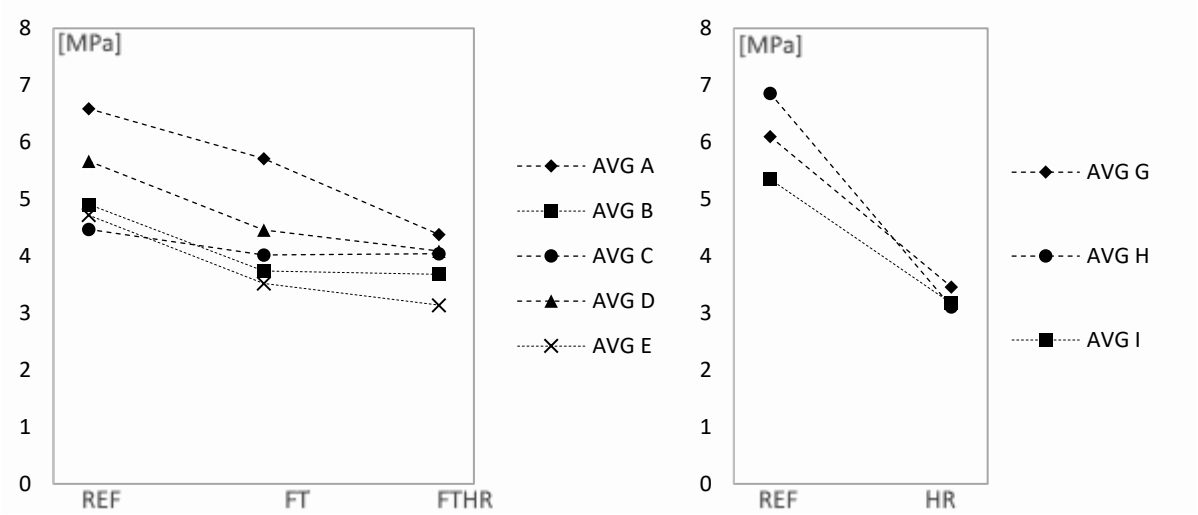

Figure 58 Ultimate stress

Table 13 Percental evolution of the ultimate stress after durability loading compared to the reference case

	A	B	C	D	E	G	H	I
REF [**MPa**]	6,59**	4,91**	4,47	5,67*	4,72*	6,1	6,86**	5,35
FT [%]	▼13,4	▼23,8	▼10,1*	▼21,3*	▼25,4	–	–	–
FTHR [%]	▼33,5	▼24,1	▼9,6*	▼27,9*	▼33,5	–	–	–
HR [%]	–	–	–	–	–	▼43,3	▼54,7*	▼40,7*

The according ultimate strains are displayed in Figure 59 and the same trend is followed as for the ultimate stress, which is a logical sequence. Although, deviations can be observed for the series B and E subjected to the FT loading case. These significant decreases in ultimate strain is caused by brittle failure. Therefore, a deeper investigation is done on series E regarding the odd behavior in the stress-strain curves obtained after mechanical loading. The relatively higher thickness of series E with values up to 13 mm instead of the nominal value of 10 mm lowers the fibre-volume fraction significantly with respect to the expected value calculated by equation (8) in section *3. Materials and Methods.* This may affect the composite behavior of the specimen since the critical fibre-volume fraction is approached, resulting in a more brittle material. Physically, this phenomenon is declared by the fact that, once the first crack is formed, the stress in the fabrics is significantly higher, resulting in fabric failure before (or during) the multiple cracking stage. This also declares the fact that barely cracks appeared on this series. Regarding these results, the study of several specimens with different fibre-volume fractions would be very interesting.

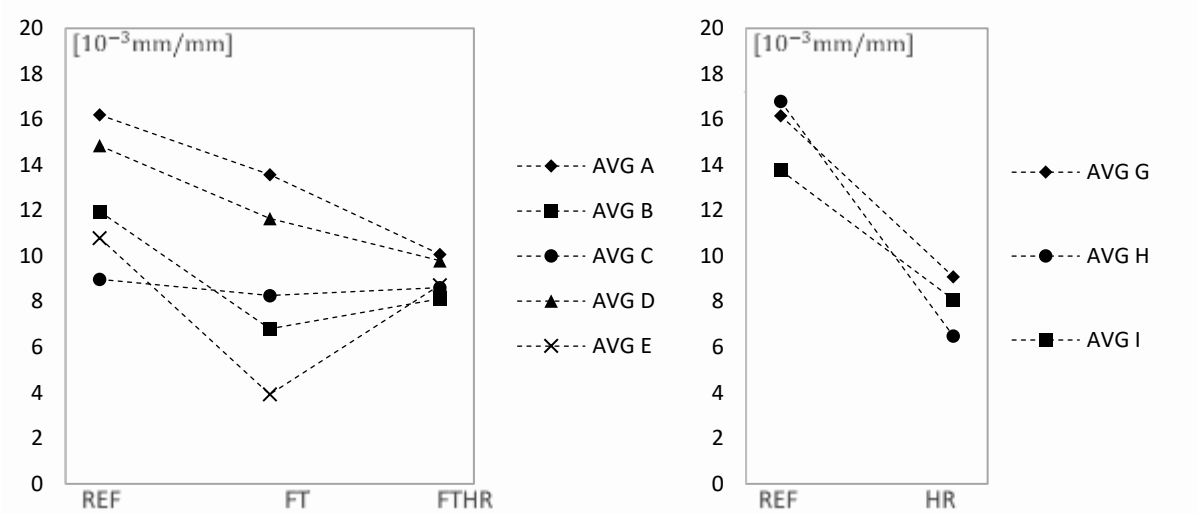

Figure 59 Ultimate strain

Table 14 Percental evolution of the ultimate strain after mechanical loading compared to the reference case

	A	B	C	D	E	G	H	I
REF $[10^{-3}]$	16,2**	11,96**	8,98	14,85*	10,8*	16,17	16,80**	13,775
FT [%]	▼16,2	▼43,1	▼7,9*	▼21,5*	▼63,6	–	–	–
FTHR [%]	▼37,8	▼32,0	▼4,0*	▼34*	▼19,2	–	–	–
HR [%]	–	–	–	–	–	▼43,7	▼61,3*	▼41,2*

In short, it can be noticed that, regarding the ULS conditions, environmental loading has a negative influence on the ultimate strength of the material which can be attributed to physical and/or chemical degradation processes. Deeper investigation of series E showed that an increased thickness has a significant effect on the composite behaviour, resulting in a more brittle material and barely crack formation.

To determine whether ultimate failure is due to fabric failure or fibre pull-out, a closer look is taken to efficiency factor of the fibres (stage III) in Figure 60. According to the specifications of the manufacturer [Knauff 2016], the ultimate load capacity of 2 fibre nets should equal 5,0 kN per 50 mm.

Within this investigation, study is done on the level of the loads at failure instead of the stresses. The efficiency factor of the fibres is defined as the ratio between effective load capacity and theoretical load capacity, as imposed by the manufacturer. Efficiency factors between 54,5% and 67,18% are observed for the reference specimens, which may be attributed to the non-planarity of the fabrics in the production process, the non-alignment of the clamps during the tensile test and physical deterioration due to the rolling process of the fabrics. Further decrease is observed after environmental loading, which may be attributed to the formation of portlandite. Another possible declaration for the degradation may be linked to the high temperatures in combination with the high alkaline environment, but cannot be confirmed since no information on pH is given by the manufacturer.

Taking into account the possible effects attributed to the testing and production process as discussed above, along with the visual failure mechanisms of the composites (Annex B), it can be concluded that all the fabrics that didn't fail in the clampers failed due to fabric failure. No pull-out was observed during this work.

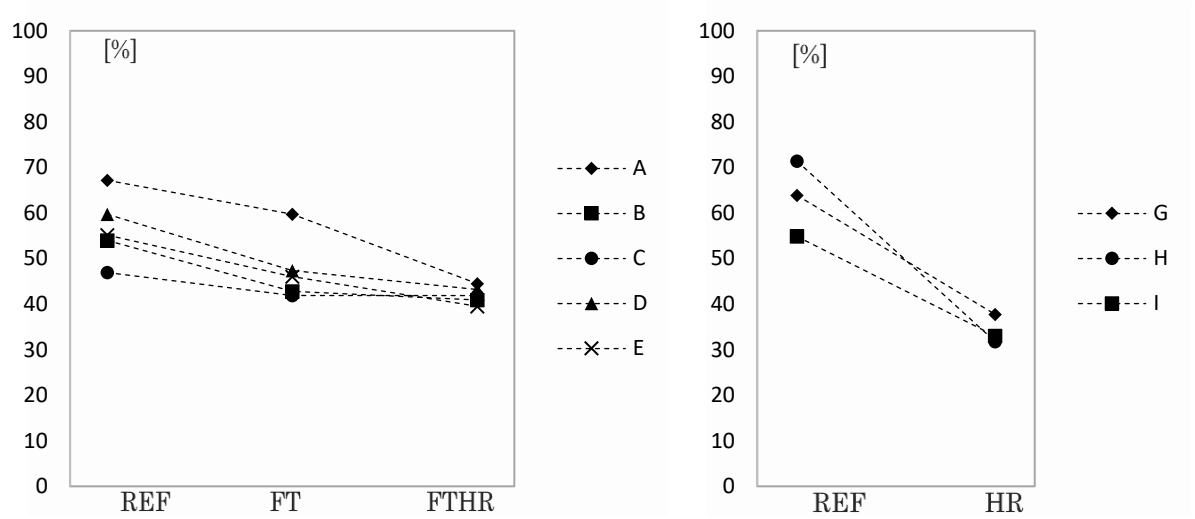

Figure 60 Efficiency factor of the fabrics

4.3.3 Crack investigation

A proper crack investigation is carried out regarding Serviceability Limit State conditions (crack occurance) and durability of the composites. The formation of cracks increase the sensitivity to aggressive substances such as OH^-, enhancing the chemical and physical degradation processes and are therefore of enormous importance considering the durable performance of the composites.

Figure 61 displays the average maximum number of cracks for all specimens that passed the multiple cracking stage. It can be noticed that the reference series having the lowest density (A, D, G, H, I) (Figure 31) show the most total number of cracks, which is a logical sequence of the ACK theory regarding the transition length which is dependent on shear stress. This is improved for higher densities, governing a better bond and therefore a better load bearing capacity, increasing this transition length and resulting in less crack formations. A small deviation of this observation is observed for plate A, but can be abandoned due to the rejection of 2 out of 3 specimens for the reference case, which is statistically incorrect.

Except for some cases, it can be noticed that durability loading reduces the number of cracks. This is against all expectations since a damaged material is more likely to show more cracks. As mentioned before during the investigation on the ultimate strength (Figure 59), the ultimate strain shows a general decrease with exceptional values for series B_FT, which are related to an increase of thickness, reducing the fibre-volume fraction and governing a brittle material behaviour due to the loss in composite interaction. The decrease of other series may be linked to the formation of portlandite in the matrix due to the environmental loading, governing a brittle material behaviour.

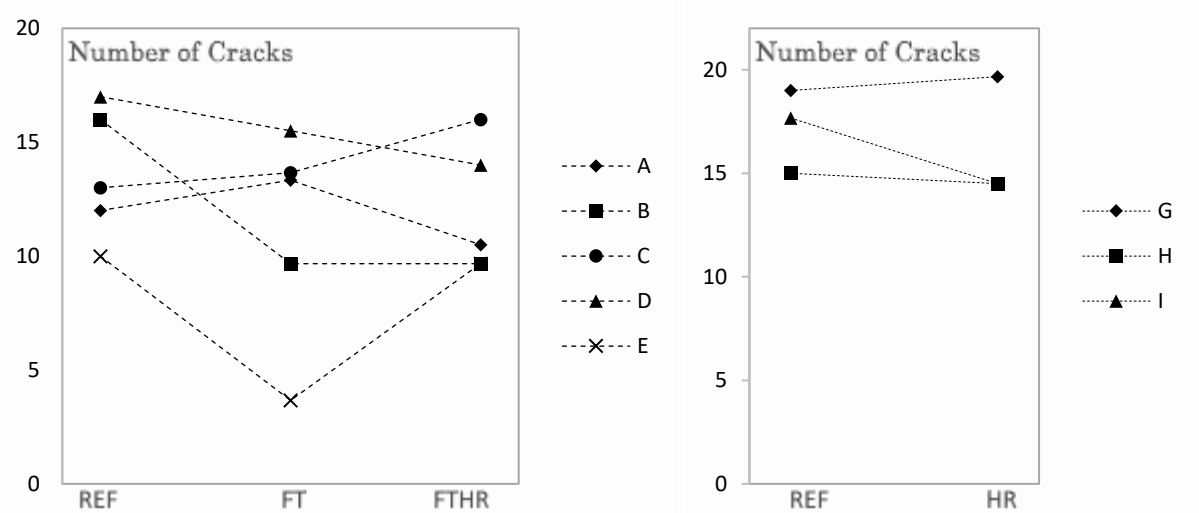

Figure 61 Maximum number of cracks

Table 15 Percental evolution of the total number of cracks after mechanical loading compared to the reference case

	A	B	C	D	E	G	H	I
REF [−]	12**	16**	13*	17*	10*	19	15**	17,7
FT [%]	▲11,1	▼39,6*	▲5,1	▼8,8	▼63,3	–	–	–
FTHR [%]	▼12,1	▼39,6	▼23,1*	▼17,6*	▼3,3	–	–	–
HR [%]	–	–	–	–	–	▲3,5	▼3,3*	▼17,9*

Figure 62 displays the average crack width for all the series and a decreasing trend is observed after durability loading. This means that, anyhow, the crack extension is limited after exposing to durability loading cases, demonstrating that a deterioration of the matrix and/or the fabrics lays at the base of these observations by the formation of portlandite, affecting the performance of both the matrix and the fabrics according to Butler et al. (2010)

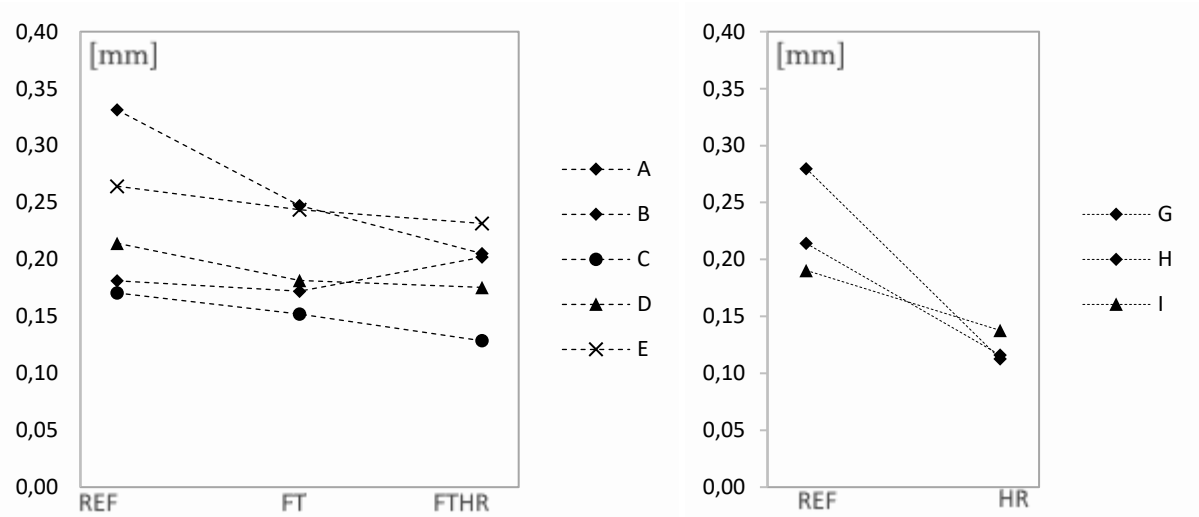

Figure 62 Average crack width

As a short conclusion, durability cycles induce the formation of less cracks than the reference situations. Although the average crack width and, consequently, the ultimate strain show a decrease, proving that durability loading has a negative influence on the mechanical performance of TRC. The fact that the average crack width is decreasing for increasing durability cycles may be seen as a beneficial characteristic, lowering the sensitivity to aggressive substances. According to Butler et al. (2010), this deterioration can be attributed to the formation of portlandite, affecting both the performance of the matrix and the fabrics. Also, the use of AR glass fibres in a high alkali environment can cause deterioration of the latter, but cannot be confirmed for this amount of cycles.

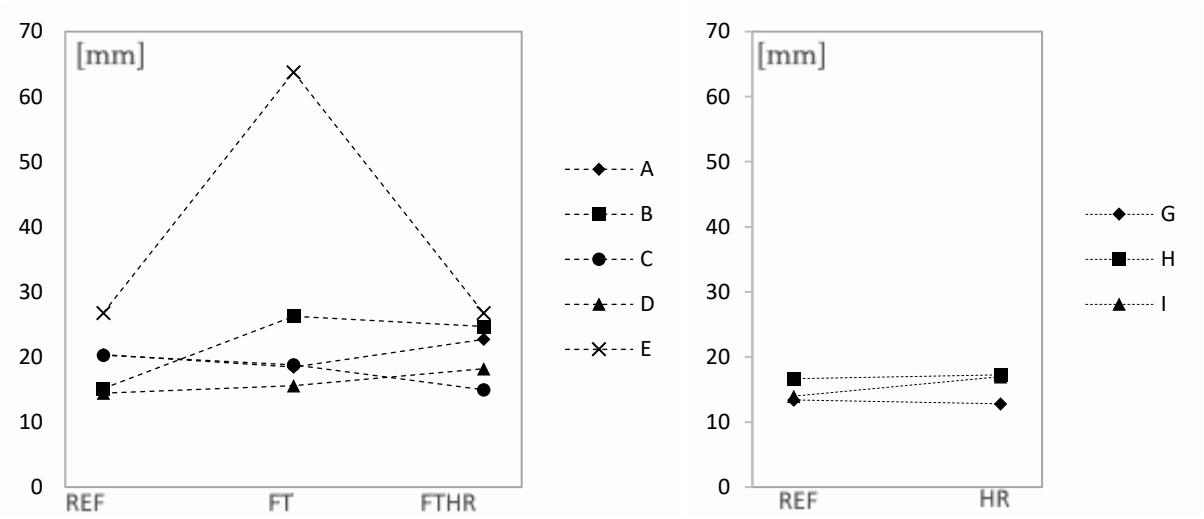

Figure 63 Average crack interdistance

Within these experimental observations, an investigation on the average distance between the cracks is evaluated and displayed in Figure 63. The observations are a logical sequence of the behaviour in strain and average crack width. A very significant increase in crack interdistance is observed for series B_FT, again proving the loss of composite behaviour to brittle behaviour. Furthermore, a general increase in crack interdistance is observed over the series, which is in accordance with the decrease in total number of cracks and the global deterioration of the mechanical performance.

Table 16 Percental evolution of the average crack interdistance after mechanical loading compared to the reference case

	A	**B**	**C**	**D**	**E**	**G**	**H**	**I**
REF [−]	20,35**	15,15**	20,27*	14,43*	26,78*	19	15**	17,7
FT [%]	▼9,4	▲73,2*	▼7,3	▲7,9*	▲138,2	–	–	–
FTHR [%]	▲11,6	▲62,9	▼16,2*	▲26,0*	▲0,1	–	–	–
HR [%]	–	–	–	–	–	▼4,4	▲3,6*	▲21,4*

In order to confirm that durability cracks are linked to the matrix's density, as observed in section 4.2, the durability cracks are compared to the total number of cracks in Figure 64. Again, it can be noticed that, after **the FT durability loading case**, the durability cracks are related to the series density, which is major for series E and B, showing minor durability cracks (up to 6,9%) and the opposite effect is seen for the lowest density, where 12,2% up to 36,6% of the total number of cracks is attributed to durability loading. For **the FTHR durability loading case**, a small decrease of amount of durability cracks is

observed, which can be attributed to late hydration processes. Series B and E show here a small increase, which can be attributed to the above statements. **The HR durability loading case** shows that 13,8% up to 50,8% of the total number of cracks can be attributed to the durability loading.

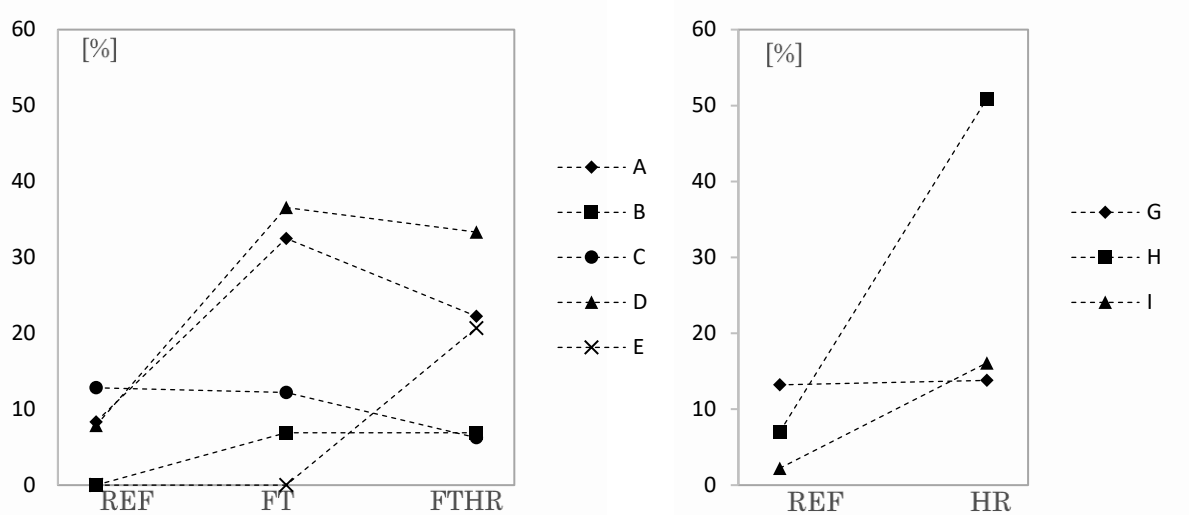

Figure 64 (Durability cracks) / (total number of cracks)

Table 17 Comparison of the durability cracks to the total number of cracks

	A	B	C	D	E	G	H	I
REF [%]	8,3**	0**	12,8*	7,8*	0*	13,2	7,0**	2,2
FT [%]	32,5	6,9*	12,2	36,6*	0	–	–	–
FTHR [%]	22,2	7,0	6,3	33,3	20,7	–	–	–
HR [%]	–	–	–	–	–	13,8	50,8*	16,1*

5. Conclusions

This work covered the influence of environmental loading on the mechanical performance of Textile Reinforced Cementitious Composites for outdoor applications of sandwich panels. This section captures a general conclusion on the effect of the different parameters considering a durable design of such sandwich panels. Within this context, the tensile behaviour of prismatic Textile Reinforced Cementitious composites with a nominal thickness of 10 mm and fibre-volume fraction of 1,69% was investigated under environmental loading according the European standards imposed by EN 12467 (2012).

It was observed that increased thickness of the specimen, attributed to the production process, lowers the fibre-volume fraction towards the critical value, inducing a loss in composite behaviour. The latter causes brittle composite failure.

An extensive study on several mechanical parameters was carried out regarding the Serviceability and Ultimate Limit state. These parameters require essential knowledge concerning the design of sandwich panel faces.

It was observed that the material's stiffness (stage I in the stress – strain curve) can be qualitatively approximated by non-destructive testing techniques such as Ultrasonic Pulse Velocity (UPV) and Resonalyser test methods. Quantitative information should be required from mechanical uniaxial testing. Hereby, it was observed that environmental loading causes initial damage due to the formation of so called durability cracks. Presence of the latter proves that the multiple cracking stage has already reached, implying a decrease in stiffness.

Freeze-thaw cycling induced a decrease in stiffness varying between around 40% and 80% compared to the reference situation, showing initial stiffness values between 9,0 GPa 15,6 GPa. Further environmental loading to heat-rain cycles caused a slight increase in stiffness which can be attributed to late hydration processes. Nevertheless, a global decrease with respect to the reference specimens was observed varying between 2% and 80%. This wide range may be attributed to the density variation on the series, influencing the late hydration processes. Heat-rain cycles induced a decrease between around 70% and 80%. It can be noticed that environmental loading may cause deterioration of the stiffness up to 80%, whatever the type of loading. Regarding the need to limit deflections for sandwich panels implied by the Serviceability Limit State conditions, this degradation in stiffness is significantly high, with the consequence of a low durable performance.

Observations showed that the first cracking strength is strongly related to the matrix density, enhancing the first cracking stress with increasing density. The first cracking strength of the investigated specimens is found between 1,9 MPa and 3,3 MPa. Regarding this observation, deterioration of this property may be attributed to physical or chemical degradation of the matrix. Freeze-thaw cycling caused no significant reduction of the first cracking strength, with sometimes even an increase for series showing a relatively higher density, pointing on late hydration processes governing the formation of CSH phases. On the opposite, a maximum decrease of 25% is observed for

the specimens with the lowest density. Further subjection of these specimens to heat-rain cycles induces a global deterioration with maximal values of around 50% for the lower density specimens, while no significant increase was observed for higher density specimens. Specimens subjected to heat-rain cycles showed a decrease between 20% and 25%. Therefore, it can be concluded that environmental loading will induce a deterioration of the first cracking strength in time, which is delayed with increasing matrix density.

The ultimate strength of the investigated composite varies from 4,5 MPa to 6,9 MPa. Environmental loading showed a decrease of the ultimate capacity, going from 10% to 25% after subjection to freeze-thaw cycles. Further exposure to heat-rain cycles enhanced the degradation of this property between approximately 10% and 35%. Heat-rain cycles separately seemed to degrade the ultimate capacity most significant with decreases between 40% and 55%. Degradations due to environmental loading may be attributed to physical and chemical processes, where the latter find cause in the formation of portlandite, affecting the ductile behaviour of the composite and the performance of the fabrics. The according ultimate strains follow the same tendency.

Deeper investigation on the crack development showed that environmental loading induces up to 50% of total number of cracks before failure, depending on the density and thickness of the specimen. The appearance of cracks may be classified under SLS conditions, but should be interpret very carefully. Some may interpret the formation of cracks as an exceedance of the SLS requirements, while others may interpret the crack formation and propagation until a certain width as an acceptable SLS condition.

In extension of this SLS conditions, it is important to have knowledge on the average width of these cracks, since the latter increase the sensitivity to aggressive substances and will cause decrease in durable performance. These average crack widths decrease slightly after environmental loading, which may be considered as beneficial regarding the durability performance of sandwich panels consisting of TRC composite faces.

6. Future Works

Within this chapter, the author enumerates some additional research that could be of interest for the investigation on durability of TRC.

Scanning Electron Microscopy

In order to get a better understanding of the influence of micro processes on the mechanical behaviour of TRC, a Scanning Electron Microscope (SEM) could be used to observe the formation of portlandite and other precipitation phases in the matrix and around the fabrics. Also, the formation of the CSH, governing the strength of the matrix, can be monitored and analyzed.

pH measurements

The pH-level of the matrix affects the performance of the fabrics. Therefore, it could be very interesting to monitor the evolution of the pH during the environmental loading to determine the latter on the mechanical performance of the fabrics.

Composition of the Matrix

Within this work, the exact cement composition was not known. For further investigations, it might be interesting to compose the cementitious matrix with well-known proportions and materials. This gives the author the freedom to add or reject specific materials such as fly ash and micro silica to buffer the pH of the matrix. Also, variations on the amount of Portland cement clinker may be adapted to have a certain control over the hydration processes and precipitation phases in time.

Variation in fibre-volume fraction

Investigation on specimens with different fibre-volume fractions could be of interest to determine the most preferable fraction with eye on durability and mechanical performance.

Micro cracks due to restricted shrinkage

When cooling down the specimens in water after exposure to high temperatures (Heat-rain cycles), micro cracks have been observed which are related to restricted shrinkage. It could be of interest to characterize the influence of these micro cracks on the crack initiation and propagation during the uniaxial tension tests. Deeper investigation on this phenomenon could be related to a decrease in stiffness after a first set of Heat-Rain cycles and can be monitored using a non-destructive technique such as the resonalyser test method or the Ultrasonic Pulse Velocity method. Within this research, the variation in fibre-volume fraction could have a significant role.

Sandwich beams

Investigation on the influence of environmental loading on the mechanical behaviour of an entire sandwich beam could be of interest to understand the global sandwich interaction. Originally, this was one of the objectives of this master thesis, but could not be realized due to technical problems with the provided climate chamber.

References

AC Tech. (1996). *Technical Bulletin 7*. (Allied Construction Technologies Inc.) Retrieved Maart 12, 2017, from http://actamerican.net/media/1061/technical-bulletin-07-alkalinity-in-concrete-slabs.pdf

ASTM International. (1997). Designation: C 666/C 666M -03. *Designation: C 666/C 666M -03 Standard Test Method for Resistance of Concrete to Rapid Freezing and Thawing*. Department of Defence, United States.

Aveston, J., Cooper, G.A. and Kelly, A. (1971). *Single and Multiple Fracture, The Properties of Fibre Composites.* Conference Proceedings National Physical Laboratories, IPC Science & Technology Press Ltd. London, 15-24.

Beckert Groz Kg. (2011). *Inside Composites*. (Orange Zero Ltd.) Retrieved March 2017, from http://www.insidecomposites.com/textile-concrete-bridge-in-albstadt-lautlingen/

Bentur, A. and Mindes, S. (2007). *Fibre Reinforced Cementitious Composites*. Taylor and Francis, New York, USA, 601 pages

Brameshuber, W. (2006). *State of the Art report of RILEM Technical Committee TC 201-TRC:Textile Reinforced Concrete*. RILEM Publications, Bagneux, France, 273 pages

Brameshuber, W. (2016) *Recommendation of RILEM TC 232 TDT: test methods and design of textile reinforced concrete.* Materials and Structures, 49:4923-4927, RILEM Technical Committee, Aachen

Butler, M., Mechtcherine, V. and Hempel, V. (2010). *Durability of textile reinforced concrete made with AR glass fibre: Effect of the matrix composition*. Materielas and Structures ISSN 1359-5997 Vol. 43, Dresden

Çavda A. (2013). *Investigation of freeze-thaw effects on mechanical properties of fibre reinforced cement mortars*. Journal of Composites: Part B 58 463-47, Faculty of Engineering, Gumushane University, Turkey

Colombo, I., Colombo, M. and di Prisco, M. (2015). *Tensile behavior of textile reinforced conctrete subjected to freezing*. Journal of Cement and Concrete Research 169-183, Department of Civil Environmental Engineeringing, Milan, Italy

Colombo, I., (2015). *Multilayer Precast Façade Panel: Structural Optimization for Energy Retrofitting*. PhD Thesis, Politecnico di Milano, Department of Civil and Environmental Engineering; pages 260

Craig, A. and Norman, A. (2004). *Material selection in sandwich beam construction.* Scripta Materialia 50, 1335-1339, Cambridge University Engineering Department, Cambridge, United Kingdom

Cuypers H. (2001). *Analysis and Design of Sandwich Panels with Brittle Matrix Composite Faces for Building Applications.* PhD Thesis, Vrije Universiteit Brussel, Facultry of Engineering Sciences, 235 pages

Cuypers, H., Tysmans, T., Waastiels, J. and Adriaenssens, S. (2008). *Structural analysis of small span textile reinforced concrete shells*. Journal of Composites Science and Technology 1790-1796, Vrije Universiteit Brussel, Faculty of Engineering Science, Brussels, Belgium

De Baere, I., Sol, H., Van Hemelrijck, D., Petreli, A., Van Paepegem, W. (2007). *Comparison of different identification techniques for measurement of quasi-zero Poisson's ratio of fabric-reinforced laminates*. journal of Composites, Part A 38 2047-2054, Belgium

De Munck M. (2014). *Het conceptueel ontwerp van een lichtgewicht gevelsysteem voor nieuwbouw en renovatie*. IWT aanvraag voor Baekelandmandaat, Vrije Universiteit Brussel, Brussels.

Gao, S.L., Mäder, E., Plonka, R. (2004). *Coatings for glass fibres in a cementitious matrix*. Acta Materialia 52:4745-4755

Harris. Devin (2017). *Digital Image Correlation*. (University of Virginia, Engineering) Retrieved April 23, 2017, from http://cee.virginia.edu/devinharris/category/digital-image-correlation/

Hegger, J., Kulas, C., Schneider, C., Brameshuber, W. (2010). *TRC Pedestrian Bridge - Design, Load-bearing behavior and production processes of a slender and light-weight construction*. International RILEM conference on Material Science,, RILEM Publications SARL, pages 353-364, Aachen

Hempel, R., Butler M., Hempel, S., Schorn, H . (2005). *Durability of textile reinforced concrete. Proceedings of the international RILEM workshop on high performance fibre reinforced cementitious composites in structural applications*. International RILEM conference on Material Science,, New York

Huang, M., Jiang, L., Liaw, P., Brooks, C., Seeley, R., Klarstrom, D. (1998). *Using Acoustic Emission in Fatigue and Fracture Materials Research*. The Minerals, Metals & Materials Society. Retrieved April 2017, 23, from http://www.tms.org/pubs/journals/JOM/9811/Huang/Huang-9811.html

Hwang, C.L. and Young, J.F. (1984). *Drying shrinkage of Portland Cement Pastes.* Journal of the American Ceramic Society, Vol. 70, Issue 5, pages 323-328, National Taiwan Institute of Technology, Taiwan

Knauf. (2017). *K445 Knauf Gitex - Gitex LW - Autex Universeel - Isoltex*. (Knauf) Retrieved October 18, 2016, from http://www.knauf.be/nl/product/isoltex

Majumdar, A.J., West, J.M. and Larner, L.J. (1977). *Properties of glass fibres in cement environment.* Journal of Material Sciences, Vol. 12, Issue 5, pages 927-936, United states

McCormick, N. and Lord, J. (2010). *Digital Image Correlation*. Materials Today, Vol. 13, Issue 12, pages 52-54, National Physical Laaboratory (NPL), United Kingdom

Neville, A. (1996). *Properties of Concrete*. Properties of Concrete, 5th edition, New York

Orlowski, J., and Raupach, M. (2008). *Durabilit model for AR-glass fibres in textile-reinforced concrete.* Journal of Materials and Structures, Vol. 41, Issue 7, pages 1225-1233, Aachen

Portal, N., Perez, I. F., Thrane, L., Lundgren, K. (2014). *Pull-out of textile reinforcement in concrete*. Elsevier. Journal of Construction and Building Materials, Vol. 71 pages 63-71, United Kingdom

Purnell, P., Short, N. R. (2001). *A static fatigue model for the durability of glass fibre reinforced cement.* Journal of Materials Science, Vol. 36, Issue 22, pages 5383-5390

Remy O. (2012). *Lightweight Stay-in-Place formwork: "a concept for future building applications"*. PhD Thesis, Vrije Universiteit Brussel, Faculty of Engineering Sciences, pages 291

Sadatoshi, O. and Hannant, D.J. (1994). *Modelling the Stress-Strain Response of Continuous Fibre Reinforced Cement composites*. Materials Journal, VOl. 91, Issue 3, Pages 306-312

Saint-Pierre, F., Philibert, A., Giroux, B., and Rivard, P. (2016). *Concrete Quality Designation based on Ultrasonic Pulse Velocity*. Construction and Building Materials, Vol. 125, Pages 1022-1027, Canada

Satoru, Y. and Go, M. (n.d.). *Digital Image Correlation*. Department of Mechanical Engineering, Aoyama Gakuin University

Sigmunde, B. (2014). *Sortenreine 3D Textilien zur Betonarmierung* (Detail) Retrieved October 22, 2016, http://www.detail.de/artikel/sortenreine-3d-textilien-zur-betonarmierung-12411/

Tillman BV (2017). *Tillman Chemische Bouwstoffen*. Retrieved October 17, 2016, from http://tillman.nl/CB/CBM/producten.htm

Tomoscheit (n.d.). *Project life Insu-Shell,* RWTH Aachen University, Aachen, Germany. Retrieved December 22, 2016, http://www.irbnet.de/daten/iconda/CIB21709.pdf

Tysmans, T., (2010). *Design of anticlastic shells in innovative textile reinforced coment composites*. PhD Thesis, Vrije Universiteit Brussel; pages 269

Vlaamse Overheid. (2016). Retrieved from EPB U Waarden: http://www2.vlaanderen.be/economie/energiesparen/epb/doc/epbuwaarden2017.pdf

Walraven, J., Agnieszka, B. and Vrouwenvelder, T. (2010). *fib Model for Concrete Structures*. fib Journal, Structural Concrete, The Netherlands

Witczak, M.W., Kaloush, K., El-Basyouny M., Pellinen, T. and Von Quintus, H. (2002). *NCHRP Report 465: Simple Performance Test for Superpave Mix Design.* Materials and Construction, Transportation Research Board, National Research Council, Washington DC

Zenckert, D. (1995). *An introduction to Sandwich Construction.* Engineering Materials Advisory Services EMAS, pages 277

Zinck, P., Mäder, E., Gerard, J.F. (2001). *Role of silane coupling agent and polymeric film former for tailoring glass fibre sizings from tensile strength measurements*. Journal of Materials Science, Vol. 36, Issue 21, pages 5245-5252, Germany

Annex A
Materials and Methods

Table A1 Characteristic dates and density of every plate

Plate	Day of production	Day of demolding	Day of cutting	Density (kg/m^3)
A	21/11/2016	23/11/2016	06/01/2017	1707.12
B	21/11/2016	23/11/2016	06/01/2017	1872.85
C	21/11/2016	23/11/2016	06/01/2017	1806.63
D	23/11/2016	19/12/2016	06/01/2017	1603.86
E	23/11/2016	19/12/2016	06/01/2017	1806.70
F	23/11/2016	06/01/2016	06/01/2017	1844.50
G	26/12/2016	10/01/2016	02/03/2017	1655.52
H	26/12/2016	10/01/2016	02/03/2017	1681.86
I	26/12/2016	10/01/2016	02/03/2017	1606.25

Table A2 Comparison of the mechanical behaviour to the ACK model values

	ACK	**A**	**B**	**C**	**D**	**E**	**G**	**H**	**I**
					σ_{mc} [MPa]				
AVG	2,25	2,89	2,40	2,80	2,31	3,34	1,96	2,25	2,09
STD	-	0,22	-	0,42	0,30	0,63	0,19	0,80	0,34
%	1,00	1,28	1,07	1,24	1,03	1,48	0,87	1,00	0,93
					E_{c1} [GPa]				
AVG	15,74	14,01	17,12	14,07	11,38	15,40	12,86	14,73	8,99
STD	-	4,02	2,12	2,40	1,08	9,27	8,73	8,05	4,10
%	1,00	0,89	1,09	0,89	0,72	0,98	0,82	0,94	0,57
					E_{c3} [GPa]				
AVG	0,59	0,41	0,28	0,27	0,30	0,30	0,35	0,37	0,31
STD	-	-	-	-	0,05	0,05	0,03	-	0,03
%	1,00	0,69	0,46	0,45	0,50	0,50	0,59	0,63	0,52

Figure A1 Freeze-thaw cycles: Planning

Figure A2 Heat-rain cycles: Plannin

Annex B
Uniaxial tension test results

Within this annex, a global overview of the stress-strain curve of every tested specimen can be found. Also, an extensive table reports the general properties and mechanical properties of every specimen tested.

The **general properties** cover the thickness, width and length measured in a statistic representative way. This means that several measurements along the thickness, width and length have been performed and are averaged afterwards. Every specimen is then weighted to determine the density.

The **mechanical properties** displayed are the following

- $\#DC$ Number of durability cracks observed with DIC
- E_1 Young's modulus in stage I according to the ACK theory. This value is determined using a best fit over the first linear stage
- σ_{fc} The first cracking strength is defined as the first load drop observed in the stress-strain curve and is checked with an abrupt appearance of the first (mechanical) crack in DIC
- σ_{lc} The last cracking strength is defined as the last load drop observed in the stress-strain curve and is checked with an abrupt appearance of the last crack in DIC
- δ_{lc}/L The strain at the end of the Multiple cracking stage is defined as the strain after the last load drop is observed and is checked with an abrupt appearance of the last crack in DIC
- $\#TC$ Total number of cracks observed with DIC after the multiple cracking stage
- δ/L The strain variation between the first and last load drop in the stress-strain curve
- E_3 Young's modulus in stage III according to the ACK theory. This value is determined using a best fit over the linear stage
- σ_{max} The ultimate stress at specimen failure
- δ_{max}/L The ultimate strain at specimen failure
- $Fail$ Defines the failure mechanism of the specimen. C designates failure in the clamps, while G defines a 'good' failure mechanism (no failure in the clamps). These mechanisms are displayed in Figure B9.

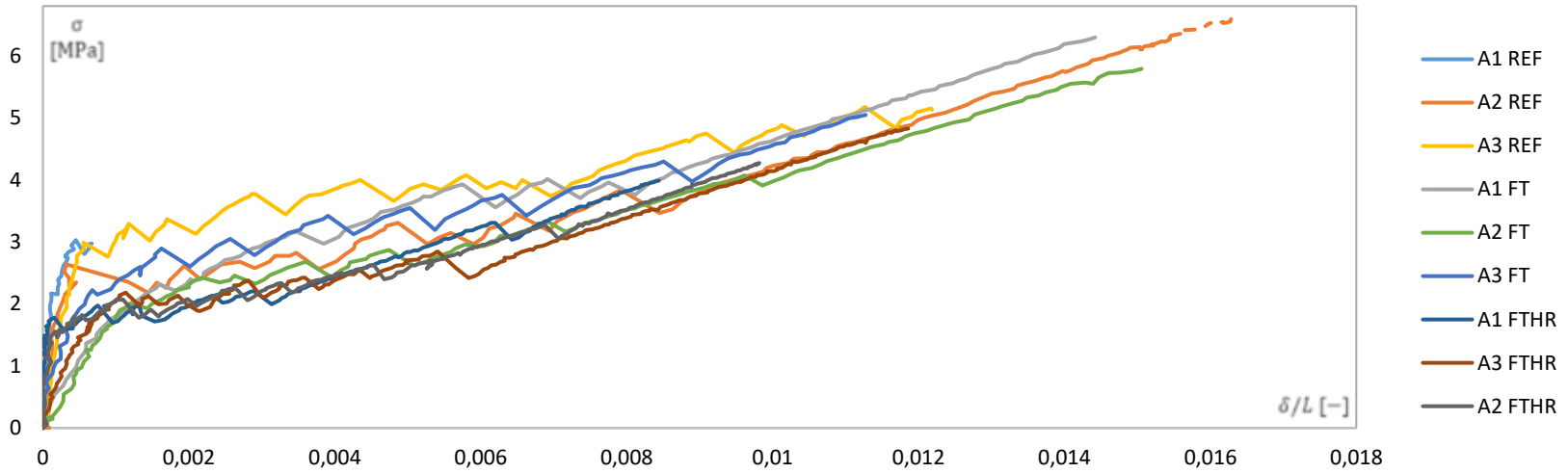

Figure B1 Stress-strain curve of Series A

Table B1 General and Mechanical properties of Series A

A		General properties					Mechanical properties									
		t	w	l	ρ	#DC	E_1	σ_{fc}	σ_{lc}	δ_{lc}/L	#TC	δ/L	E_3	σ_{max}	δ_{max}/L	Fail
		mm	mm	mm	kg/m^3	–	GPa	MPa	MPa	10^{-3}	–	10^{-3}	GPa	MPa	10^{-3}	–
REF	A1	10,466	50,89	475	1675,9	1	17,88	3,03	-		-	-	-	-	-	C
	A2	10,016	50,89	475	1738,9	1	14,30	2,64	3,84	8,45	12	8,12	0,406	6,59	16,20	C
	A3	9,948	50,89	475	1800,6	1	9,86	2,99	-	-	-	-	-	-	-	C
FT	A1	10,074	50,89	475	1687,8	5	1,74	2,32	3,96	8,11	13	6,52	0,372	6,30	14,00	G
	A2	10,436	50,89	475	1704,5	5	2,04	2,00	4,07	9,86	16	8,67	0,287	5,79	15,31	G
	A3	10,332	50,89	475	1709,7	3	5,77	2,22	4,54	10,05	11	9,37	0,380	5,05	11,42	G
FTHR	A1	10,094	50,89	475	1733,6	2	19,23	1,78	3,31	6,43	9	6,27	0,354	3,99	8,46	G
	A2	10,182	50,89	475	1673,9	1	14,95	1,56	3,27	7,07	12	6,90	0,410	4,25	9,78	G
	A3	9,742	50,89	475	1639,1	4	3,24	1,69	2,85	5,66	12	4,99	0,287	4,89	12,00	G

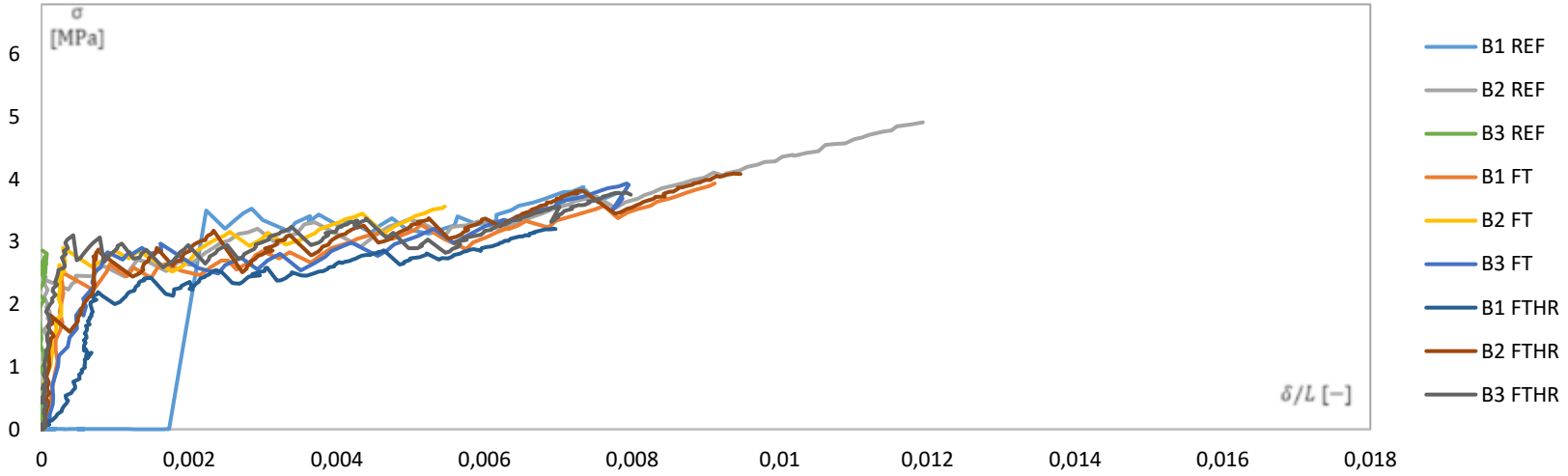

Figure B2 Stress-strain curve of Series B

Table B2 General and Mechanical properties of Series B

B		General propzerties					Mechanical properties										
		t	w	l	ρ	#DC	E_1	σ_{fc}	σ_{lc}	δ_{lc}/L	#TC	δ/L	E_3	σ_{max}	δ_{max}/L	Fail
		mm	mm	mm	kg/m^3	–	GPa	MPa	MPa	10^{-3}	–	10^{-3}	GPa	MPa	10^{-3}	–
REF	B1	10,632	50,91	475	1878,5	-	-	-	-	-	-	-	-	-	-	C
	B2	10,798	50,91	475	1918,5	0	15,62	2,40	3,73	7,77	16	7,74	0,275	4,91	11,96	G
	B3	10,742	50,91	475	1589,8	-	-	-	-	-	-	-	-	-	-	C
FT	B1	11,282	50,91	475	1924,2	1	7,43	2,51	3,33	6,86	12	6,59	0,424	3,94	9,04	G
	B2	11,278	50,91	475	1932,2	0	7,42	2,91	-	-	7	-	-	3,57	5,70	G
	B3	11,162	50,91	475	1911,5	1	3,22	2,84	3,21	5.59	10	4,69	0,390	3,70	5,70	G
FTHR	B1	10,966	50,91	475	1911,8	2	1,68	2,14	2,81	5,38	10	4,56	0,298	3,21	7,00	G
	B2	11,03	50,91	475	1893,2	0	9,04	1,83	3,82	7,77	9	7,65	0,207	4,08	9,40	G
	B3	10,752	50,91	475	1896,0	0	13,89	3,10	3,04	5,47	10	5,04	0,253	3,75	8,00	G

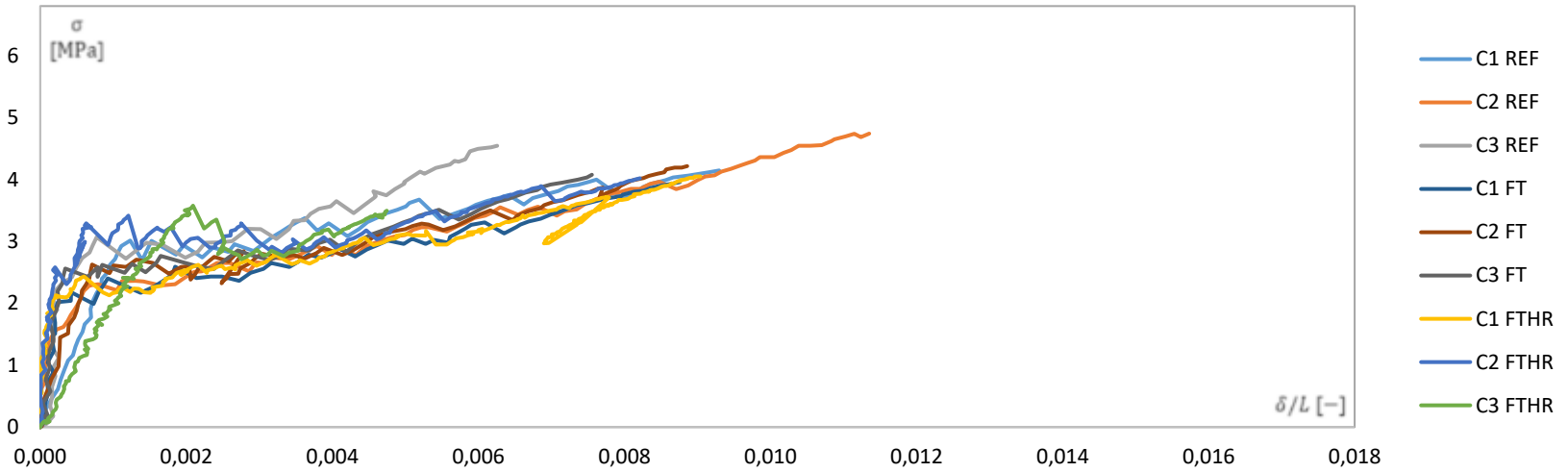

Figure B3 Stress-strain curve of Series C

Table B3 General and Mechanical properties of Series C

C		General properties					Mechanical properties									
		t	w	l	ρ	#DC	E_1	σ_{fc}	σ_{lc}	δ_{lc}/L	#TC	δ/L	E_3	σ_{max}	δ_{max}/L	Fail
		mm	mm	mm	kg/m^3	–	GPa	MPa	MPa	10^{-3}	–	10^{-3}	GPa	MPa	10^{-3}	–
REF	C1	10,776	51,05	471	1644,2	2	2,82	3,01	4	7,98	12	6,75	-	4,14	9,33	G
	C2	10,426	51,05	471	1791,2	2	12,38	2,31	3,97	8,71	18	7,91	0,265	4,74	11,35	G
	C3	9,664	51,05	471	1794,7	2	15,77	3,07	-	-	9	-	-	4,54	6,26	G
FT	C1	10,294	51,05	471	1850,5	1	6,61	2,18	3,31	6,35	14	5,93	0,269	3,95	9,00	G
	C2	10,18	51,05	471	1871,2	2	4,24	2,63	3,50	6,47	15	5,76	0,352	-	-	C
	C3	10,152	51,05	471	1851,8	2	7,83	2,56	3,51	5,73	12	5,39	0,336	4,08	7,54	G
FTHR	C1	10,326	51,05	471	1832,7	2	12,78	2,13	3,57	7,24	17	7,03	0,342	4,05	9,04	G
	C2	10,002	51,05	471	1808,9	0	15,46	2,58	3,90	7,046	15	6,84	0,345	4,02	8,20	G
	C3	9,582	51,05	471	1814,4	-	-	-	-	-	-	-	-	-	-	C

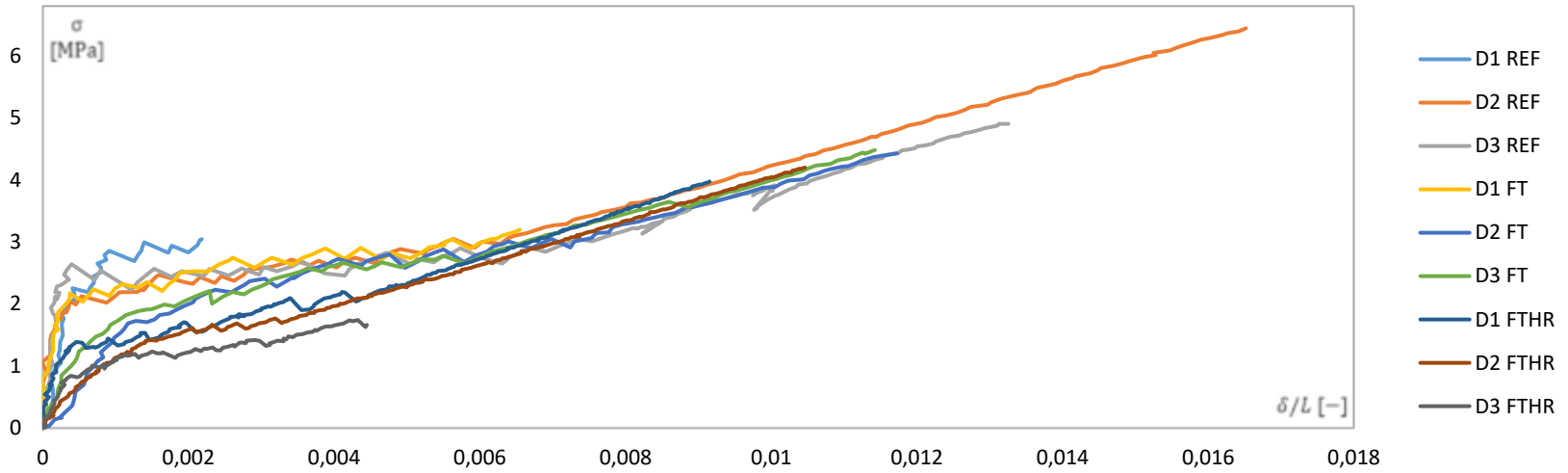

Figure B4 Stress-strain curve of Series D

Table B4 General and Mechanical properties of Series D

D		General properties					Mechanical properties									
		t	w	l	ρ	#DC	E_1	σ_{fc}	σ_{lc}	δ_{lc}/L	#TC	δ/L	E_3	σ_{max}	δ_{max}/L	Fail
		mm	mm	mm	kg/m^3	–	GPa	MPa	MPa	10^{-3}	–	10^{-3}	GPa	MPa	10^{-3}	–
REF	D1	10,624	50,83	475	1590,5	1	10,41	2,25	-	-	-	-	-	-	-	C
	D2	10,308	50,83	475	1611,1	2	12,55	2,05	3,01	6,28	17	5,92	0,336	6,44	16,50	G
	D3	10,438	50,83	475	1587,1	1	11,17	2,64	3,04	7,55	17	7,15	0,26	4,90	13,20	C
FT	D1	10,378	50,83	475	1616,2	2	3,97	2,49	-	-	12	-	-	-	-	C
	D2	10,5	50,83	475	1581,7	8	1,85	1,99	3,65	8,86	16	7,20	0,349	4,48	11,50	G
	D3	10,414	50,83	475	1610,6	7	1,44	1,73	2,91	7,29	15	6,02	0,292	4,43	11,80	G
FTHR	D1	10,404	50,83	475	1612,2	3	4,34	1,38	2,18	4,30	11	3,76	0,391	3,97	9,10	G
	D2	10,402	50,83	475	1608,5	9	1,13	1,23	1,77	3,27	17	2,12	0,401	4,20	10,50	G
	D3	10,374	50,83	475	1616,8	2	1,89	0,84	-	-	-	-	-	-	-	G

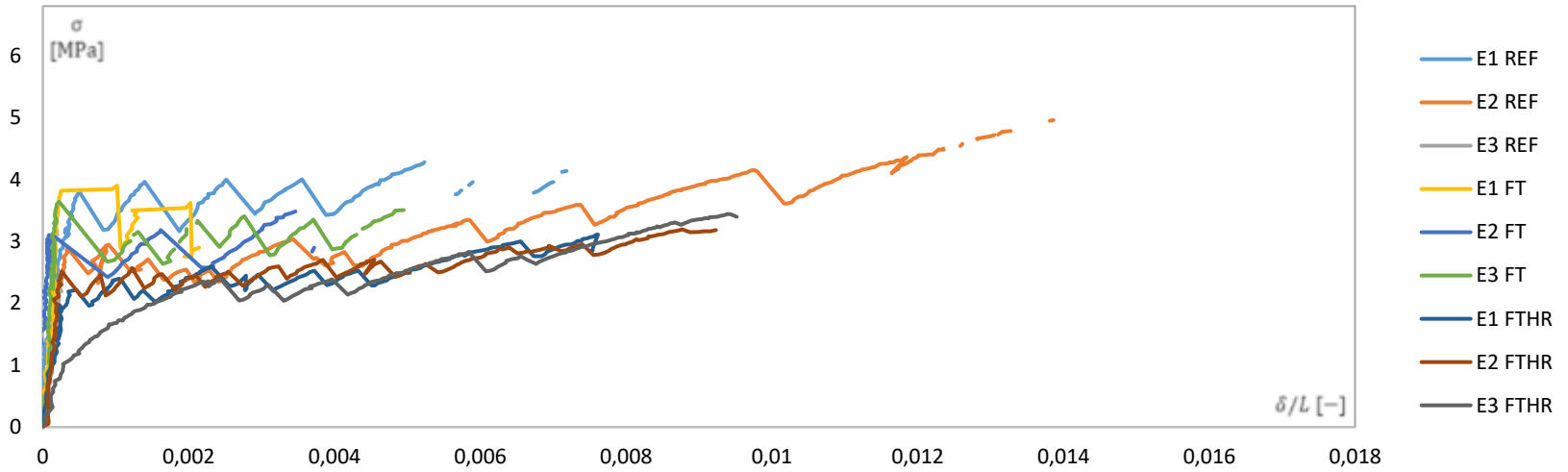

Figure B5 Stress-strain curve of Series E

Table B5 General and Mechanical properties of Series E

E		General properties					Mechanical properties									
		t	w	l	ρ	#DC	E_1	σ_{fc}	σ_{lc}	δ_{lc}/L	#TC	δ/L	E_3	σ_{max}	δ_{max}/L	Fail
		mm	mm	mm	kg/m^3	–	GPa	MPa	MPa	10^{-3}	–	10^{-3}	GPa	MPa	10^{-3}	–
REF	E1	11,124	50,82	479	1802,1	0	20,52	3,79	4,292	6,74	7	6,225	0,336	4,48	7,7	G
	E2	11,832	50,82	479	1822,8	0	8,63	2,90	4,14	10,17	13	9,83	0,260	4,96	13,90	G
	E3	11,534	50,82	479	1755,9	-	-	-	-	-	-	-	-	-	-	G
FT	E1	12,69	50,82	479	1845,2	0	16,73	3,90	-	-	4	-	-	3,58	3,30	G
	E2	13,188	50,82	479	1788,0	0	22,86	3,10	3,90	2,17	2	2,05	0,349	3,48	3,50	G
	E3	12,704	50,82	479	1830,2	0	20,77	3,64	3,35	3,97	5	3,75	0,292	3,51	5,00	G
FTHR	E1	12,362	50,82	479	1840,9	4	3,33	2,39	2,77	6,63	8	4,19	0,391	3,40	9,40	G
	E2	12,534	50,82	479	1805,9	1	5,72	1,89	3,00	6,73	8	6,51	0,401	2,85	7,60	G
	E3	12,236	50,82	479	1769,3	1	13,61	2,51	2,96	7,55	13	7,29	-	3,18	9,20	G

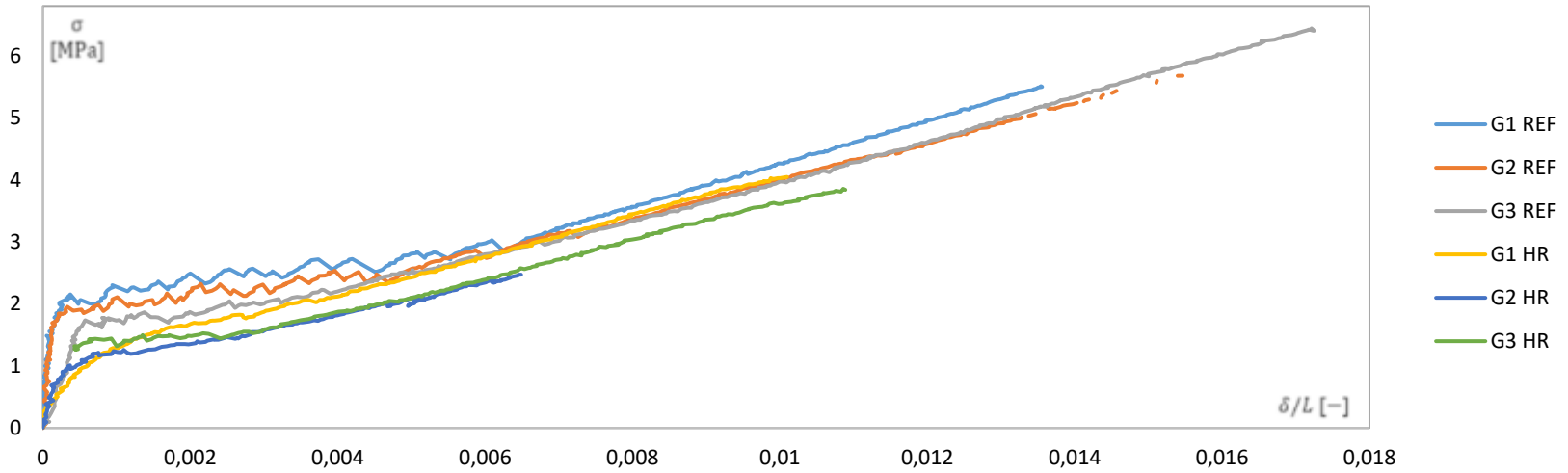

Figure B6 Stress-strain curve of Series G

Table B6 General and Mechanical properties of Series G

G		General properties					Mechanical properties									
		t	w	l	ρ	#DC	E_1	σ_{fc}	σ_{lc}	δ_{lc}/L	#TC	δ/L	E_3	σ_{max}	δ_{max}/L	Fail
		mm	mm	mm	kg/m^3	–	GPa	MPa	MPa	10^{-3}	–	10^{-3}	GPa	MPa	10^{-3}	–
REF	G1	10,216	49,74	485	1635,1	1	20,38	2,15	3,03	6,25	16	5,875	0,375	5,51	13,6	G
	G2	10,756	49,74	485	1649,4	1	14,90	1,96	3,18	7,26	22	6,93	0,323	6,35	17,70	G
	G3	10,572	49,74	485	1658,5	2	3,29	1,77	3,01	6,81	22	5,92	0,35	6,44	17,20	G
HR	G1	10,848	49,74	485	1665,9	12	1,37	1,65	2,06	3.71	17	1,83	0,262	4,05	10,00	G
	G2	11,158	49,74	485	1641,9	12	4,24	1,65	1,57	2,98	13	1,11	0,309	2,47	6,40	G
	G3	11,008	49,74	485	1649,3	6	2,83	1,44	1,55	2,85	21	2,14	0,263	3,85	10,90	G

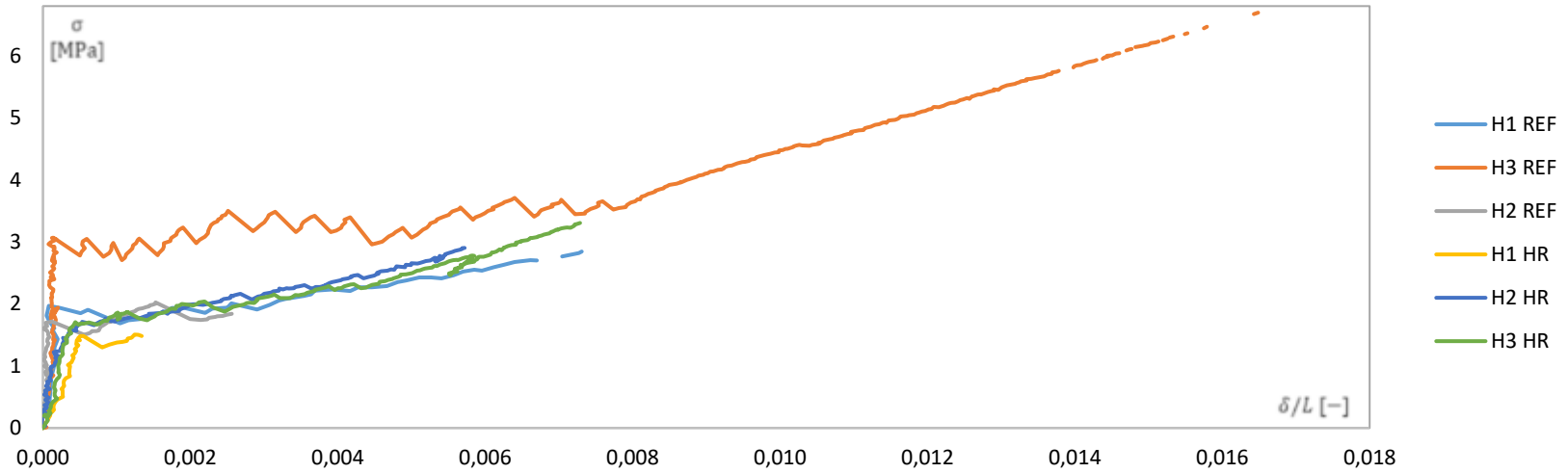

Figure B7 Stress-strain curve of Series H

Table B7 General and Mechanical properties of Series H

H		General properties					Mechanical properties									
		t	w	l	ρ	#DC	E_1	σ_{fc}	σ_{lc}	δ_{lc}/L	#TC	δ/L	E_3	σ_{max}	δ_{max}/L	Fail
		mm	mm	mm	kg/m^3	–	GPa	MPa	MPa	10^{-3}	–	10^{-3}	GPa	MPa	10^{-3}	–
REF	H1	10,908	49,64	484	1656,2	0	7,56	1,97	-	-	-	-	-	-	-	G
	H2	10,596	49,64	484	1657,8	1	23,44	1,72	-	-	-	-	-	-	-	G
	H3	10,486	49,64	484	1691,0	0	13,19	3,07	3,56	7,92	15	7,78	0,37	6,86	16,80	G
HR	H1	10,47	49,64	484	1677,7	2	2,76	-	-	-	-	-	-	-	-	G
	H2	10,26	49,64	484	1675,5	3	7,59	1,71	2,72	5,35	15	4,82	0,419	2,90	5,70	G
	H3	10,366	49,64	484	1694,6	2	3,96	1,71	2,32	4,31	14	3,88	0,319	3,31	7,30	G

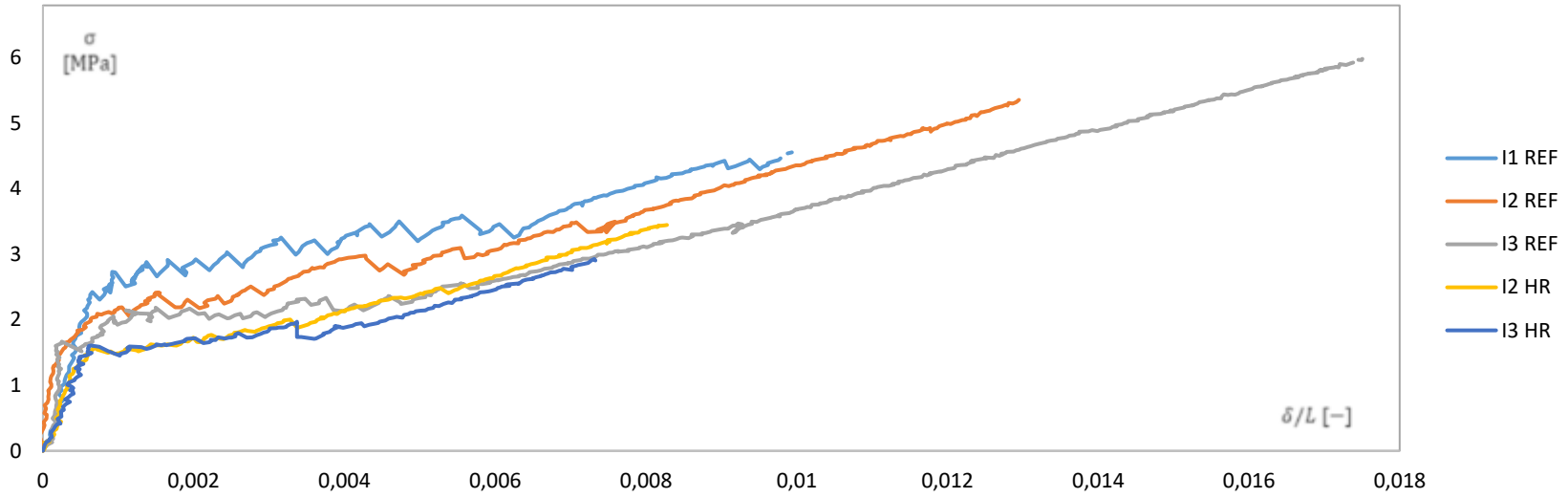

Figure B8 Stress-strain curve of Series I

Table B8 General and Mechanical properties of Series I

I		General properties					Mechanical properties									
		t	w	l	ρ	#DC	E_1	σ_{fc}	σ_{lc}	δ_{lc}/L	#TC	δ/L	E_3	σ_{max}	δ_{max}/L	Fail
		mm	mm	mm	kg/m^3	–	GPa	MPa	MPa	10^{-3}	–	10^{-3}	GPa	MPa	10^{-3}	–
REF	I1	10,054	50,06	483	1625,1	3	4,96	2,42	3,46	6,25	17	5,59	0,296	4,71	10,9	G
	I2	10,281	50,06	483	1616,6	4	8,86	2,19	3,49	7,22	17	6,17	0,336	5,36	13,00	C
	I3	10,356	50,06	483	1598,3	0	13,17	1,67	2,55	5,66	19	5,41	0,28	5,98	17,40	G
HR	I1	10,131	50,06	483	1620,1	-	-	-	-	-	-	-	-	-	-	-
	I2	10,305	50,06	483	1610,4	3	2,47	1,55	2,48	5.38	14	4,66	0,292	3,44	8,30	G
	I3	10,512	50,06	483	1562,7	1	2,38	1,61	2,22	5,25	15	4,62	0,319	2,90	7,90	G

Figure B9 Failure mechanism of Series A, B, C, E, G, H and I

Annex C
DIC images of Durability Cracks

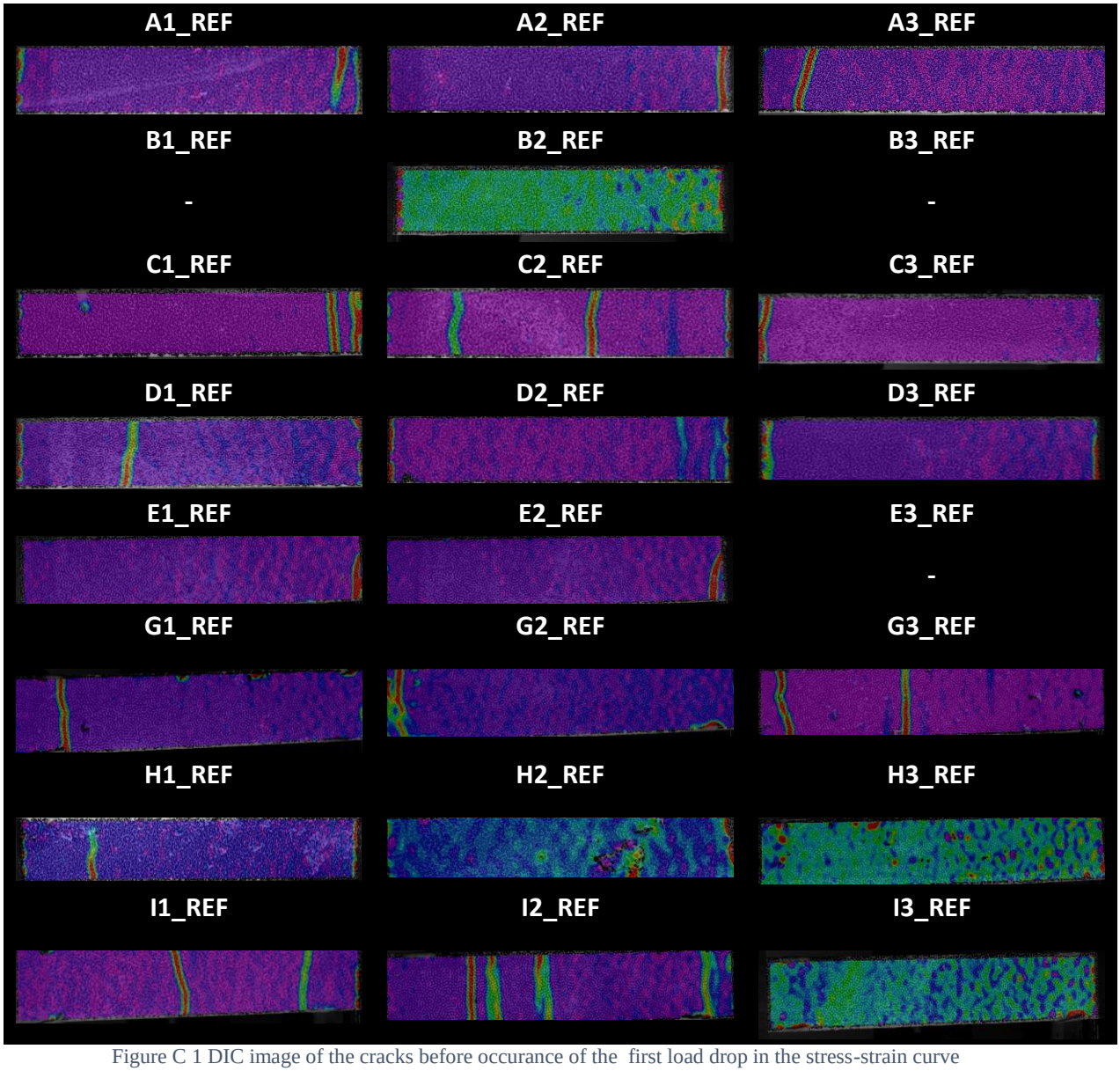

Figure C 1 DIC image of the cracks before occurance of the first load drop in the stress-strain curve

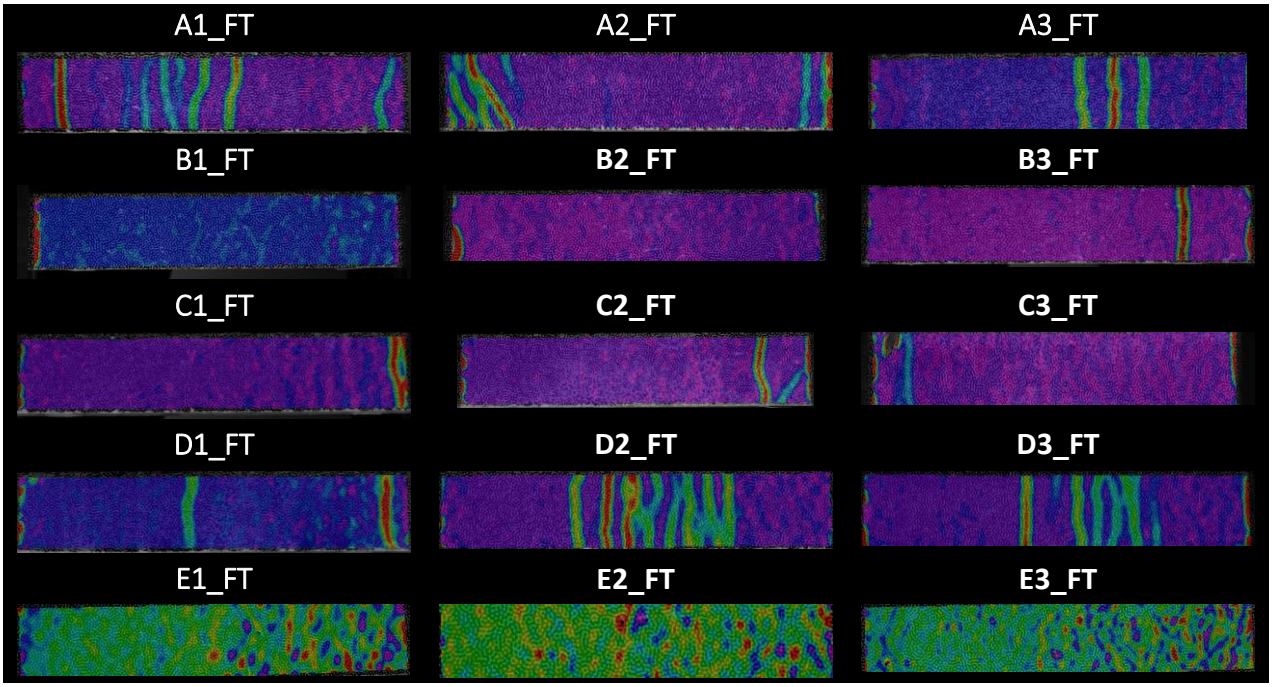

Figure C 2 DIC image of the durabliity cracks for the FT loading case

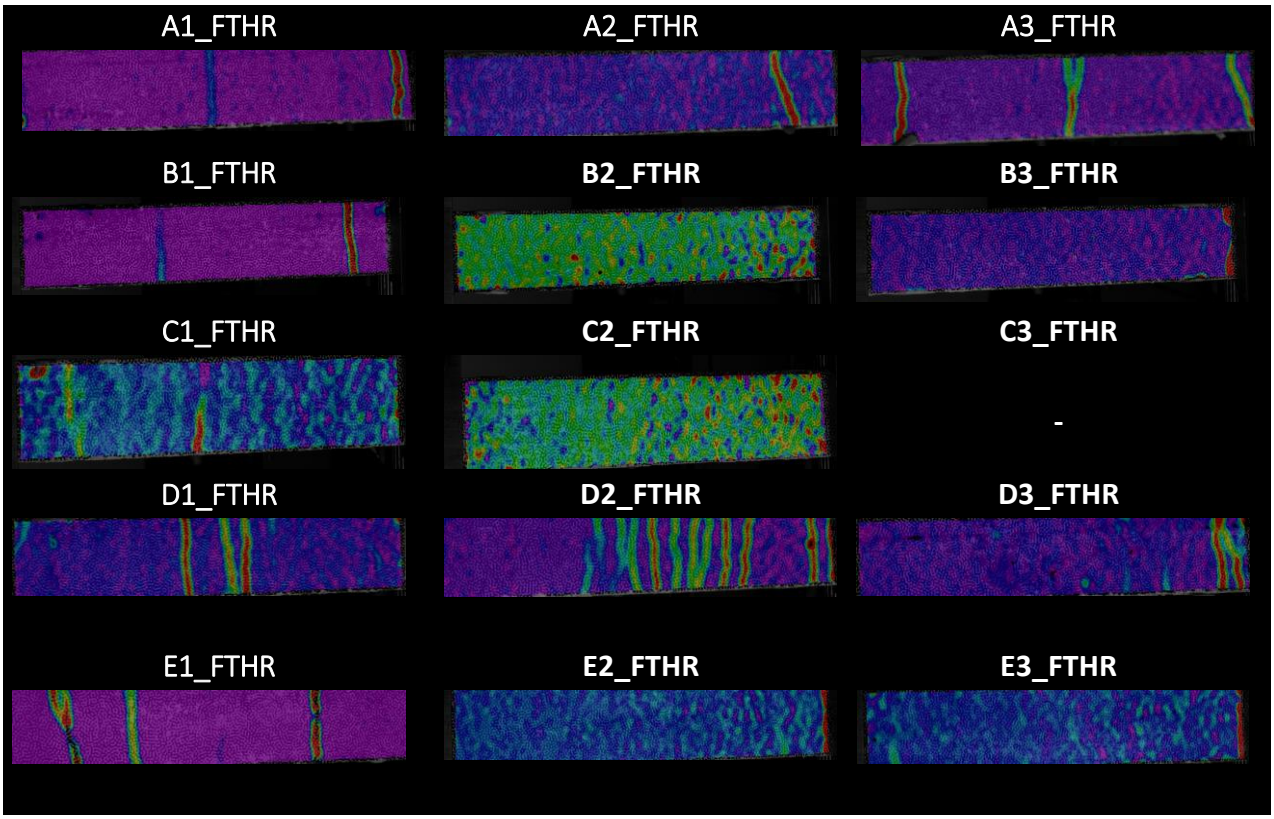

Figure C 3DIC image of the durabliity cracks for the FTHR loading case

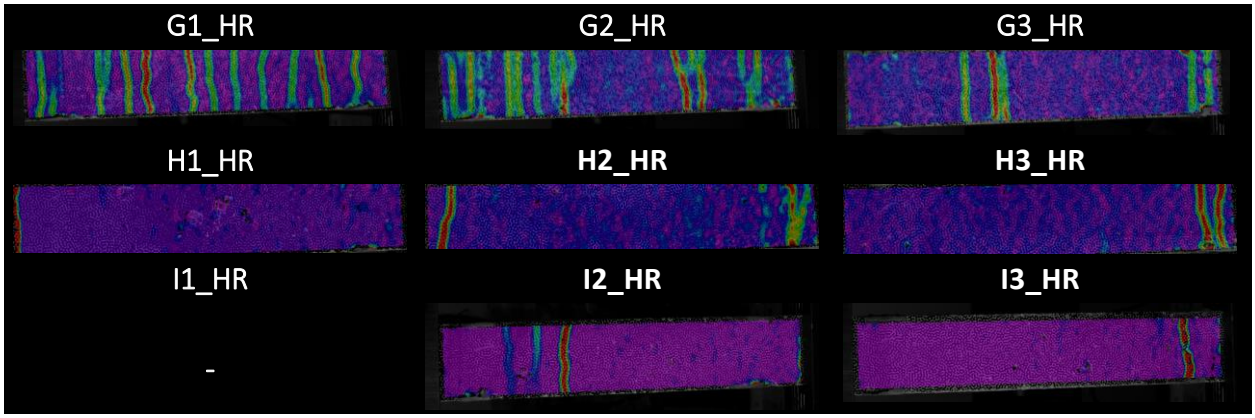

Figure C 4 DIC image of the durabliity cracks for the HR loading case

Annex D
Averaged Mechanical Properties

Table D 1 Young's modulus according to Resonalyser test method for specimen subjected to FTHR (series A to E) and HR (series G to I)

	A_{FTHR}	B_{FTHR}	C_{FTHR}	D_{FTHR}	E_{FTHR}	F_{FTHR}	G_{HR}	H_{HR}	I_{HR}
AVG	15,5	20,7	14,9	10,8	22,6	25,7	11,5	14,9	13,7
STD	4,19	5,51	4,88	2,67	0,81	2,85	2,84	0,84	1,27

Table D2Young's modulus according to Ultrasonic Pulse Velocity for specimen subjected to FTHR (series A to E) and HR (series G to I)

	A_{FTHR}	B_{FTHR}	C_{FTHR}	D_{FTHR}	E_{FTHR}	F_{FTHR}	G_{HR}	H_{HR}	I_{HR}
AVG	18,9	25,3	21,9	14,3	23,1	24,9	15,0	16,5	14,7
STD	0,73	0,40	1,43	1,17	0,18	1,68	0,50	0,40	0,53

Table D3 First cracking strength

		REF (MPa)	DUR 1 (MPa)	DUR 2 (MPa)	REF (MPa)	DUR 3 (MPa)		
Plate A								**Plate G**
	AVG	2,885	2,179	1,678	1,960	1,582	**AVG**	
	STD	0,216	0,166	0,112	0,190	0,124	**STD**	
	%	1,000	0,755	0,582	1,000	0,807	**%**	
Plate B								**Plate H**
	AVG	2,400**	2,752	2,356	2,251	1,708	**AVG**	
	STD	-	0,210	0,666	0,719	0,005	**STD**	
	%	1,000	1,147	0,982	1,000	0,752	**%**	
Plate C								**Plate I**
	AVG	2,796	2,456	2,354*	2,094	1,575*	**AVG**	
	STD	0,422	0,243	0,321	0,338	0,043	**STD**	
	%	1,000	0,878	0,842	1,000	0,752	**%**	
Plate D								
	AVG	2,313	2,068	1,147				
	STD	0,302	0,386	0,276				
	%	1,000	0,894	0,496				
Plate E								
	AVG	3,340*	3.549	2,295				
	STD	0,628	0.405	0,280				
	%	1,000	1.063	0,687				

(*) 1 out of 3 specimens is rejected due to early failure in the clamps or missing DIC results.

(**) 2 out of 3 specimens is rejected due to early failure in the clamps or missing DIC results.

Table D4 Strain at the end of the Multiple cracking stage

		REF (10^{-3})	DUR 1 (10^{-3})	DUR 2 (10^{-3})	REF (10^{-3})	DUR 3 (10^{-3})	
Plate A							**Plate G**
	AVG	8,446**	9,341	6,383	6,772	3,181	**AVG**
	STD	–	1,067	0,704	0,509	0,463	**STD**
	%	1,000	1,106	0,756	1,000	0,470	**%**
Plate B							**Plate H**
	AVG	7,774**	5,694	6,207*	7,923**	4,833*	**AVG**
	STD	–	1,118	1,353	–	0,735	**STD**
	%	1,000	0,732	0,798	1,000	0,610	**%**
Plate C							**Plate I**
	AVG	8,345*	6,186	7,143*	6,378	5,316*	**AVG**
	STD	0,515	0,395	0,137	0,788	0,089	**STD**
	%	1,000	0,741	0,856	1,000	0,833	**%**
Plate D							
	AVG	6,914*	7,345*	3,789*			
	STD	0,893	1,493	0,722			
	%	1,000	1,062	0,548			
Plate E							
	AVG	8,451*	3,073*	6,97			
	STD	2,427	1,27	0,5055			
	%	1,000	0,364	0,825			

(*) 1 out of 3 specimens is rejected due to early failure in the clamps or missing DIC results.

(**) 2 out of 3 specimens is rejected due to early failure in the clamps or missing DIC results.

Table D5 Last cracking strength

		REF (MPa)	DUR 1 (MPa)	DUR 2 (MPa)	REF (MPa)	DUR 3 (MPa)	
Plate A							**Plate G**
	AVG	3,839**	4,188	3,141	3,093	1,727	**AVG**
	STD	–	0,307	0,256	0,122	0,291	**STD**
	%	1,000	1,091	0,818	1,000	0,558	**%**
Plate B							**Plate H**
	AVG	3,727**	3,329*	3,222	3,56**	2,519*	**AVG**
	STD	–	0,172	0,526	–	0,280	**STD**
	%	1,000	0,893	0,865	1,000	0,708	**%**
Plate C							**Plate I**
	AVG	3,982*	3,44	3,732*	3,018	2,35*	**AVG**
	STD	0,321	0,024	0,23	0,664	0,19	**STD**
	%	1,000	0,864	0,937	1,000	0,779	**%**
Plate D							
	AVG	3,345*	3.278*	1,974*			
	STD	0,026	0,521	0,293			
	%	1,000	0,980	0,59			
Plate E							
	AVG	4,215*	3.675*	2,909			
	STD	0,110	0.376	0,121			
	%	1,000	0.824	0,690			

(*) 1 out of 3 specimens is rejected due to early failure in the clamps or missing DIC results.

(**) 2 out of 3 specimens is rejected due to early failure in the clamps or missing DIC results.

Table D6 E modulus (stage I)

		REF (GPa)	DUR 1 (GPa)	DUR 2 (GPa)	REF (GPa)	DUR 3 (GPa)		
Plate A								**Plate G**
	AVG	14,013	3,182	12,474	12,856	2,814	**AVG**	
	STD	4,02	2,245	8,277	8,729	1,437	**STD**	
	%	1,000	0,227	0,890	1,000	0,219	**%**	
Plate B								**Plate H**
	AVG	15,623**	6,022	14,12	14,73	4,772	**AVG**	
	STD	–	2,43	1,896	8,049	2,515	**STD**	
	%	1,000	0,590	1,383	1,000	0,324	**%**	
Plate C								**Plate I**
	AVG	10.321	6,229	10,047*	8,991	2,421*	**AVG**	
	STD	6.716	1,828	7,182	4,102	0,063	**STD**	
	%	1,000	0,604	0,973	1,000	0,269	**%**	
Plate D								
	AVG	11,379	2,426	2,453				
	STD	1,084	1,376	1,676				
	%	1,000	0,213	0,216				
Plate E								
	AVG	14,576*	20,122	7,554				
	STD	8,408	3,115	5,376				
	%	1,000	1,380	0,518				

(*) 1 out of 3 specimens is rejected due to early failure in the clamps or missing DIC results.

(**) 2 out of 3 specimens is rejected due to early failure in the clamps or missing DIC results.

Table D7 E modulus (stage III)

		REF (GPa)	DUR 1 (GPa)	DUR 2 (GPa)	REF (GPa)	DUR 3 (GPa)		
Plate A								**Plate G**
	AVG	0,406**	0,346	0,35	0,35	0,278	**AVG**	
	STD	–	0,051	0,061	0,026	0,027	**STD**	
	%	1,000	0,852	0,862	1,000	0,794	**%**	
Plate B								**Plate H**
	AVG	0,275**	0,297*	0,253	0,372**	0,369*	**AVG**	
	STD	–	0,024	0,065	–	0,071	**STD**	
	%	1,000	1,080	0,920	1,000	0,992	**%**	
Plate C								**Plate I**
	AVG	0,265**	0,319*	0,345*	0,305	0,305*	**AVG**	
	STD	–	0,044	0.024	0,028	0,019	**STD**	
	%	1,000	1,204	1,302	1,000	1,000	**%**	
Plate D								
	AVG	0,298*	0,320*	0,396*				
	STD	0,054	0,041	0,007				
	%	1,000	1,074	1,329				
Plate E								
	AVG	0,298*	0,320*	0,396*				
	STD	0,054	0,041	0,007				
	%	1,000	1,074	1,329				

(*) 1 out of 3 specimens is rejected due to early failure in the clamps or missing DIC results.

(**) 2 out of 3 specimens is rejected due to early failure in the clamps or missing DIC results.

Table D8 Ultimate tensile stress

		REF (MPa)	DUR 1 (MPa)	DUR 2 (MPa)	REF (MPa)	DUR 3 (MPa)	
Plate A							**Plate G**
	AVG	6,59**	5,71	4,36	6,099	3,458	**AVG**
	STD	–	0,526	0,185	0,513	0,86	**STD**
	%	1,000	0,867	0,661	1,000	0,567	**%**
Plate B							**Plate H**
	AVG	4,911**	3,73	3,68	6,86**	3,10*	**AVG**
	STD	–	0,187	0,444	–	0.285	**STD**
	%	1,000	0,760	0,750	1,00	0,452	**%**
Plate C							**Plate I**
	AVG	4,44	4,01*	4,02*	6,86	3,104	**AVG**
	STD	0,424	0,891	–	–	0,285	**STD**
	%	1,000	0,904	0,905	1,000	0,452	**%**
Plate D							
	AVG	5,67*	4,03*	4,09*			
	STD	1,088	0,039	0,16			
	%	1,000	0,711	0,721			
Plate E							
	AVG	4,72*	3,52	3,14			
	STD	0,342	0,048	0,272			
	%	1,000	0,747	0,667			

(*) 1 out of 3 specimens is rejected due to early failure in the clamps or missing DIC results.

(**) 2 out of 3 specimens is rejected due to early failure in the clamps or missing DIC results.

Table D 9 Ultimate strain

		REF (10^{-3})	DUR 1 (10^{-3})	DUR 2 (10^{-3})	REF (10^{-3})	DUR 3 (10^{-3})	
Plate A							**Plate G**
	AVG	16,2**	13,58	10,08	16,18	9,12	**AVG**
	STD	–	1,979	1,788	0,22	0,24	**STD**
	%	1,000	0,838	0,622	1,00	0,56	**%**
Plate B							**Plate H**
	AVG	11,96**	6,81	8,13	16,80**	6,50*	**AVG**
	STD	–	1,928	1,205	–	0,11	**STD**
	%	1,000	0,569	0,680	1,00	0,39	**%**
Plate C							**Plate I**
	AVG	8,98	8,27*	8,62*	13,75	8,10*	**AVG**
	STD	2,562	1,032	0,593	0,34	0,03	**STD**
	%	1,000	0,921	0,960	1,00	0,59	**%**
Plate D							
	AVG	14,85*	11,65*	9,81*			
	STD	2,333	0,212	0,989			
	%	1,000	0,785	0,660			
Plate E							
	AVG	10,80*	3,93	8,73			
	STD	4,384	0,929	0,986			
	%	1,000	0,364	0,808			

(*) 1 out of 3 specimens is rejected due to early failure in the clamps or missing DIC results.

(**) 2 out of 3 specimens is rejected due to early failure in the clamps or missing DIC results.

Table D10 Total number of cracks

		REF (-)	DUR 1 (-)	DUR 2 (-)	REF (-)	DUR 3 (-)	
Plate A							**Plate G**
	AVG	12,0**	13,3	10,5	19,0	19,7	**AVG**
	STD	–	3,536	2,121	3,000	2,082	**STD**
	%	1,000	1,111	0,875	1,000	1,035	**%**
Plate B							**Plate H**
	AVG	16,0**	9,7	9,7	15,0**	14,5*	**AVG**
	STD	–	2,517	0,577	–	0,707	**STD**
	%	1,000	0,604	0,604	1,000	0,967	**%**
Plate C							**Plate I**
	AVG	13,0	13,7	16,0*	17,7	14,5*	**AVG**
	STD	4,583	1,528	1,414	1,155	0,707	**STD**
	%	1,000	1,051	1,231	1,00	0,821	**%**
Plate D							
	AVG	17,0*	15,5	14,0*			
	STD	0,000	0,707	4,243			
	%	1,000	0,912	0,824			
Plate E							
	AVG	10,0*	3,7	9,7			
	STD	4,243	1,528	2,887			
	%	1,000	0,367	0,967			

(*) 1 out of 3 specimens is rejected due to early failure in the clamps or missing DIC results.

(**) 2 out of 3 specimens is rejected due to early failure in the clamps or missing DIC results.

Table D11 Average crack width

		REF (mm)	DUR 1 (mm)	DUR 2 (mm)	REF (mm)	DUR 3 (mm)		
Plate A								**Plate G**
	AVG	0,33**	0,25	0,21	0,21	0,12	**AVG**	
	STD	–	0,012	0,021	0,021	0,032	**STD**	
	%	1,00	0,746	0,619	1,00	0,54	**%**	
Plate B								**Plate H**
	AVG	0,18**	0,17	0,20	0,28**	0,11*	**AVG**	
	STD	–	0,031	0,043	–	0,023	**STD**	
	%	1,00	0,950	1,115	1,00	0,40	**%**	
Plate C								**Plate I**
	AVG	0,17	0,15	0,13*	0,19	0,14*	**AVG**	
	STD	0,02	0,001	0,003	0,032	0,014	**STD**	
	%	1,00	0,892	0,754	1,00	0,72	**%**	
Plate D								
	AVG	0,21*	0,18	0,18*				
	STD	0,03	0,011	0,038				
	%	1,00	0,847	0,819				
Plate E								
	AVG	0,26*	0,24	0,23				
	STD	0,01	0,051	0,058				
	%	1,00	0,922	0,876				

(*) 1 out of 3 specimens is rejected due to early failure in the clamps or missing DIC results.

(**) 2 out of 3 specimens is rejected due to early failure in the clamps or missing DIC results.

Table D12 Average crack interdistance

		REF (mm)	DUR 1 (mm)	DUR 2 (mm)	REF (mm)	DUR 3 (mm)		
Plate A								**Plate G**
	AVG	20,35**	18,44	22,70	13,39	12,80	**AVG**	
	STD	–	4,812	4,050	2,102	1,373	**STD**	
	%	1,000	0,906	1,116	1,000	0,956	**%**	
Plate B								**Plate H**
	AVG	15,15**	26,24	24,68	16,65**	17,25*	**AVG**	
	STD	–	7,328	1,700	–	0,776	**STD**	
	%	1,000	1,732	1,629	1,000	1,036	**%**	
Plate C								**Plate I**
	AVG	20,27	18,79	14,96*	13,98	16,97*	**AVG**	
	STD	6,753	2,047	1,322	0,843	1,043	**STD**	
	%	1,000	0,927	0,738	1,000	1,214	**%**	
Plate D								
	AVG	14,4*	15,57	18,19*				
	STD	0,094	0,643	5,677				
	%	1,000	1,079	1,260				
Plate E								
	AVG	26,78*	63,77	26,79				
	STD	11,349	18,218	6,946				
	%	1,000	2,382	1,001				

(*) 1 out of 3 specimens is rejected due to early failure in the clamps or missing DIC results.

(**) 2 out of 3 specimens is rejected due to early failure in the clamps or missing DIC results.